DOKUZ EYLÜL UNIVERSITY

GRADUATE SCHOOL OF NATURAL AND APPLIED SCIENCES

AUTOMATION AND FINITE ELEMENT ANALYSIS OF A DESKTOP CNC LATHE

by

Uğur TUTKUN

October, 2020

İZMİR

AUTOMATION AND FINITE ELEMENT ANALYSIS OF A DESKTOP CNC LATHE

A Thesis Submitted to the
Graduate School of Natural and Applied Sciences of Dokuz Eylül University
In Partial Fulfillment of the Requirements for the Degree of Master of Science
in Mechatronics Engineering Program

by

Uğur TUTKUN

October, 2020
İZMİR

M.Sc. THESIS EXAMINATION RESULT FORM

We have read the thesis entitled **"AUTOMATION AND FINITE ELEMENT ANALYSIS OF A DESKTOP CNC LATHE"** completed by **UĞUR TUTKUN** under supervision of **ASST.PROF.DR. MURAT AKDAĞ** and we certify that in our opinion it is fully adequate, in scope and in quality, as a thesis for the degree of Master of Science.

………………………………………..

Asst.Prof.Dr. Murat AKDAĞ

Supervisor

…………………………………….

Prof. Dr. Zeki KIRAL

(Jury Member)

…………………………………….

Asst.Prof.Dr. Fatih Cemal CAN

(Jury Member)

Prof.Dr. Özgür ÖZÇELİK

Director

Graduate School of Natural and Applied Sciences

ACKNOWLEDGMENTS

Foremost, I would like to express my sincere gratitude to my family for their endless support. I would like to thank to my advisor Asst. Prof. Dr. Murat Akdağ for his patience, motivation and immense knowledge. I thank to my manager Mr. Murat Varol for letting me to study in the university laboratories for my project on weekdays. I would like to thank to Prof. Dr. Kubilay Aslantaş and his student Mr. Fuat Kara who shared their studies and experiment data for my thesis. I would like to thank to mechanical design engineer Mr. Mert Kanık for his supports. And I would like to thank to Dokuz Eylül University Mechanical Engineering student Mr. Ali Demir for his support and help to this study.

Uğur TUTKUN

AUTOMATION AND FINITE ELEMENT ANALYSIS OF A DESKTOP CNC LATHE

ABSTRACT

This study contains the realistic modelling, finite element analysis, automation and turning experiments of a desktop CNC lathe. For the analysis model, a multi-body flexible system has been created and the static analyzes have been performed on this multi-body model. The assembly model consists of motion sub-assemblies which are called members. Each member consists of models of parts or sub-assemblies which have a common rigid body motion. The stress obtained from the static analyzes and especially the amount of displacement of the insert was examined and it was tried to establish a relationship with the precision of the parts to be produced on the machine. After the analysis part, the turning experiments have been performed. For the experiments, 316-L stainless steel bar has been used as the workpiece. With different cutting parameter levels, six experiments have been done. With these experiments, the relationships between cutting parameters and surface quality have been established. Also, the optimum working range of the lathe has been determined. For the automation part of the study, the tool holder has been automated with the adjustments on the MACH3 program. In addition, the pneumatic part on the tool holder and the speed control of the spindle motor has been automated with the codes in the program too.

Keywords: CNC lathe, cutting parameters on a CNC lathe, analysis of a CNC lathe, automation of a CNC lathe, MACH3, Modus, Brain

MASAÜSTÜ BİR CNC TORNANIN OTOMASYONU VE SONLU ELEMANLAR YÖNTEMİ İLE ANALİZİ

ÖZ

Bu çalışma, bir masaüstü CNC torna tezgahının realistik modellenmesi, sonlu elemanlar analizi, otomasyonu ve tornalama deneylerini içermektedir. Analiz modeli için çok gövdeli esnek bir sistem oluşturulmuş ve bu çok gövdeli model üzerinde statik analizler yapılmıştır. Montaj modeli, eleman olarak adlandırılan hareket alt montajlarından oluşmaktadır. Her eleman, ortak bir rijit gövde hareketine sahip parça veya alt montaj modellerinden oluşmaktadır. Statik analizlerden elde edilen gerilme ve özellikle kesici ucun yer değiştirme miktarı incelenmiş ve tornada üretilecek parçaların hassasiyeti ile ilgili bir ilişki ortaya konulmaya çalışılmıştır. Analiz bölümünden sonra tornalama deneyleri yapılmıştır. Deneyler için, iş parçası olarak 316-L paslanmaz çelik çubuk kullanılmıştır. Farklı kesme parametre seviyeleri ile altı deney yapılmıştır. Bu deneylerle kesme parametreleri ve yüzey kalitesi arasındaki ilişkiler ortaya çıkarılmıştır. Ayrıca torna tezgahının optimum çalışma aralığı da belirlenmiştir. Çalışmanın otomasyon kısmı için, takım tutucu MACH3 programındaki ayarlarla otomatikleştirilmiştir. Ayrıca, takım tutucu üzerindeki pnömatik parça ve spindle motorunun hız kontrolü de MACH3'e yazılan kodlarla otomatikleştirilmiştir.

Anahtar kelimeler: CNC torna, CNC tornadaki kesme kuvvetleri, CNC torna analizi, CNC torna otomasyonu, MACH3, Modbus, Brain

CONTENTS

LIST OF FIGURES

Page

LIST OF TABLES

Page

CHAPTER ONE

INTRODUCTION

1.1 Introduction

The accessibility of companies in the market today relies upon staying aware of the creating innovation. In the assembling segment, consumer loyalty can be given by assembling the quality item less expensive and quicker. To create quality items, the parts must be delivered reliable and in the desired size range. Parts can be created more exact and quicker on CNC machines contrasted with conventional turning machines.

1.2 History of the CNC Lathes

Historically, numerical control (NC) systems have been made with computerization of lathe tools which promotes dynamically material machining. Therefore, new researches and improvements brought out the computerized numerical control (CNC) innovation. Very first NC machines were improved in 1940s and 1950s that are powered by motors that leads to linear movements of the axes. Very first products are made on the lathe frame were taped or punched on the tool table. In Figure 1.1 first European NC machine tool is shown.

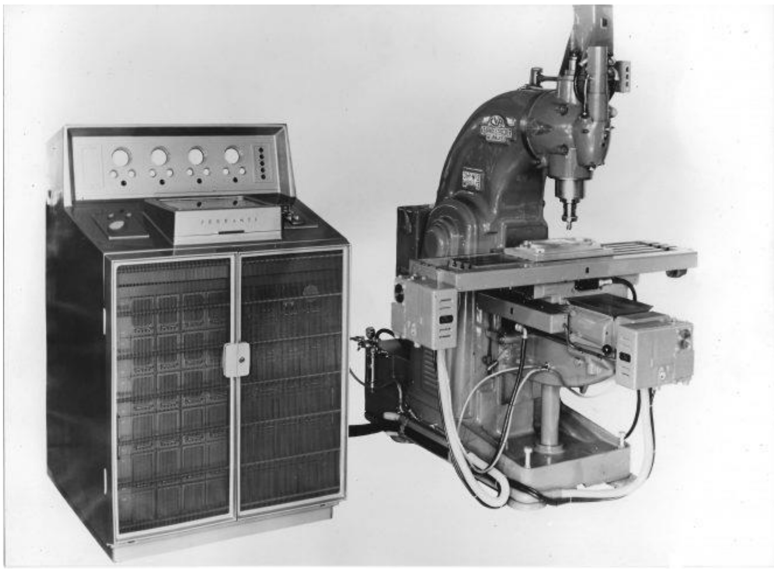

Figure 1.1 First NC machine tool (The First NC Machine Tool, 1956)

Servomechanisms have been quickly increased with simple and advanced PCs, making the modern CNC machines that have reformed the machining processes. In

1952, Arma Company which had accomplished lots of things in defence industry during the war, declared the numerically controlled turning machine. The cost of PC cycles fell radically during the 1960s with the far reaching of presentation of helpful minicomputers. In the end it turned out to be more affordable to deal with the engine control and feedback with a PC program than it was with committed servo systems. Small PCs were committed to a single mill, putting the whole process in a little box. In Figure 1.2 a vertical machining centre from 1962 is shown.

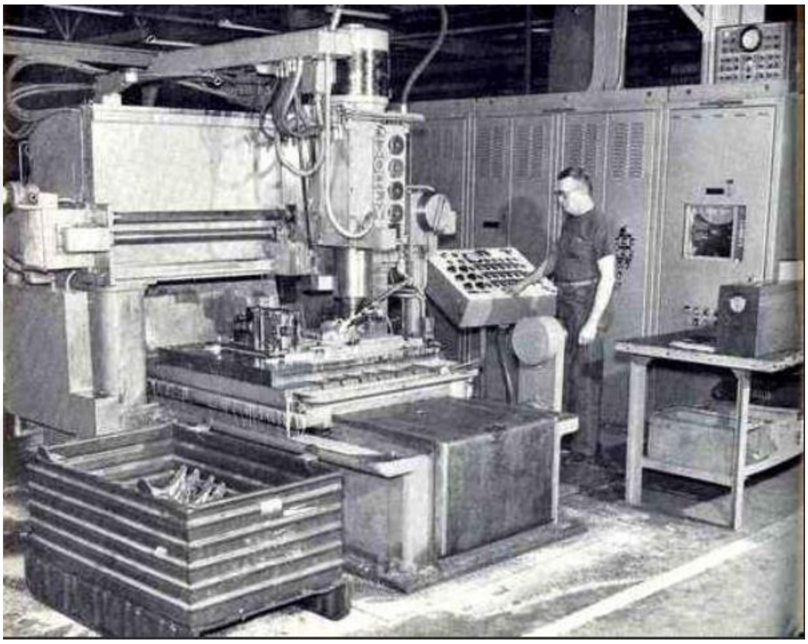

Figure 1.2 A vertical machining center (A magnetic tape controlled vertical profiler, 1962)

In 1973 Dr. Koren invented the world's initially computerized controller for a processing machine, some time before PCs which had been widely utilized in industrial applications. Koren designed the controller and coded the all algorithms of the software (whole memory of the PC was 4K). This control idea involves letting the machine controller calculate the most productive speed continuously, during processing, to upgrade performance (namely, boost productivity while maintaining accuracy). Koren therefore spearheaded the improvement of versatile control algorithms for different manufacturing processes to upgrade their productivity while keeping up part quality. In Figure 1.3 Yoram Koren controls the world's first CNC milling machine that he designed.

Figure 1.3 CNC milling machine (Koren, 1973)

CNC automation decreased the frequency of errors and gave CNC operators time for extra works. CNC automation allows greater capacity for serial production than the conventional lathes. With the helping of the computers, production with the CNC machines ensure the more precision. A modern CNC machine is shown in Figure 1.4

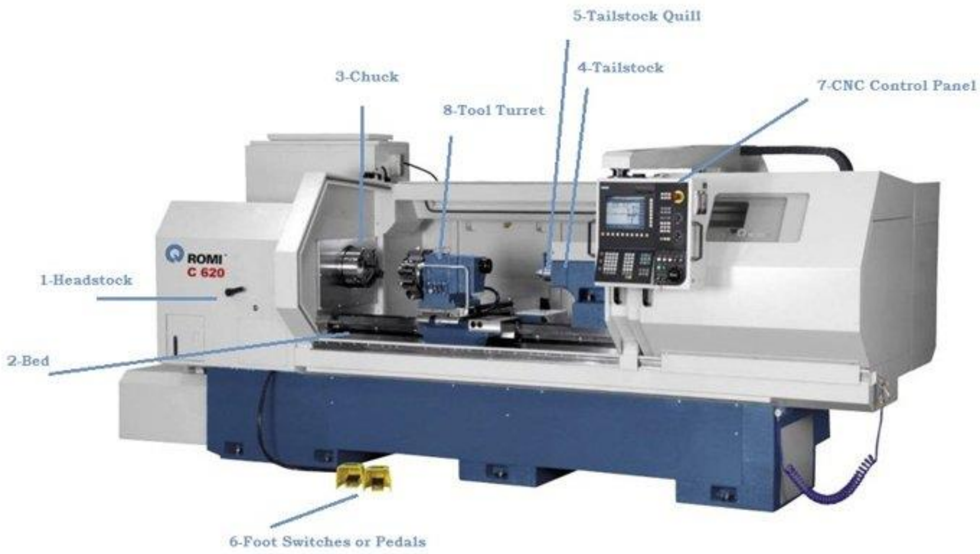

Figure 1.4 View of a modern cnc lathe (Parts of the CNC Lathe, 2020)

1.3 Literature review

For this thesis the literature review has been done under two different captions. The first caption is about the realistic modelling and finite element analyses of manufacturing machines. And the second caption is about the cutting forces and their effects on the workpiece in a turning process.

1.3.1 Modelling and finite element analysis

Erkekli has been made a study about mechanical designing and testing of a quadruped robot. The study includes the processes of design, analyse and production of this 4-leg robot. Besides, the test processes of this robot with a hydraulic actuator are shown (Erkekli, 2017).

Xing and Moan looks at in detail the displaying and analysis of a planet carrier of a wind turbine gearbox part. The examination is acted in multi-parts just like this thesis. They create a multi-body model and make the analysis environment for the planet carrier. The result from this investigation is the creation of proper and correct analysis model of planet carrier of a wind turbine (Xing & Moan, 2012).

Maniar, Patel and Vakharia presented the design of an apparatus for machining production. The study gives the 3D assembled and detonated perspective of the apparatus. The modelling of this fixture is performed with a balanced mass. Finite element analysis of the apparatus is additionally performed (Patel, Maniar, & Vakharia, 2009).

Çakır and Işık investigated the FEA of cutting tools before crack. For the cutting force data, they use force dynamometers. Beside the static analyzes, the study also gives the harmonic and modal analyzes of the cutter. The analyzes are carried on ANSYS (Işık & Çakır, 2005).

Abuthakeer, Mohanram and Kumar gave structure models of machining tools with the assistance of making basic adjustments made in tool bed. After the finite element simulations, bed models were manufactured with quick prototyping and tested (Authakeer, Mohanram, & Kumar, 2011).

In Arali and Kulkarni's investigation goal is to perform the static, fatigue analyzes of spindle structure for the greatest cutting force condition and foreseeing life of the bearings. Proportional rotating stress, factor of safety and life of the axle is found by fatigue analysis. In the study, the analysis results are compared with the analytical calculations of stress values (Arali & Kulkarni, 2014).

Vrtanoski and Dukovski investigated the structural analysis of main spindle covering structure made by various materials. The metal structure of the main model is replaced by the structure made with polymer concrete. This work is a commitment to the practicability of the utilization of polymer concrete in machine tool design. It tends to be seen that the significant advantage of polymer concrete in comparison with cast iron is a vastly improved damping ratio, which may prompt improve dynamic performance of the machine. Different attributes of polymer concrete are generously more regrettable in comparison with the cast iron, which requires suitable redesigning of the structure to have the option to accomplish attractive performances (Vrtanoski & Dukovski, 2005).

One of the targets of this thesis is making a right reasonable analysis model and performing finite element analysis of the current CNC lathe. For analysis model, a multi-body adaptable framework has been made and the static analyzes have been performed on this multi-body model.

1.3.2 Cutting forces and their affects in a turning process

Analysing cutting forces and their effects on the workpiece in a turning process is still an important subject.

In Das, Rai and Saha's study an exploratory methodology is introduced for the measurement of the surface quality of the machined surface produced by basic turning operation. The boundaries used in the test were determined as three cutting boundaries which are cutting speed, depth of cut and feed rate. Different boundaries, for example, device nose radius, workpiece length, workpiece width, and workpiece material were taken as stable. The impacts of the process boundaries in particular cutting rate and feed ware monitored with the analyzes during this examination. Trials were completed with cutting speed and depth of cut as steady and feed rate as factor (Das, Rai, & Saha, 2012).

Kumar, Bhatta and Mishra study the looking at of parameters that influence the cutting forces during the turning of mild steel. These turning parameters are cutting speed, feed rate and depth of chip. The depth of chip has been found as the most critical boundary affecting the tool force in the turning process followed by feed rate and a minor impact of cutting speed. In the investigation, the tests were completed on a high-speed machine (MGL-54) which empowers to operate at higher speeds for machining and production of workpieces (Kumar, Bhatta, & Mishra, 2014).

In Kurniawan, Handawi and Mohd's examination, turning process with least amount lubrication (50mL/h flow rate and 5 bar air pressure) at different cutting speeds (100, 135, and 170 m/min) and feeds (0.16, 0.20, and 0.24 mm/rev) has been finished. The machining reactions are tool life, surface roughness, and cutting forces. All machining reactions were fundamentally impacted by the cutting speed and feed. Tool life becomes longer when to cutting speed and feed are kept in low levels. Surface roughness is conversely corresponding to cutting speed yet relative to feed. A mix of low cutting speed and feed is important to accomplish long tool life, low surface roughness, and low cutting forces (Kurniawan, Handawi, & Mohd, 2015).

In Yao, Zhou and Zhang's investigation the cutting force impacts in turning process are inspected. The face-turning of high-temperature alloy Inconel718 with carbide and ceramic cutters have been studied and the cutting forces on the cutting boundaries have been studied. The cutting force has positive connection with feed rate and the chip depth. The aftereffects of the examinations have been shown for the two cutter types. During the expanding process of the cutting rate, the cutting force occures around 96 N with the carbide cutter. For the ceramic cutter, the cutting force expanded to around 380 N initially and then reduces when the cutting force expanded (Yao, Zhou, & Zhan, 2017).

Umbert investigated the cutting forces and the possible effects of these forces in a turning process. Besides, issues like vibrations or deflection have been contemplated. Tests with various cutters and expanding depth of cut have been acted in the lathe with a force estimation framework to analyse the exact contrasts experienced in the cutting forces. These tests affirm that the radial force presents an expanding characteristic until the depth of cut is more noteworthy than the nose radius of the tool, after this second the radial force becomes stable (Umbert, 2012).

Eker, Ekici, Kurt and Bakır investigates the machining of magnesium alloy at various cutting conditions by researching machining processes and contrasting turning processes through their ideal cutting parameters. In the investigation, outside insignificant amount lubrication framework was utilized as least amount oil framework. This framework improves the tool life. In dry machining, more friction and adhesion between the tool and the workpiece happen on the grounds that they are exposed to higher temperature. Hence, tool wear rises and device life reduces (Eker, Ekici, & Bakır, 2014).

Shetty and Kumar explore the impacts of cutting boundaries in the turning process of carbon alloy steels with a CNC lathe. The boundaries are the spindle speed and feed rate which are changed to examine their impacts on surface roughness. Five distinctive carbon alloy steels have been chosen for turning processes which are SAE8620, EN8, EN19, EN24 and EN47. The examination shows that the surface roughness is affected by the spindle speed and feed rate. It is seen that the surface roughness rises with expanded feed rate and it is higher at lower speeds (Shetty & Kumar, 2012).

In Yadav, Narang and Attri's examination the impacts of machining boundaries (cutting velocity, feed rate and depth of cut) on surface roughness are researched. Analysis of difference (ANOVA) and the signal-to-noise (S/N) proportion are utilized in this investigation. Tests are made on STALLION-100 HS CNC machine. The ideal estimation of the surface toughness (Ra) comes out to be 0.89. Feed rate is the most critical factor influencing surface roughness followed by depth of cut. Cutting speed is the least noteworthy factor influencing surface roughness (Kumar, Narang, & Attri, 2012).

In Aslantaş, Çiçek and Kara's examination, a prescient modelling is performed for the cutting forces produced during the turning process of AISI 316 L stainless steel. An artificial neural organization (ANN) is used in the study. The boundaries of the ANN model are the cutting speed, feed rate and coating type. In the model, tungsten carbide cutting tools, uncoated and two coatings (TiCN and Al2O3) are utilized. The difference in the main cutting force acquired under similar conditions for each cutter coatings. Rising in the main cutting force rely upon expanded feed rate. Since the increment in the feed rate causes an expansion in the chip cross section, the pressure influences the cutting tool will likewise rise. Therefore, the force required for cutting process will rise. As the cutting speed rises, the cutting temperature in the primary distortion zone rises and thermal softening happens in the cutting zone. This thusly prompts a decline in the cutting force (Aslantaş, Çiçek, & Kara, 2015).

1.4 Cutting forces in a turning process

There are a few issues to be considered in CNC lathe design and manufacturing. Some significant subjects of these issues are rigidity of the body, figuring of the cutting forces and the open workplace environment on the machine. The bench must have a compact structure and the body material must be impervious to high moment forces.

The figuring of the cutting forces happening on the lathe ought to be done effectively. Three sorts of cutting forces happen during the cutting process. The first of the forces is the main cutting force (Fc) which is opposite to the cutter. Increments in the main cutting force rely upon an expanded feed rate. Since the expansion in the feed rate prompts an increment in the chip cross segment, the pressure influencing the cutting tool will likewise increment. As the cutting rate expands, the cutting temperature in the deformation zone increments and thermal softening happens in the cutting zone. This thusly prompts a lessening in the cutting force. Another force is the feed force (Ff) which happens on the parallel axis of the workpiece. Contingent upon the expanded feed rate, the feed forces additionally increase. Moreover, contingent upon the increasing cutting speed, the feed forces decline. The last force is the radial force (Fr) which is opposite to the unrelated force and towards the lathe. Radial cutting force increments as the tool nose radius increments. There is no critical connection between radial force and cutting parameters like cutting speed or feed rate. Cutting forces in a turning cycle are shown in Figure 1.5.

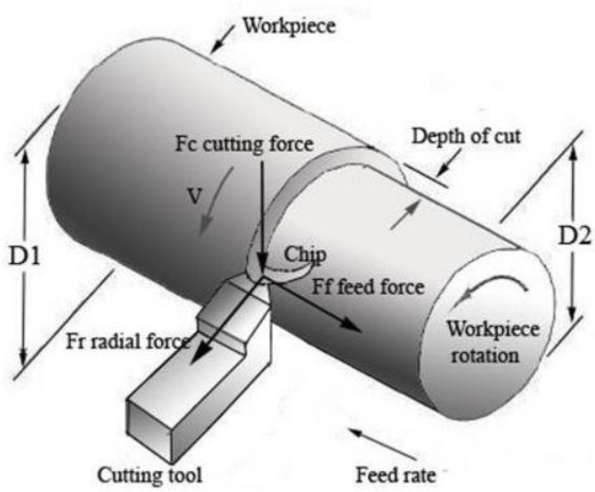

Figure 1.5 Cutting forces in a turning process (Cutting Forces, 2020)

1.5 Main parts and features of the existing lathe

The CNC lathe has a rigid structure with its cast iron body and smallness. With the 45-degree sideways structure, the lathe has a comfortable working chance and has protection from the moments made by the forces. Movement on the lathe is given by stepper motors, ball screws, rail and car frameworks. The existing work area CNC machine is shown in Figure 1.6.

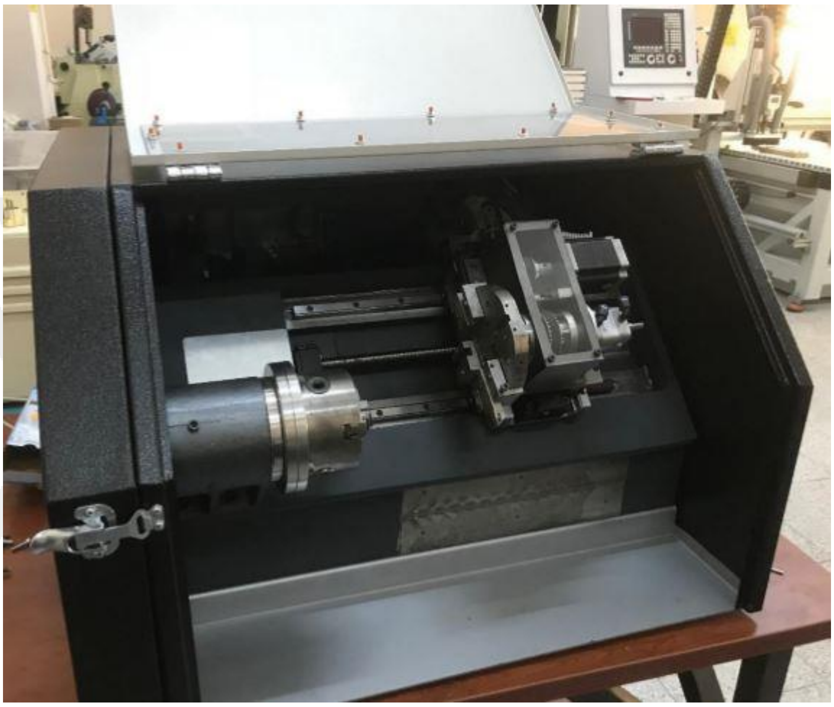

Figure 1.6 View of the CNC lathe (Personal archive, 2020)

The lathe has a 1.1 kW AC electric motor that can work at 3000 rpm. It can handle the steel pieces that has 90 mm distance across and 200 mm length. Turret holder, states on the x-axis and has 8 tool holders. With the 6-bar pressure-resistant pneumatic cylinder, the turret moves forward comfortably. After the linear movement, the stepper motor runs and the turret turns. In Table 1.1, the properties of the lathe are given.

Table 1.1 Properties of the lathe

Lathe body material	Cast iron
Lathe dimensions	739x701x499 mm
Maximum workpiece length	200 mm
Maximum workpiece diameter	90 mm
Spindle motor	1.1 kW AC motor
Maximum speed of the motor	3000 rev/min
Axis motors	Step motor
Movement of the z-axis	240 mm
Movement of the x-axis	110 mm

The dimensions of the turret body are 170 mm as length and 60 mm as width. The diameter of the tool holder is 124 mm. The turret can hold eight cutter and with the upgrades in this study, the turret can change the tools automatically. The turret mechanism is shown in Figure 1.7.

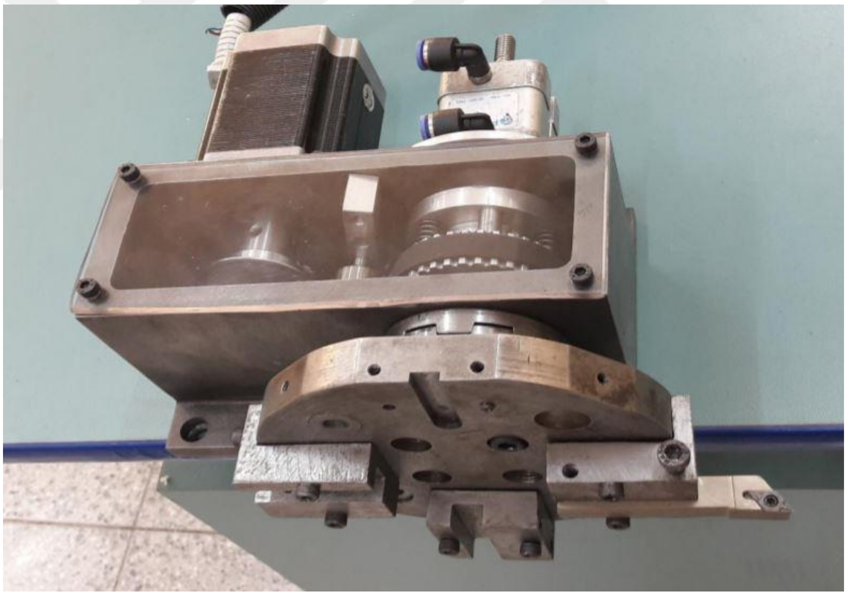

Figure 1.7 The turret mechanism (Personal archive, 2020)

1.6 Organization of the thesis

This thesis consists of five chapters (including the introduction and the conclusions) and the appendices.

In chapter one the history of CNC lathes, literature review, information about cutting forces in a turning process, main parts of the exist lathe and organization of the thesis are given.

In chapter two, the creation of 3D analysis model of the lathe and the processes of the static analysis of this analysis model are given. The detailed explanations of all stages of the modelling and analysis steps are given in chapter two.

In chapter three, the turning experiments under certain cutting parameters of the lathe are given. The optimum working parameters, effects of different cutting parameter levels and surface roughness of the workpieces are shown in this chapter.

In chapter four, the electronical part of the thesis like automatic movement of turret, automatic movement of pneumatic cylinder and the automatic control of the spindle speed are given. The detailed steps of the electronical part are shown in this chapter.

In chapter five, the conclusions and the suggestions for the future developments of the lathe are given.

CHAPTER TWO

FINITE ELEMENT MODELLING AND ANALYZES

2.1 3D model of the lathe

The importance of realistic analysis is increasing in design studies in order to achieve to increase the precision of the designed machines. In this study, the CNC lathe under consideration has been created as a multi-body flexible model and the static analyzes have been performed on this multi-body flexible model. Since the model consists of elements with relative movements to each other, the contact conditions between these elements must be considered during the static analyzes. The assembly model consists of motion sub-assemblies which are called members. Each member consists of models of parts or sub-assemblies which have a common rigid body motion. Members are connected by joints to each other (Tutkun & Akdağ, 2020). The designed model of the lathe is shown in Figure 2.1.

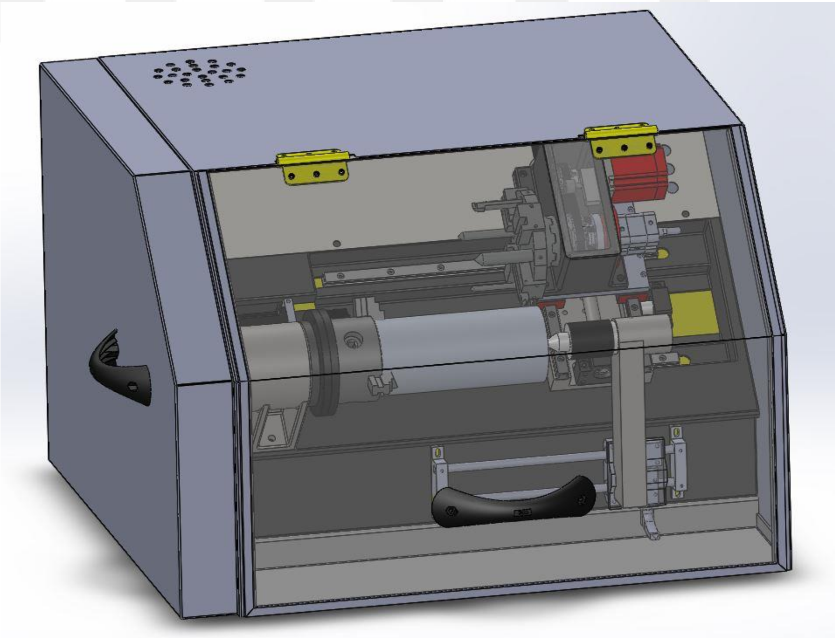

Figure 2.1 3D model of the lathe

3D model of the lathe has been created in SolidWorks. In the design model of the lathe, sub-assemblies and the main assembly have been created. All of the sub-assemblies and electronical parts like step motors have been added in the design model.

The main assembly consists of three members. These are the main lathe body, the x-axis, and the z-axis. The x-axis member includes the turret. Since the turret is close to the cutting area, the turret was considered as a separate part for a more realistic model. In this way, the deviation on the end point of the cutter has been monitored better.

In the production model, all of the details like fan holes, position of the electrical motor, protective parts have been designed. In Figure 2.2, the production model of the lathe is shown.

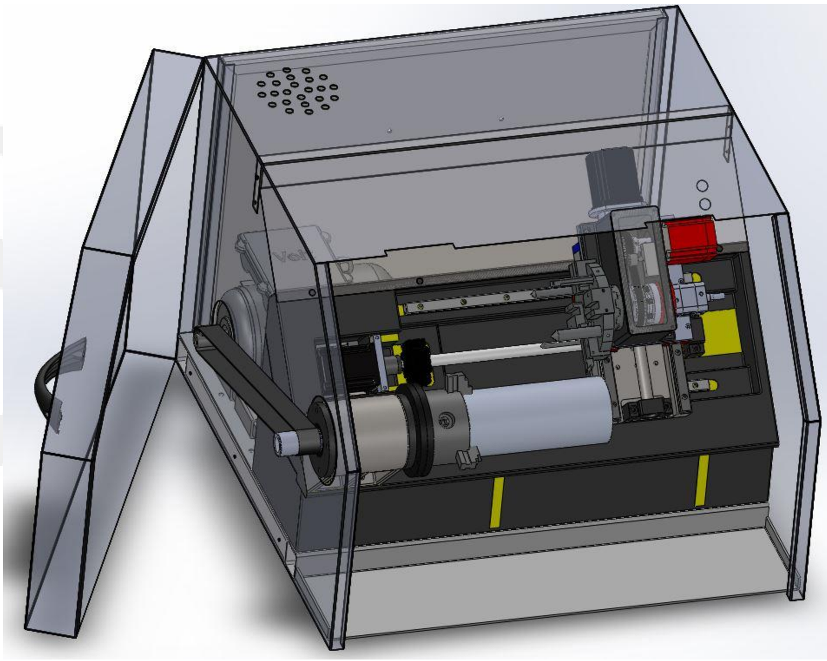

Figure 2.2 Production model of the lathe

2.2 Analysis models of the members

Before the static analyzes of whole system, static analyzes of the members have been made seperately. In this way the reactions of the members against cutting forces have been observed separately.

2.2.1 Analysis model of the lathe body

In the main lathe body, bolt holes which state on the bodies and have diameters less than 5 mm have been ignored. It has been considered that there will be no effect to the analysis results of these bolt holes. Because these small bolt holes state on the strong bodies like main body, rails and the body of the tool holder. Front and back views of the design model of the main lathe body are shown in Figure 2.3 and Figure 2.4. Front and back views of the analysis model of the main lathe body are shown in figure 2.5 and 2.6.

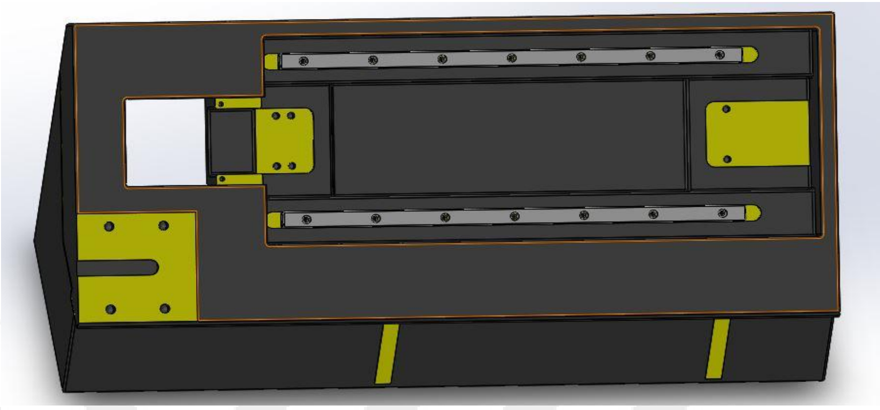

Figure 2.3 Front view of designed model of the main lathe body

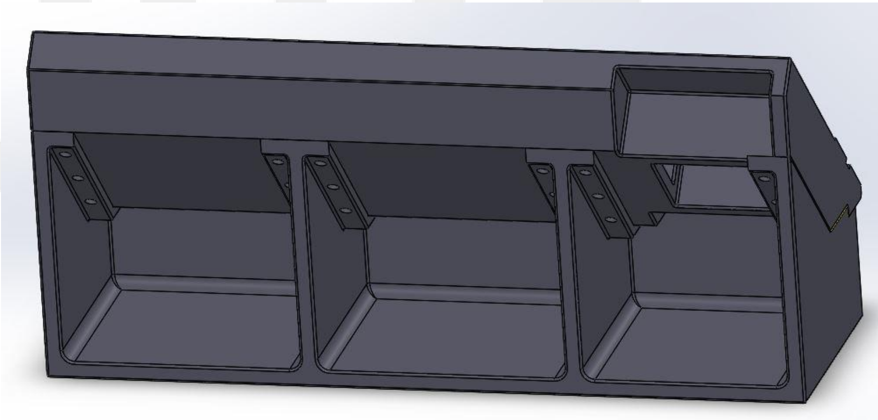

Figure 2.4 Back view of designed model of the main lathe body

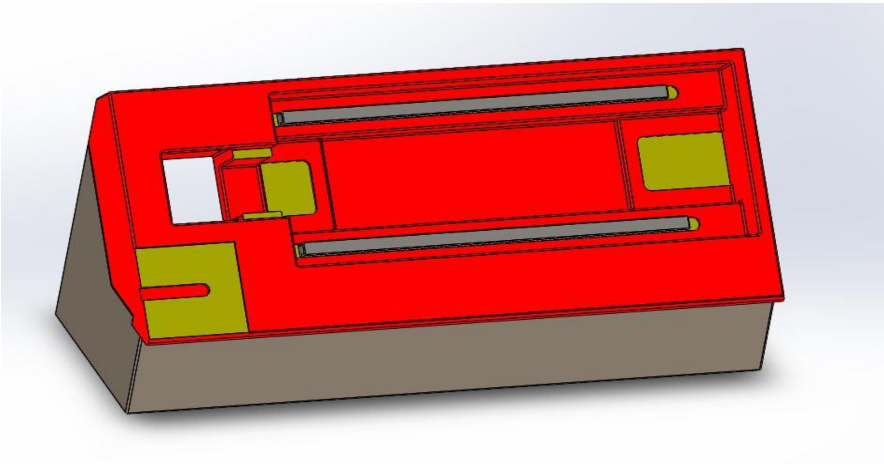

Figure 2.5 Front view of analysis model of the main lathe body

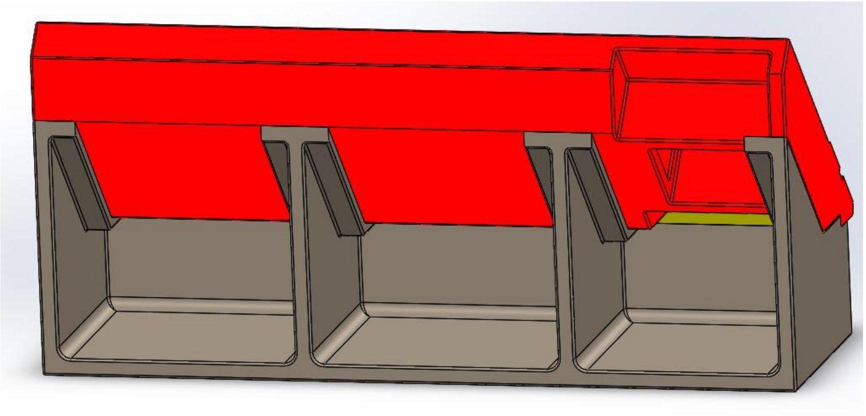

Figure 2.6 Back view of analysis model of the main lathe body

Other simplifications have been made on the rail and car profiles. The holes on the rails and cars have been ignored and the profiles of the rails and cars have been simplified. The original and simplified rail and car profiles have been shown in Figure 2.7 and 2.8.

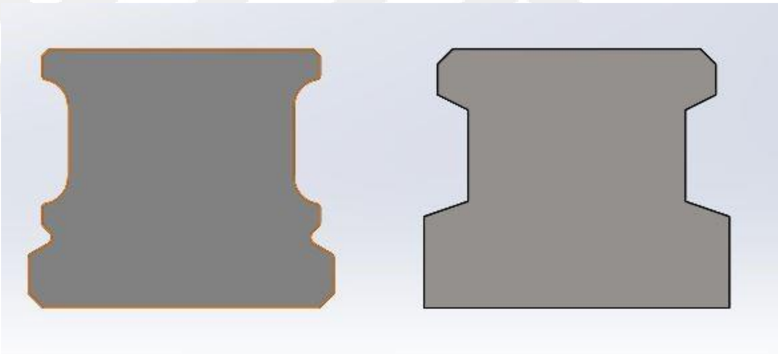

Figure 2.7 Original and simplified profiles of the rails

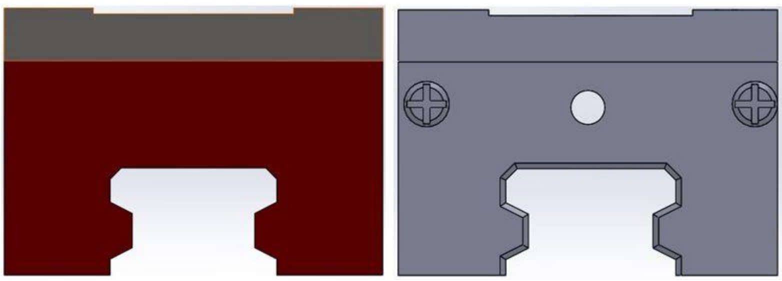

Figure 2.8 Original and simplified profiles of the cars

2.2.2 Analysis model of the z-axis

Another member is the z-axis. This member includes the cars that contacts to the rails, ball screw and nut which provide the movement with rotation, shaft bearings and the plates that carry the x-axis. In the z-axis, the important thing is the ball nut carries the axial force that occur in cutting process, and the cars carry the radial force. Model of the z-axis is shown in Figure 2.9.

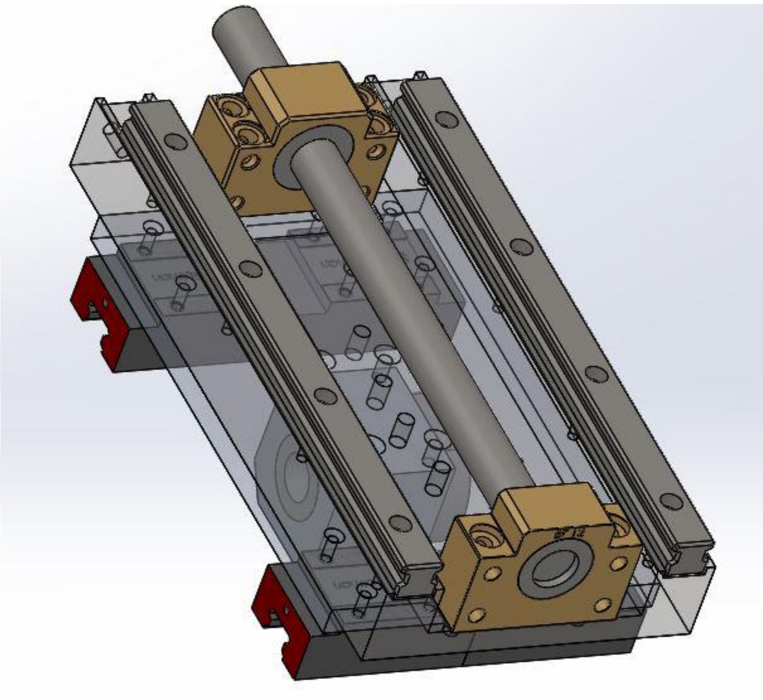

Figure 2.9 Design model of the z-axis

In the z-axis member, the surfaces between the cars that carry the z-axis and the rails that allow the movement of the z-axis on the main body have been chosen as the contact surfaces. These contact surfaces have been determined as no penetration. Analysis model of the z-axis is shown in Figure 2.10.

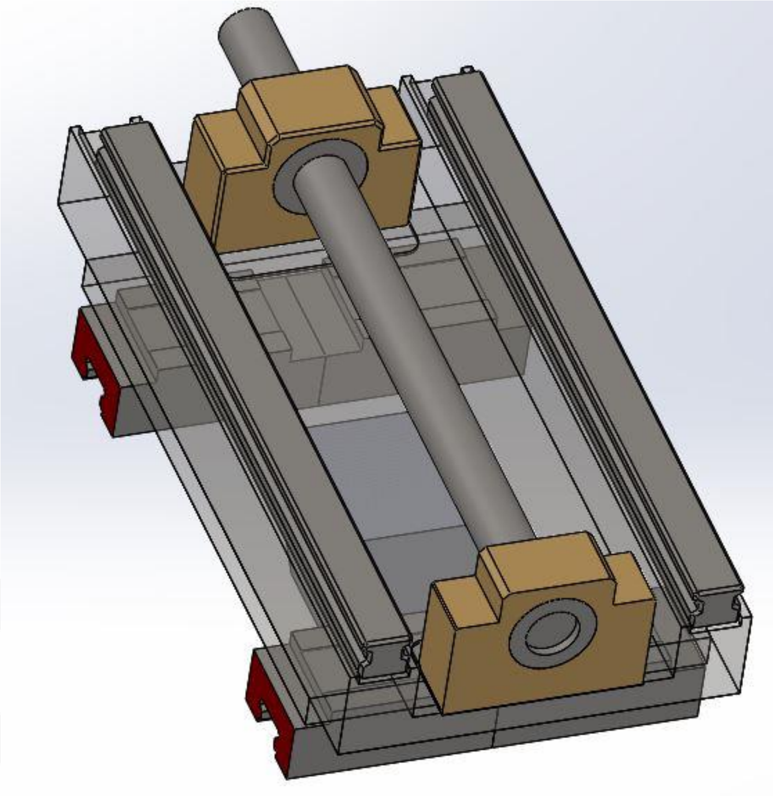

Figure 2.10 Analysis model of the z-axis

2.2.3 Analysis model of the x-axis

Another member is the x-axis. This member includes the cars that contacts to the rails, ball screw and nut which provide the movement with rotation, shaft bearings and the plates that carry the turret. In the x-axis member, the surfaces between the cars that carry the x-axis and the rails that allow the movement of the x-axis on the z-axis have been chosen as the contact surfaces. These contact surfaces have been determined as no penetration. Design model of the x-axis is shown in Figure 2.11 and analysis model of the x-axis is shown in Figure 2.12.

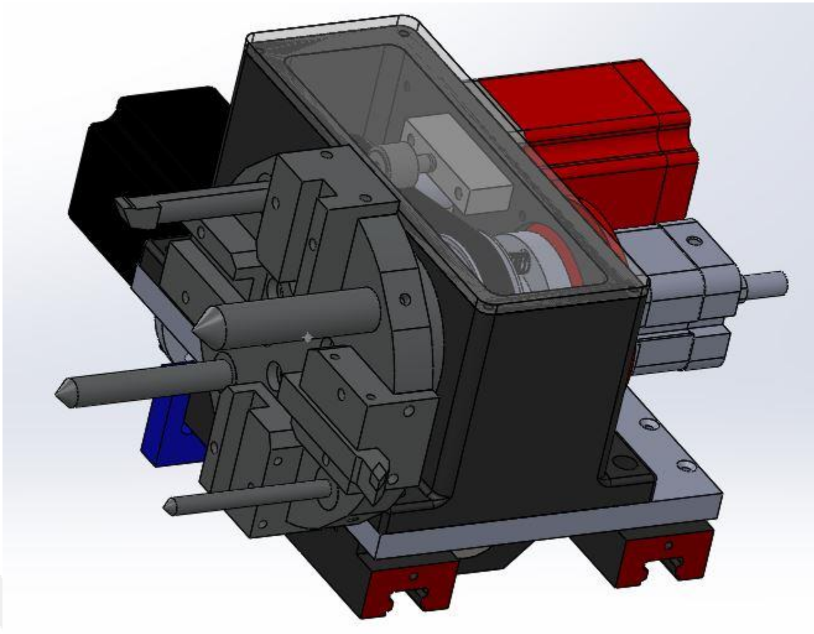

Figure 2.11 Design model of the x-axis

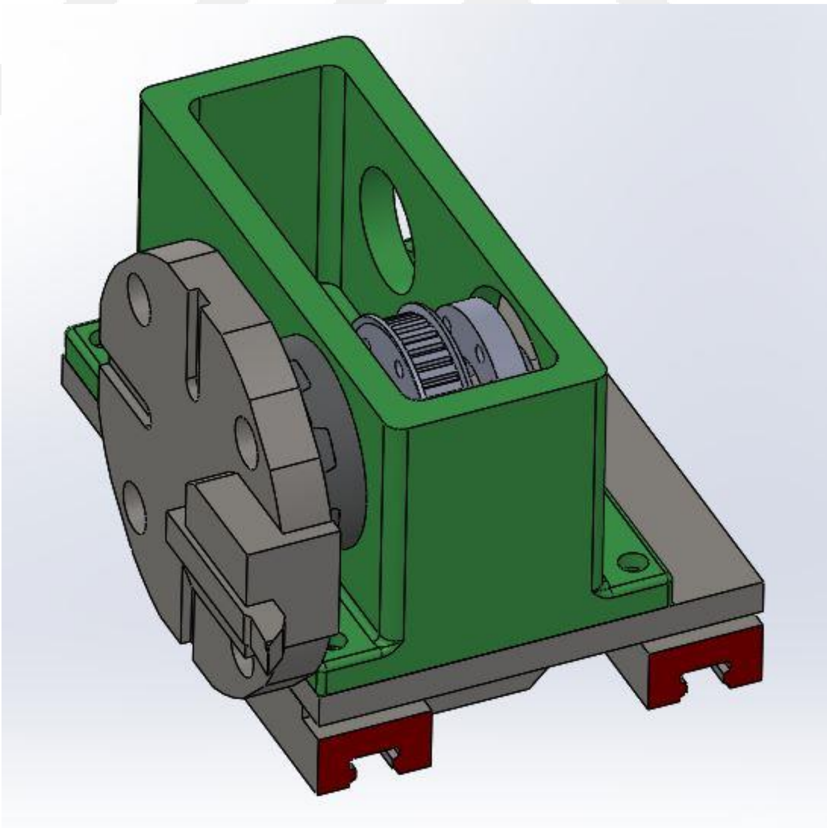

Figure 2.12 Analysis model of the x-axis

2.2.4 Analysis model of the turret

The turret has been examined separately to achieve realistic analysis results. In this way, the deviation on the end point of the cutter has been monitored specifically. The turret includes the body, movement mechanism with gears and shafts, tool changer and the cutting tools. In the sense of deviations at the cutting point, the most important part of the lathe is the tool holder. Because the analysis model of this part directly affects the displacement of the cutter under the cutting forces. The design and the analysis models of the turret are shown in Figures 2.13 and 2.14.

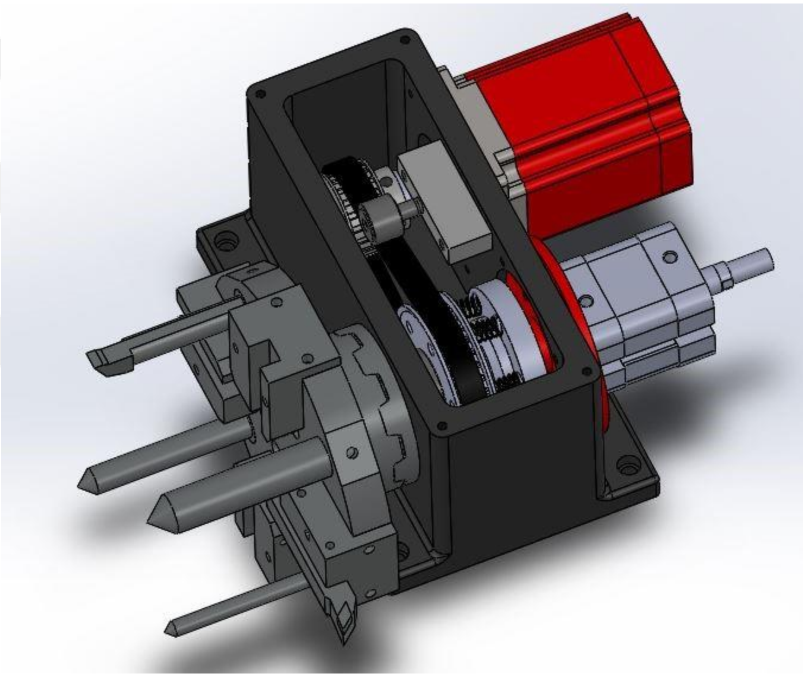

Figure 2.13 Design model of the turret

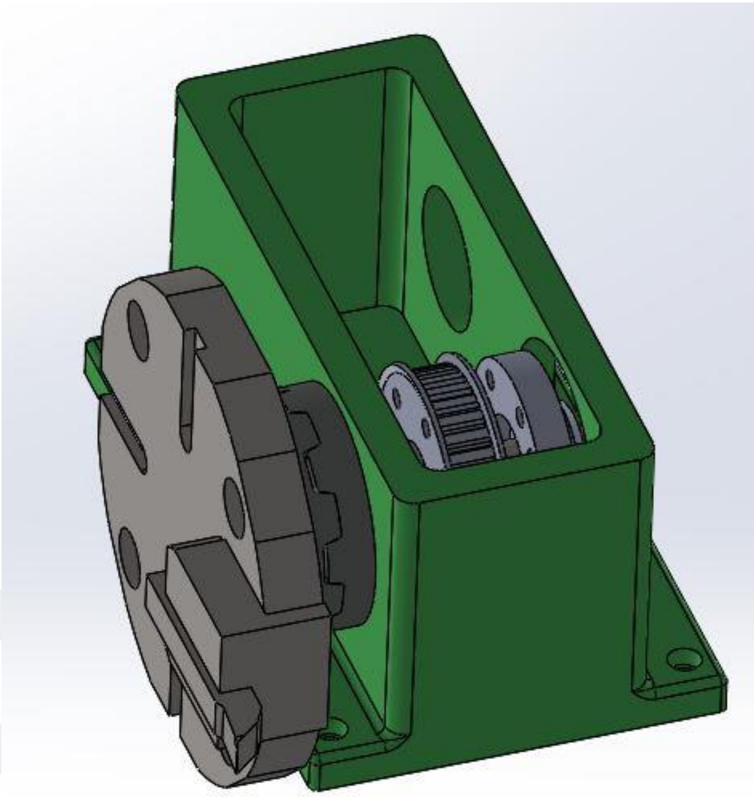

Figure 2.14 Analysis model of the turret

2.3 Cutting forces in the static analyzes

After creating the models correctly, the static analyzes have been carried out. These analyzes have been made under two different cutting forces. These cutting forces obtained from the experimental studies that Professor Kubilay Aslantaş made in University of Afyon Kocatepe.

In the real system, all of the cutting parameters have been taken as the same as the cutting parameters in Aslantaş's experiments. Experiments that Aslantaş made are shown in Table 2.1.

Table 2.1 Experiments of the Kubilay Aslantaş (Aslantaş, Çiçek, & Kara, 2015).

Experiment No	Tool	Cutting speed (m/min)	Feed (mm/rev)	Fc (N)	Ff (N)	Fr (N)
1	TiCN	75	0.05	414	420	8
2			0.1	651	633	18
3			0.2	1121	942	44
4			0.3	1585	1200	66
5		100	0.05	416	439	13
6			0.1	620	587	22
7			0.2	1070	874	43
8			0.3	1501	1037	76
9		150	0.05	337	325	7
10			0.1	587	537	21
11			0.2	1007	773	49
12			0.3	1410	902	65
13		200	0.05	354	363	7
14			0.1	563	505	19
15			0.2	933	672	49
16			0.3	1329	804	61
17		250	0.05	361	384	8
18			0.1	562	504	21
19			0.2	964	654	49
20			0.3	1266	760	62

Cutting force 1 is the force which related to cutting parameters in experiment no 16 (the line coloured with grey) and cutting force 2 is the force which related to cutting parameters in experiment no 14 (the line given by blue) in the Table 2.1. Cutting force 1 and cutting force 2 are shown in Table 2.2.

Table 2.2 Cutting forces in the analyses

Cutting Forces	Cutting Speed (m/min)	Feed (mm/rev)	Fc (N)	Ff (N)	Fr (N)
Cutting force 1	200	0.3	1329	804	61
Cutting force 2	200	0.1	563	505	19

2.4 Static analyzes of the members

Before the static analyzes of the main lathe model, all of the members have been analyzed separately. Main lathe body, z-axis and x-axis have been analyzed separately. The turret has been examined in the main analysis because of its close position to the cutting forces. Total displacements of the members under determined cutting forces have been monitored. The areas where the maximum and minimum stress values of the members have also been seen.

In a finite element analysis, mesh parameters, mesh size, mesh quality (aspect ratio for triangular mesh) are important. SolidWorks creates tetrahedral 3D solid elements for all solid components. 3D tetrahedral element type is shown in Figure 2.15.

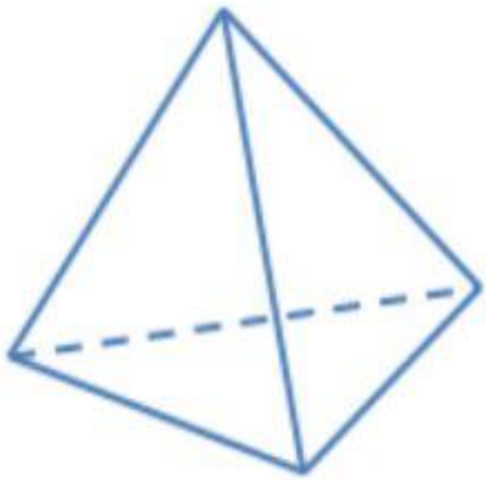

Figure 2.15 3D tetrahedral mesh element type

2.4.1 Static analyzes of the main lathe body

After the realistic analysis model of the main lathe body had been created, mesh parameters and boundary conditions have been arranged, also the own weight of the body has been added in the static analyses. The mesh sizes have been set as 5 mm. The cutting forces which appear in the turning operations have been added. Two different static analyzes have been performed with cutting force 1 and cutting force 2 which have been given before in Table 2.2. Meshed view of the body is shown in Figure 2.16.

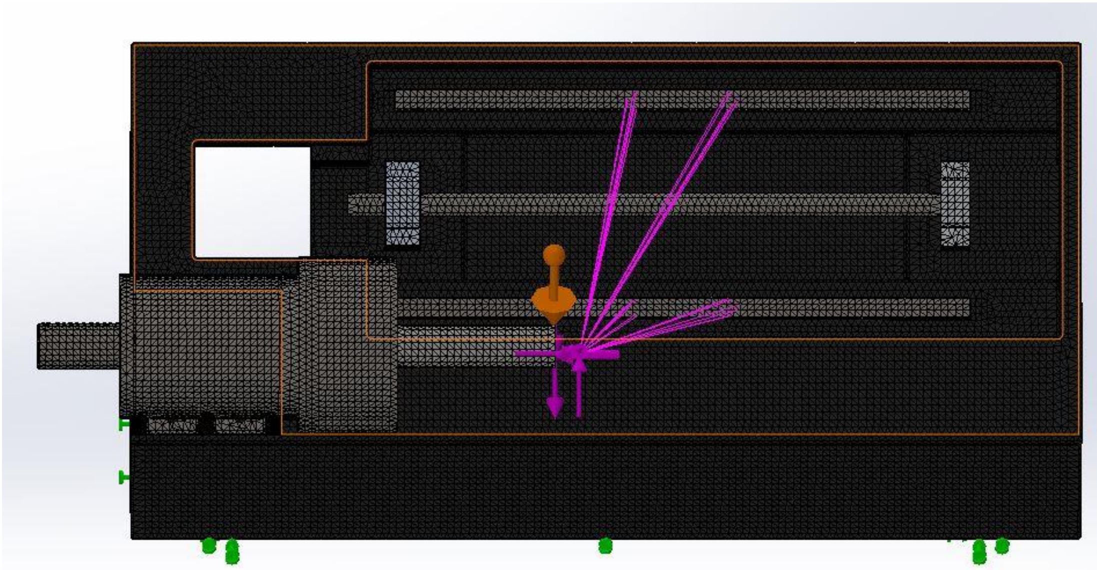

Figure 2.16 Meshed view of the body

Cutting forces in the system have been added in the analysis environment. Remote load has been used for the cutting forces. The point which the cutting forces placed on has been arranged where the cutter contacts with the workpiece. Cutting force 1 has been added and static analysis using cutting force 1 has been performed. Stress results of the main lathe body with respect to cutting force 1 is shown in Figure 2.17 and displacement results of the main lathe body with respect to cutting force 1 is shown in Figure 2.18.

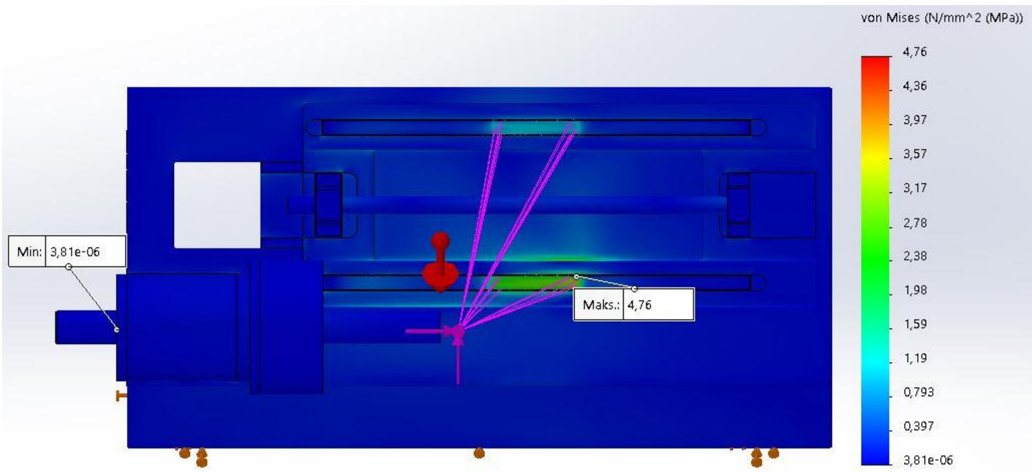

Figure 2.17 Stress results of the body with respect to cutting force 1

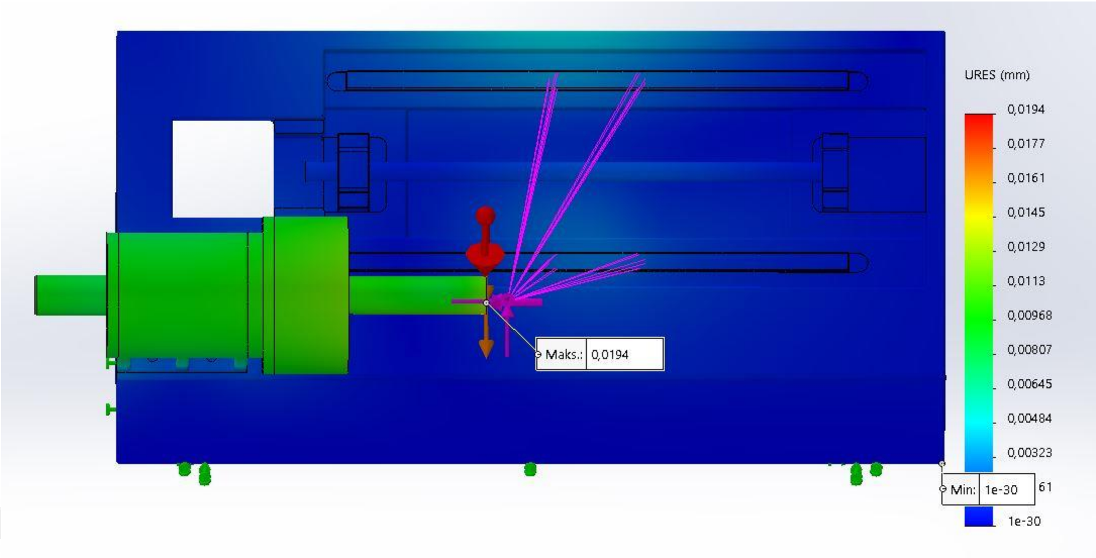

Figure 2.18 Displacement results of the body with respect to cutting force 1

After the static analysis with cutting force 1 had been performed, the cutting forces changed and the static analysis with cutting force 2 has been performed. Stress results of the main lathe body with respect to cutting force 2 is shown in Figure 2.19 and displacement results of the main lathe body with respect to cutting force 2 is shown in Figure 2.20.

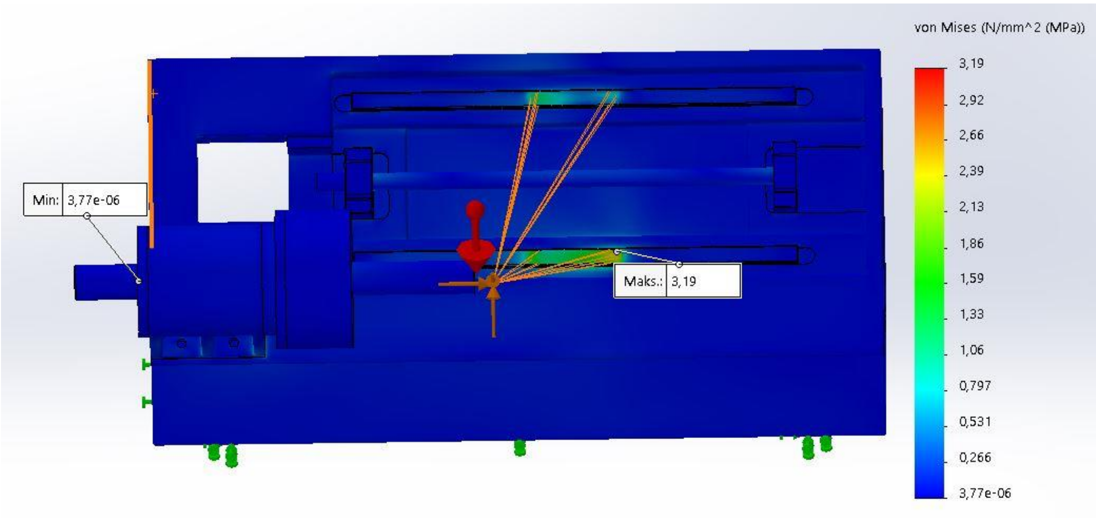

Figure 2.19 Stress results of the body with respect to cutting force 2

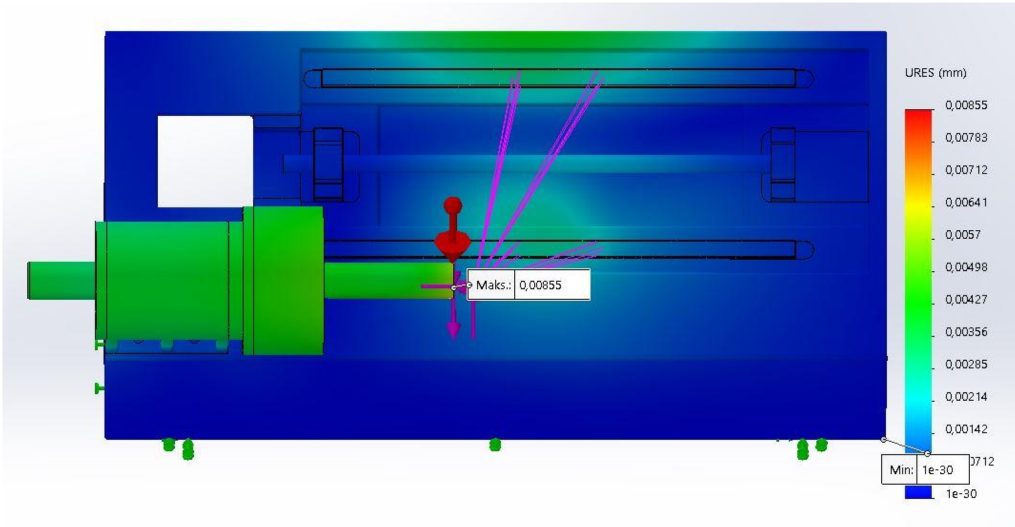

Figure 2.20 Displacement results of the body with respect to cutting force 2

2.4.2 Static analyzes of the z-axis

After the realistic analysis model of the z-axis had been created, mesh parameters and boundary conditions have been arranged, also the own weight of the z-axis has been added in the static analyzes. The mesh sizes have been set as 2 mm. The cutting forces which appear in the turning operations have been added. Two different static analyzes have been performed with cutting force 1 and cutting force 2 which have been given before in Table 2.2. Meshed view of the z-axis is shown in Figure 2.21.

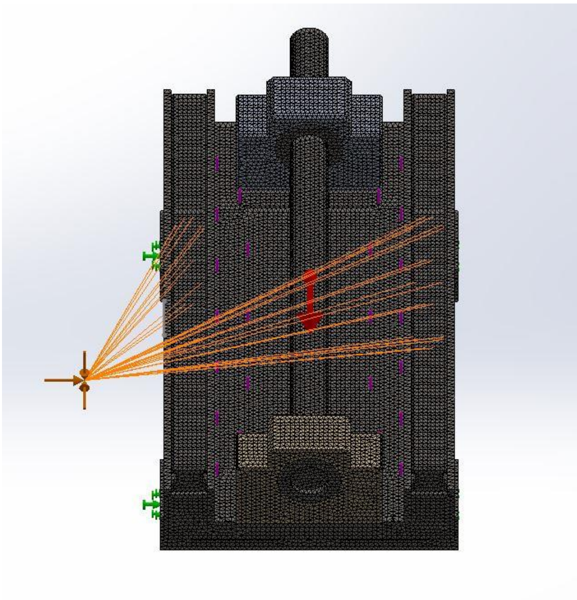

Figure 2.21 Meshed view of the z-axis

Cutting forces in the system have been added in the analysis environment. Remote load has been used for the cutting forces. The point which the cutting forces placed on has been arranged where the cutter contacts with the workpiece. Cutting force 1 has been added and static analysis with respect to cutting force 1 has been performed. Stress results of the z-axis with respect to cutting force 1 is shown in Figure 2.22 and displacement results of the z-axis with respect to cutting force 1 is shown in figure 2.23.

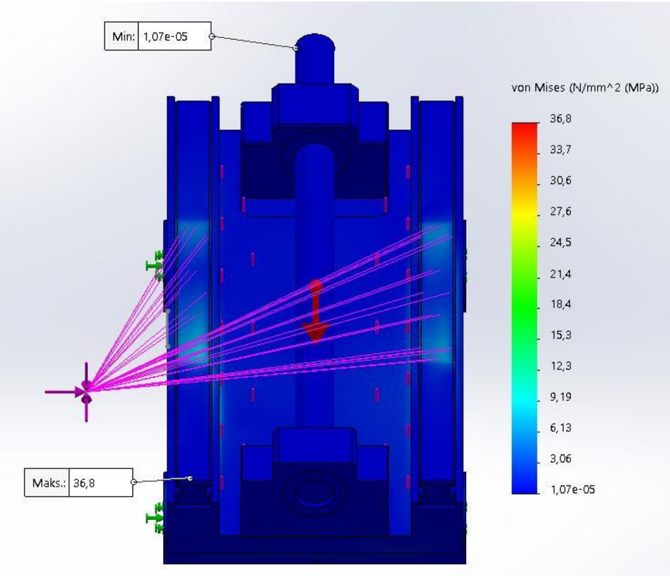

Figure 2.22 Stress results of the z-axis with respect to cutting force 1

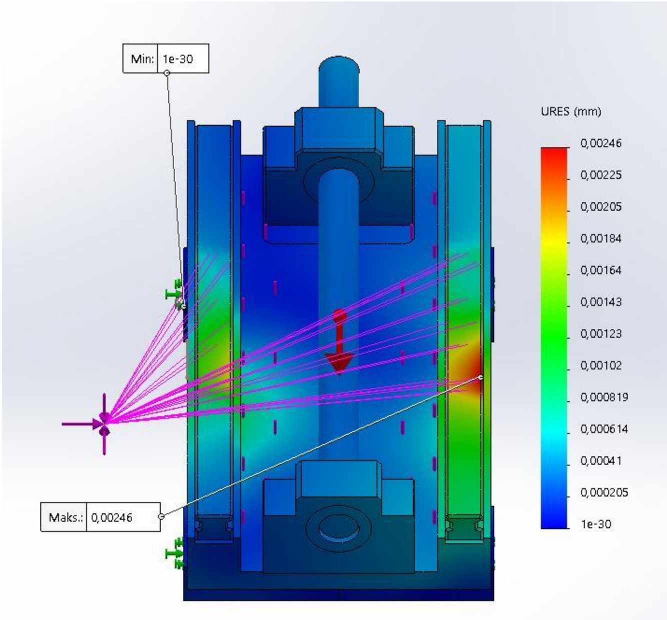

Figure 2.23 Displacement results of the z-axis with respect to cutting force 1

After the static analysis with cutting force 1 had been performed, the cutting forces changed and the static analysis with cutting force 2 has been performed. Stress results of the z-axis with respect to cutting force 2 is shown in Figure 2.24 and displacement results of the z-axis with respect to cutting force 2 is shown in Figure 2.25.

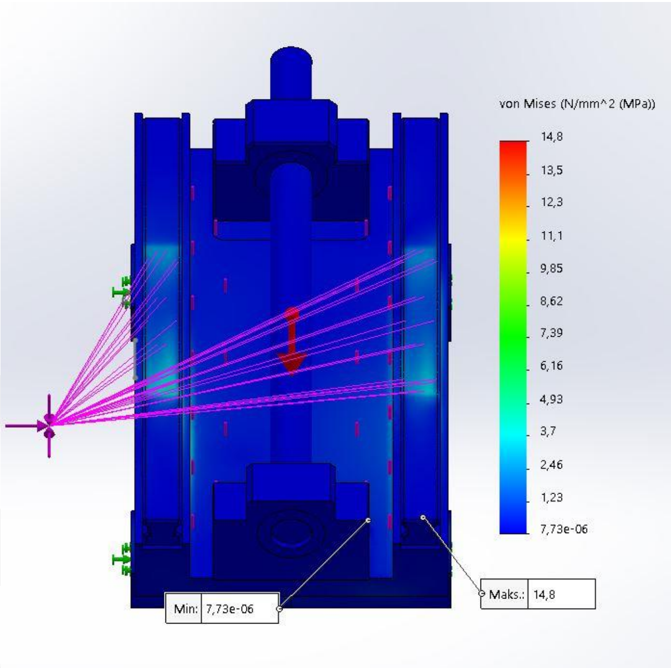

Figure 2.24 Stress results of the z-axis under cutting force 2

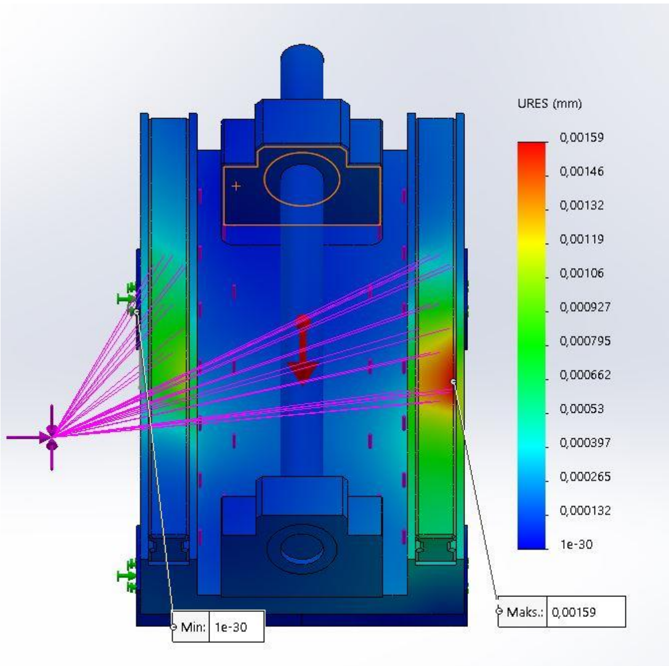

Figure 2.25 Displacement results of the z-axis under cutting force 2

2.4.3 Static analyzes of the x-axis

After the realistic analysis model of the x-axis had been created, mesh parameters and boundary conditions have been arranged, also the own weight of the x-axis has been added in the static analyzes. In the wider and non-critical surfaces like the surfaces of the turret body, the mesh sizes have been set as 3 mm. The critical and narrow surfaces like the tip of the cutter the mesh sizes have been set as 0.2 mm. The cutting forces which appear in the turning operations have been added. Two different static analyzes have been performed with cutting force 1 and cutting force 2 which have been given before in Table 2.2. Meshed view of the x-axis is given in Figure 2.26.

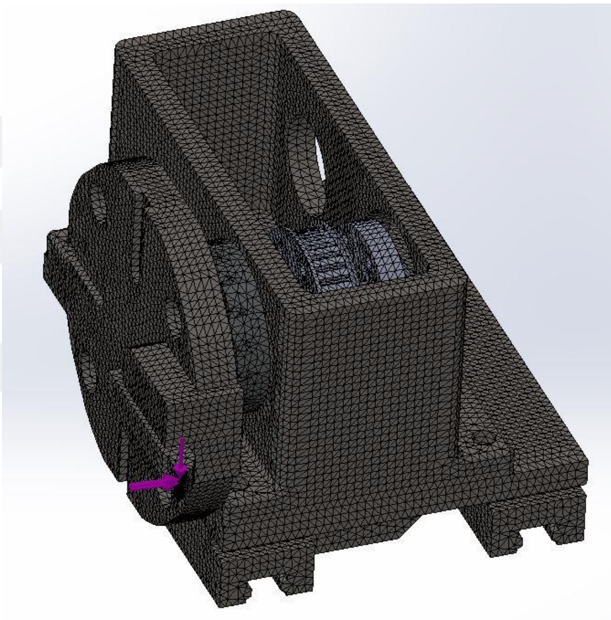

Figure 2.26 Meshed view of the x-axis

Cutting forces in the system have been added in the analysis environment. Cutting force 1 has been added and static analysis using cutting force 1 has been performed. Stress results of the x-axis with respect to cutting force 1 is shown in Figure 2.27 and displacement results of x-axis using cutting force 1 is shown in Figure 2.28.

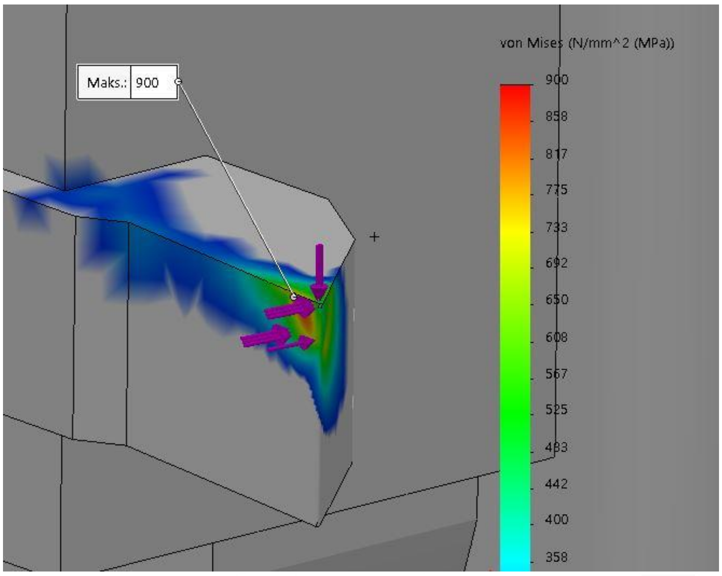

Figure 2.27 Stress results of the x-axis under cutting force 1

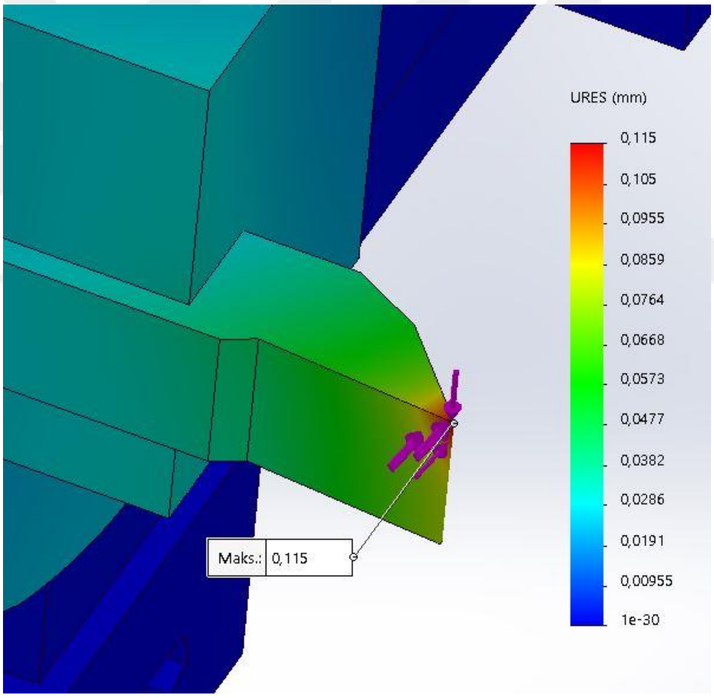

Figure 2.28 Displacement results of the x-axis under cutting force 1

After the static analysis with cutting force 1 had been performed, the cutting forces changed and the static analysis with cutting force 2 has been performed. Stress results of the x-axis with respect to cutting force 2 is shown in Figure 2.29 and displacement results of the x-axis with respect to cutting force 2 is shown in Figure 2.30.

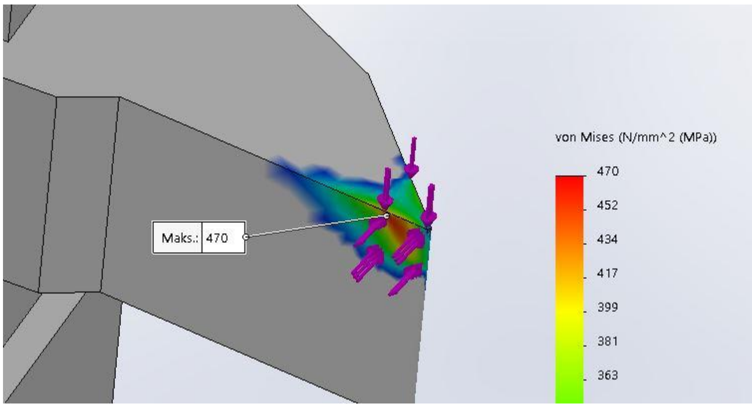

Figure 2.29 Stress results of the x-axis under cutting force 2

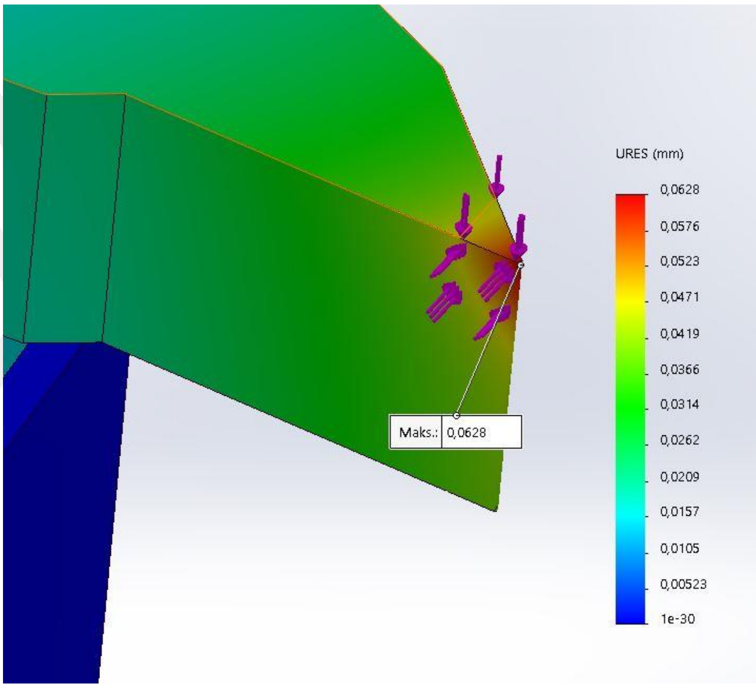

Figure 2.30 Displacement results of the x-axis under cutting force 2

2.4.4 Static analyzes of the turret

After the realistic analysis model of the turret had been created, mesh parameters and boundary conditions have been arranged, also the own weight of the turret has been added in the static analyzes. In the wider and non-critical surfaces like the surfaces of turret body, the mesh sizes have been set as 3 mm. The critical and narrow surfaces like the tip of the cutter, the mesh sizes have been set as 0.2 mm. The cutting forces which appear in the turning operations have been added. Two different static analyzes have been performed with cutting force 1 and cutting force 2 which have been given before in Table 2.2. Meshed view of the turret is given in Figure 2.31.

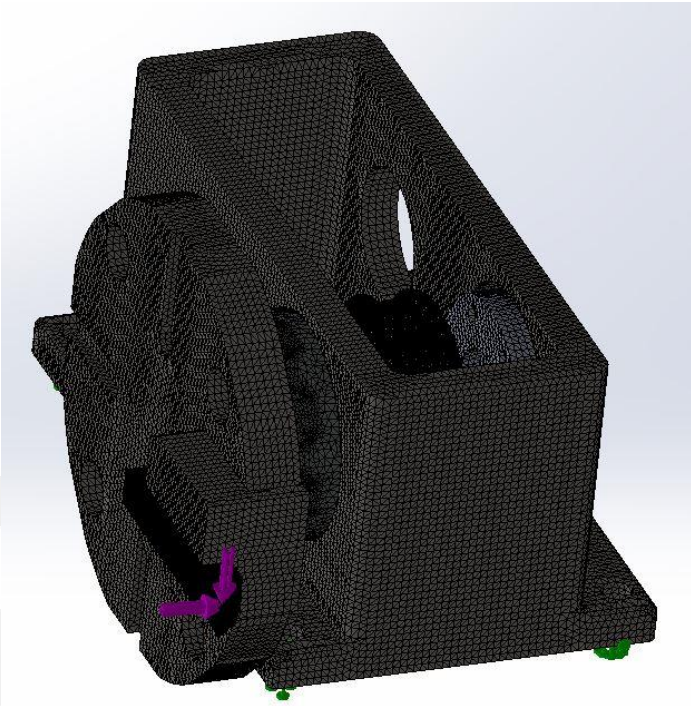

Figure 2.31 Meshed view of the turret

Cutting forces in the system have been added in the analysis environment. Cutting force 1 has been added and static analysis with respect to cutting force 1 has been performed. Stress results of the turret with respect to cutting force 1 is shown in Figure 2.32 and displacement results of the turret with respect to cutting force 1 is shown in Figure 2.33.

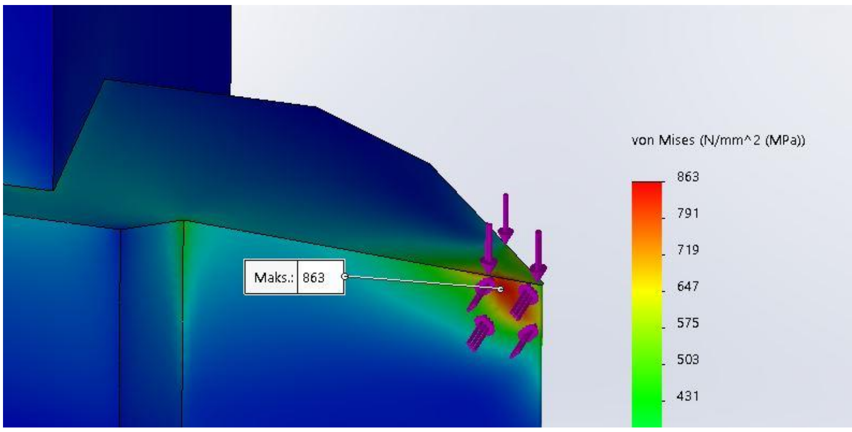

Figure 2.32 Stress results of the turret under cutting force 1

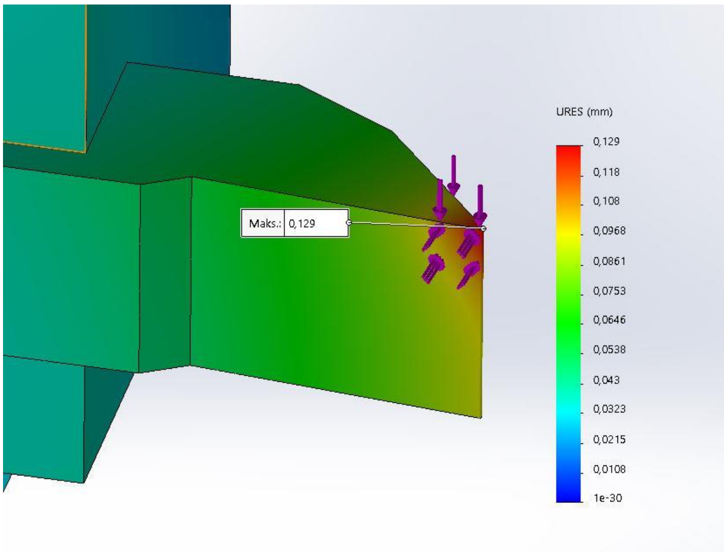

Figure 2.33 Displacement results of the turret under cutting force 1

After the static analysis with cutting force 1 had been performed, the cutting forces changed and the static analysis with cutting force 2 has been performed. Stress results of the turret with respect to cutting force 2 is shown in Figure 2.34 and displacement results of the turret with respect to cutting force 2 is shown in Figure 2.35.

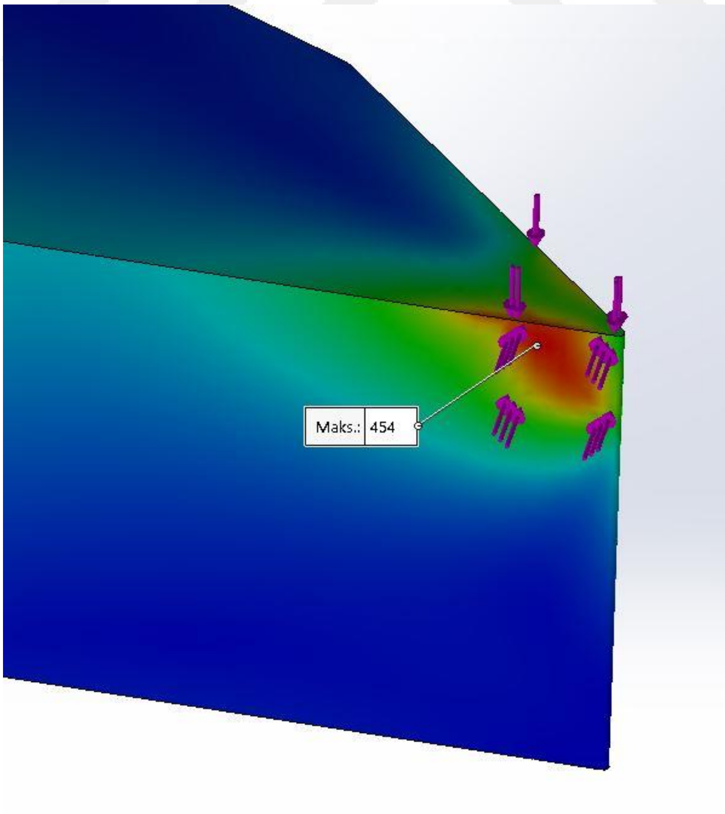

Figure 2.34 Stress results of the turret under cutting force 2

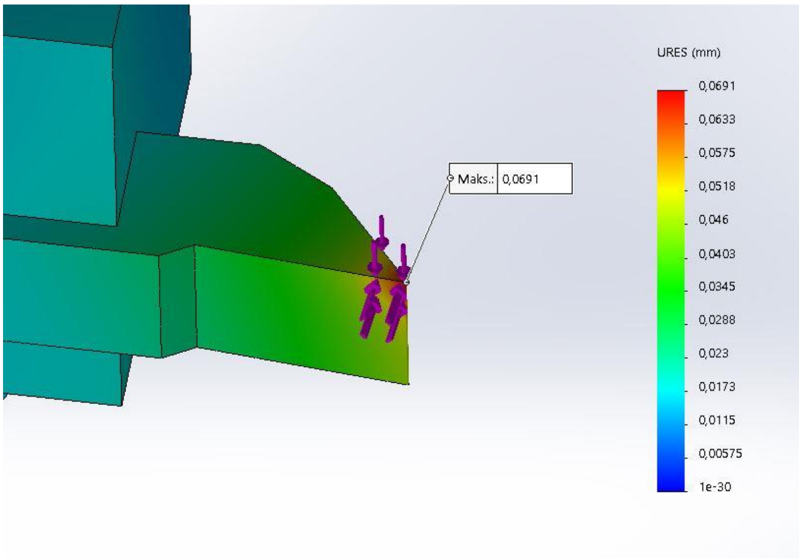

Figure 2.35 Displacement results of the turret under cutting force 2

2.5 Static analyzes of the multi-body lathe model

After the static analyzes of the members, static analyzes of the multi-body lathe model have been performed.

2.5.1 Analysis model of the multi-body lathe model

Before the getting to the analysis environment, some simplifications have been made on the model. These simplifications have been made by removing small details and small holes that not likely to affect the analysis results. With these simplifications, the analysis time became shorter and important parts that under cutting forces observed better. The transmission elements at the junction points of these members are drawn by simplifying and the contacts are considered in the analysis. In this way, the analysis model of the lathe has been made very similarly to the real system. Design model of the lathe is shown in Figure 2.36 and simplified model of the lathe is shown in Figure 2.37.

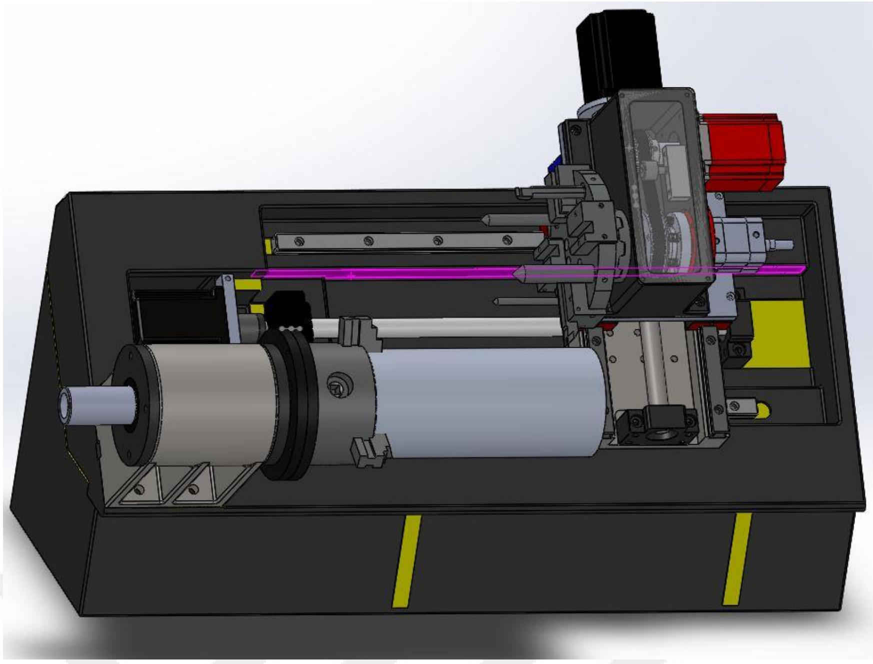

Figure 2.36 Designed model of the lathe

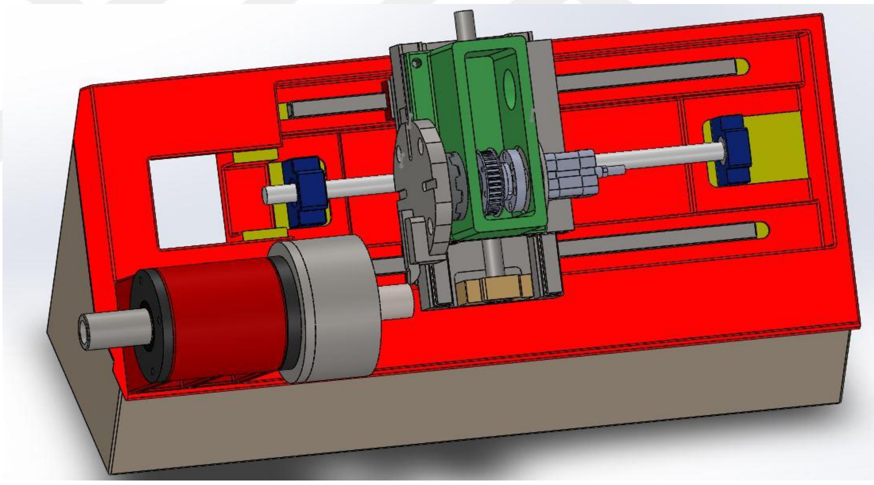

Figure 2.37 Simplified analysis model of the lathe

2.5.2 Mesh parameters and cutting forces in the multi-body lathe model

After the realistic analysis model had been created, mesh parameters have been arranged. Different mesh sizes have been used on the model. Mesh sizes have been kept high where the effects of the cutting forces insignificant and on the large surface but mesh sizes were kept low where the effects of the forces were significant and on the narrow areas. In the wider and non-critical surfaces of the members, the mesh sizes have been set as 10 mm to 40 mm. The critical and narrow surfaces as cutter tip, the tool and tool changer body, the mesh sizes have been set as 0.2 mm to 5 mm. The choosing of the correct mesh parameters affect the results of the analyzes directly. The meshed view of the lathe is shown in Figure 2.38.

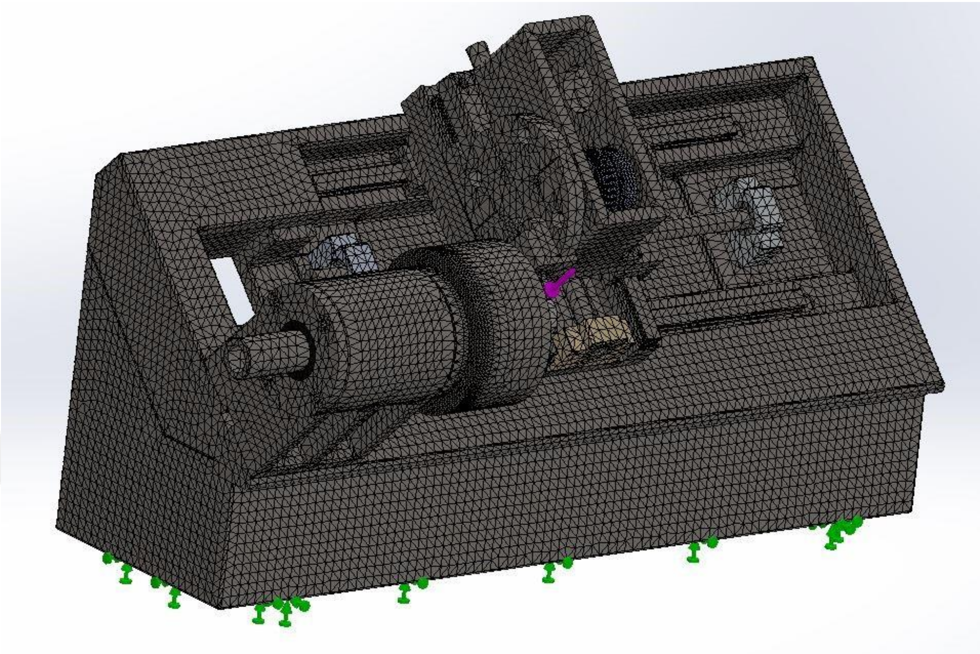

Figure 2.38 Meshed 3D view of the lathe

The tool and the cutter insert of the turret has been examined in a detailed way. It's considered that these regions are more critical in the analysis. The reason of the criticality of these regions is the cutting forces of the turning process affect directly the tool and the cutter. For the tool, 5 mm mesh size has been arranged. The meshed view of the tool is shown in Figure 2.39.

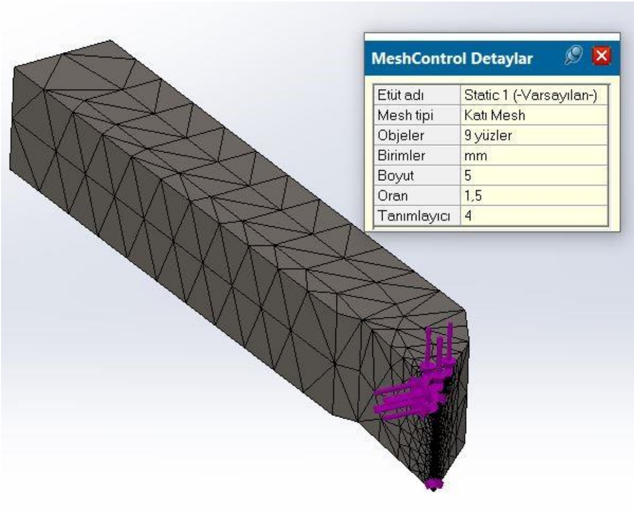

Figure 2.39 Mesh parameters of the tool

The tip of the tool where the cutter insert states, has been examined more detailed. The size of the mesh of the cutter insert region has been arranged as 0.2 mm. With these mesh size, the response of the insert under the cutting forces has been examined more realistically. The meshed view of the tool insert is shown in Figure 2.40.

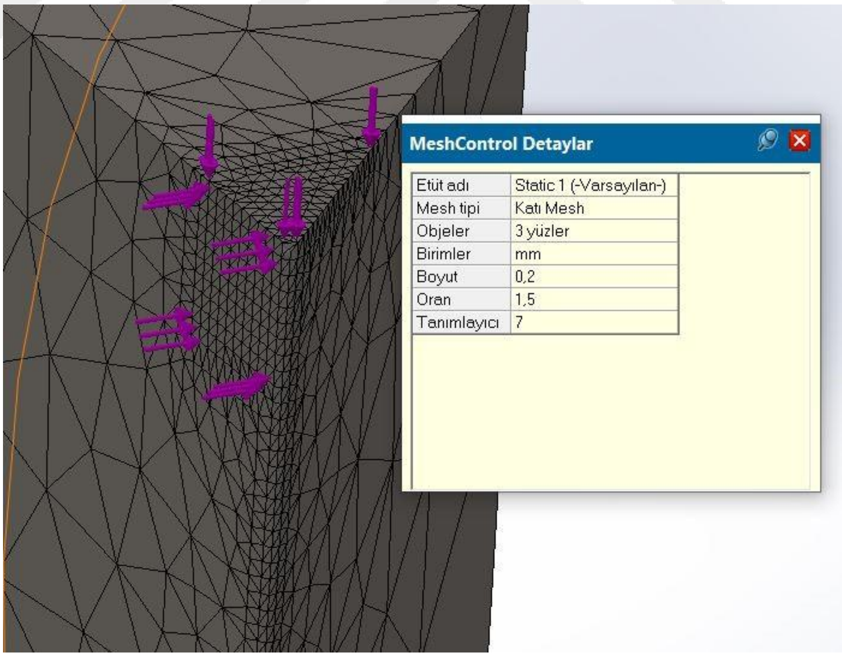

Figure 2.40 Mesh parameters of the tool insert

Boundary conditions of the members have been arranged and the own weight of the model has been added in the analysis. The cutting forces which affect the lathe have been added to tip of the cutter and workpiece. The reaction forces on the workpiece have been added with the same magnitude of the cutting forces but to the opposite directions. In this way, the flexion of the workpiece has been considered in the analysis. So, the total amount of displacement has been monitored as a realistic model. Cutting parameters, workpiece material and chip depth have been taken the same with the real experiment system. The directions of the cutting forces affect to the lathe are shown in Figure 2.41.

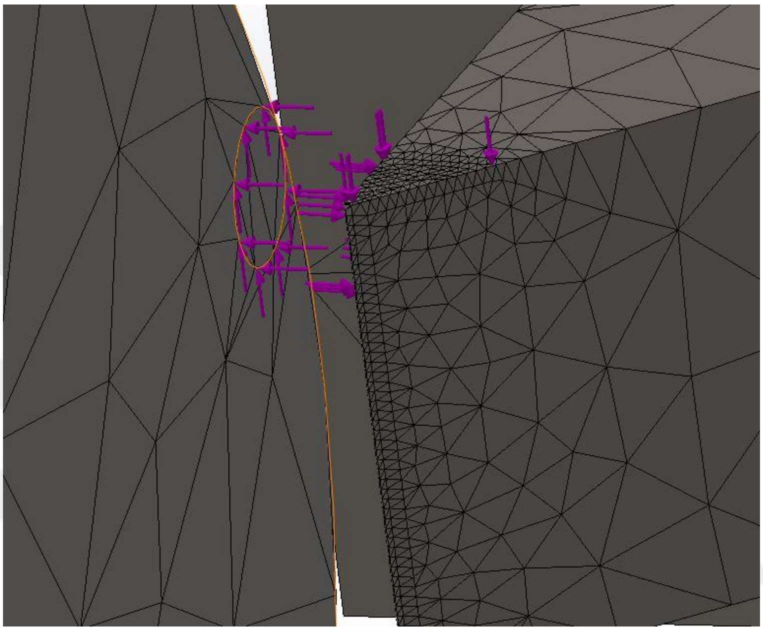

Figure 2.41 Cutting forces on the model

2.6 Results of the static analyzes of the multi-body lathe model

Two different static analyzes have been performed with cutting force 1 and cutting force 2. The cutting parameters that reveal cutting force 1 were specified as 0.3 mm/rev feed with a cutting speed of 200 m/min and 1 mm chip depth. According to the analysis results the area where the highest stress occured was the cutter tip. Under the determined forces, it was observed that there was a high stress value in the cutter tip region as 900 MPa. The stress increment on the sharp edge is called as stress singularity. In the reality, these stress values do not occur. In these sharp edges, the displacement values are more realistic. Stress results should be considered carefully in the corner edges. For this stress value, the displacement of the cutting tool has monitored as 0.115 mm. The stress results of the lathe under cutting force 1 are shown in Figure 2.42. Displacement results of the lathe are also shown in Figure 2.43.

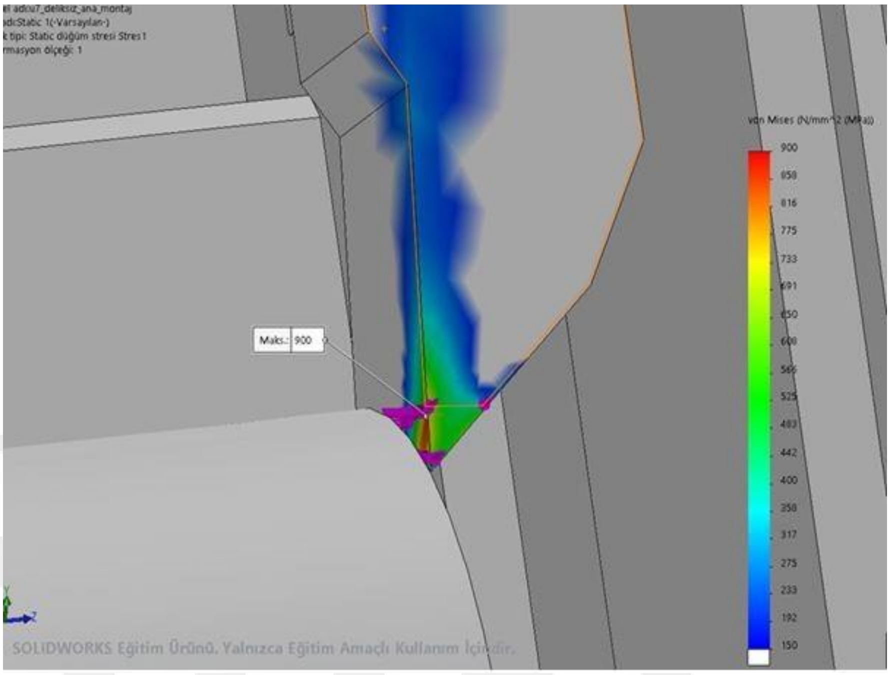

Figure 2.42 Stress results of cutting force 1

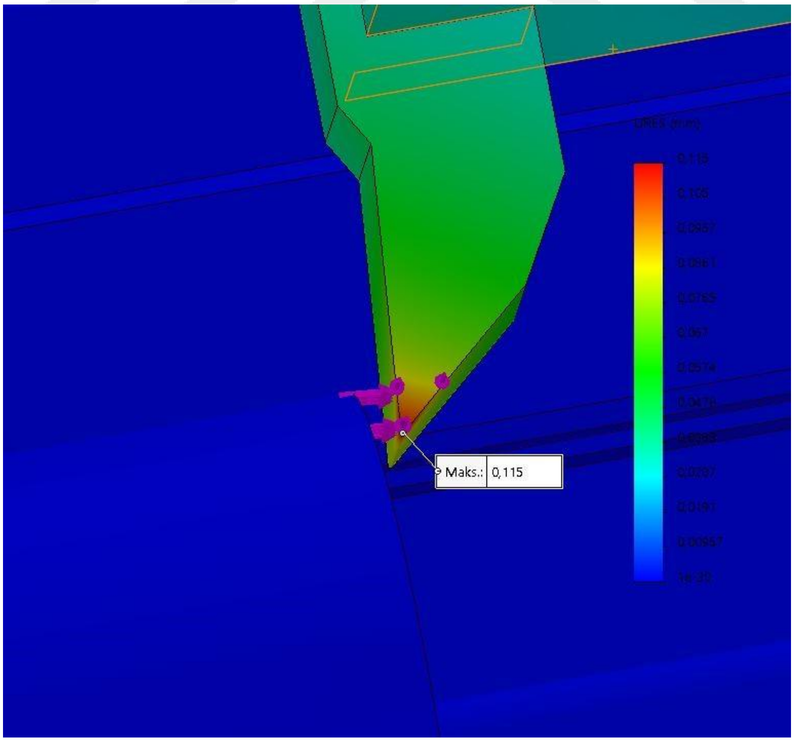

Figure 2.43 Displacement results of cutting force 1

Displacement results of the workpiece has also been considered. The important thing is here the amount of total displacement in the analysis. The displacement of the workpiece has been monitored as 0.029 mm. So, the total displacement of the system is 0.145 mm. Displacement results of workpiece under the cutting force 1 is shown in Figure 2.44.

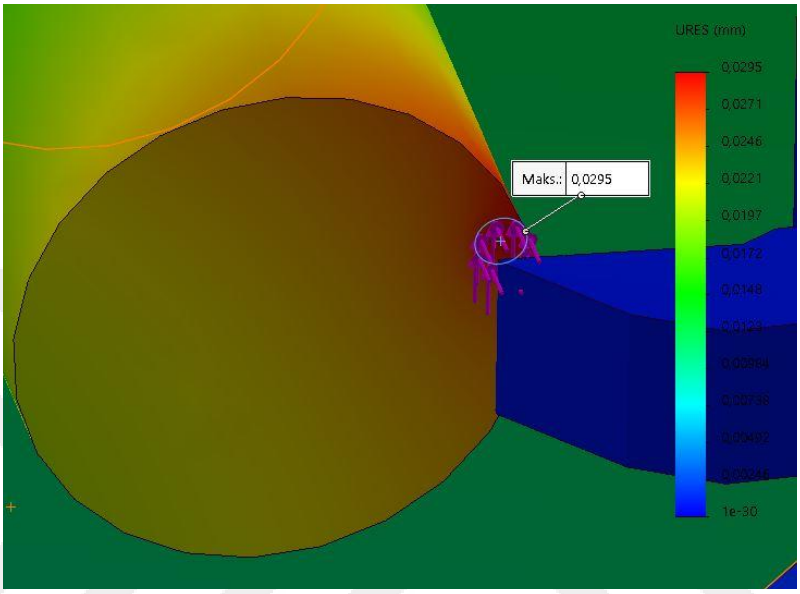

Figure 2.44 Displacement results of workpiece under cutting force 1

After this analysis, cutting parameters were changed and a new analysis has been made with cutting force 2. The cutting parameters that reveal cutting force 2 were specified as 0.1 mm/rev feed with a cutting speed of 200 m/min and 1 mm chip depth. Stress was observed on the cutter tool as 469 MPa maximum. The cutter region in this analysis was safer than the first analysis. For these values, the displacement value of the cutting tool has monitored as 0.0639 mm. The stress results of the lathe under cutting force 2 are shown in Figure 2.45 and displacement results of the lathe are also shown in Figure 2.46.

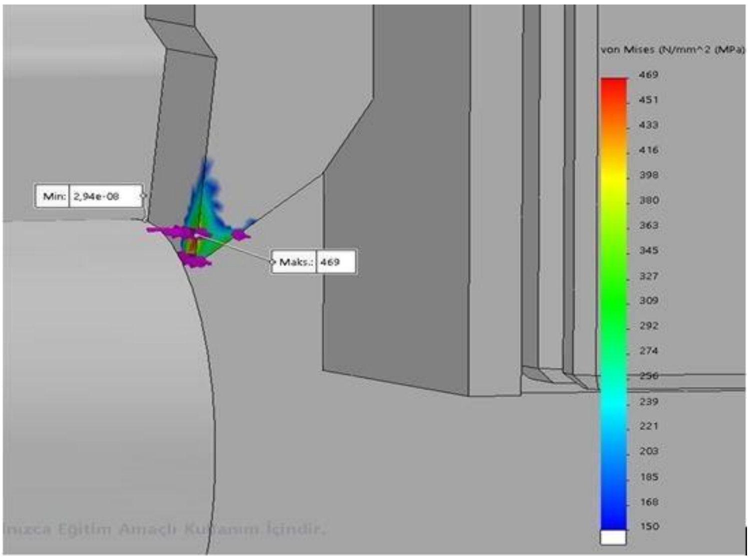

Figure 2.45 Stress results of cutting force 2

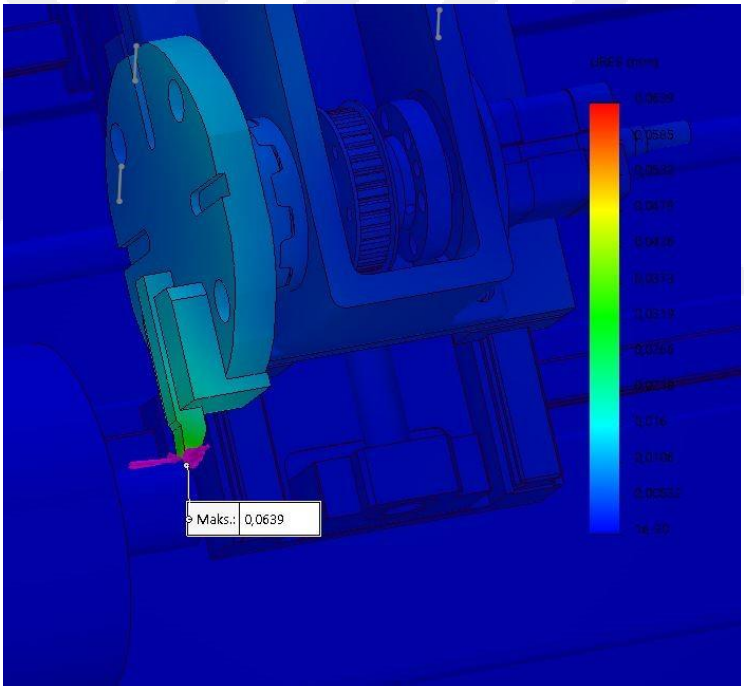

Figure 2.46 Displacement results of cutting force 2

Displacement results of the workpiece has also been considered. The important thing is here the amount of total displacement in the analysis. The displacement of the workpiece has been monitored as 0.0138 mm. So, the total displacement in the system is 0.0777 mm. Displacement results of workpiece under the cutting force 1 is shown in Figure 2.47.

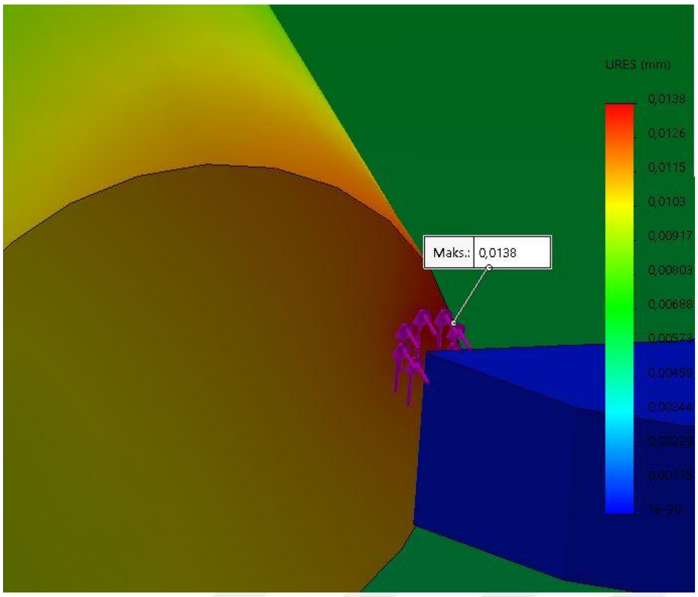

Figure 2.47 Displacement results of workpiece under cutting force 2

For a better performance of the lathe, a revision study has been done. The design of the tool has been reconsidered for better analysis results. For this purpose, the tool has been reinforced. This support piece can be produced with milling easily and it can be assembled with the bolts that have 3 mm diameters. In the analysis, these holes have been ignored for a better performance. The model view of the support piece is shown in Figure 2.48.

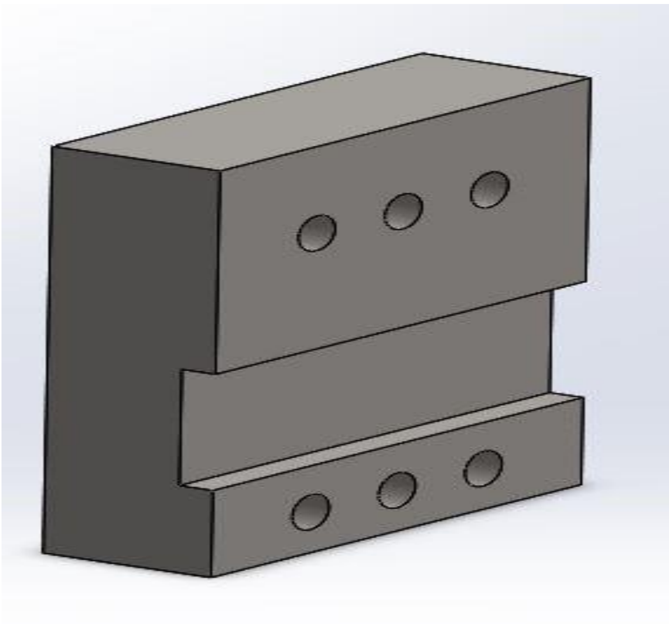

Figure 2.48 Model of the support piece for tool holder

With the support piece on the tool, the displacement value on the cutter under cutting force 1, has been reduced from 0.115 mm to 0.0608 mm. So, under this cutting force 1, total displacement has been reduced from 0.145 mm to 0.0908 mm. The displacement results of the exist lathe under cutting force 1 are shown in Figure 2.49 and the displacement results of the lathe with addition of the support piece are shown in Figure 2.50.

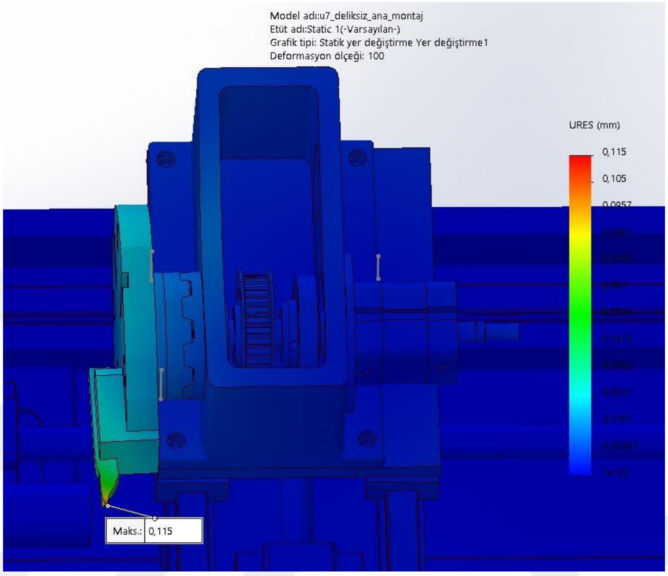

Figure 2.49 The current displacement results

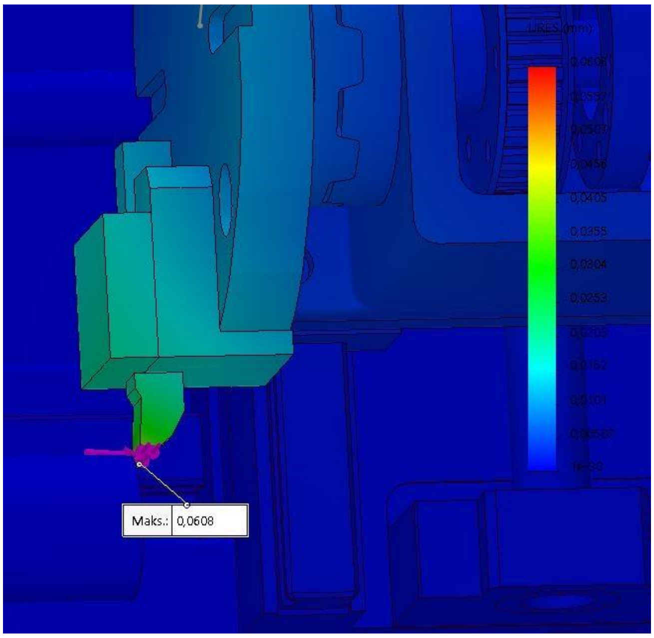

Figure 2.50 The displacement results with support piece

CHAPTER THREE

EXPERIMENTS

3.1 Pre-experimental processes

After the analysis steps, preparations for the turning experiments of the lathe have been started. Workpieces to be machined in the turning experiments were chosen as 316 L stainless steel. Two 316 L stainless steel bars with 200 mm length and 30 mm diameter were provided as the workpieces. These steel bars were cut into 65 mm length pieces to increase the number of experiments. The workpieces are shown in Figure 3.1

Figure 3.1 The workpieces (Personal archive, 2020)

Type 316 steel contains 3% molybdenum. It is an austenitic chromium-nickel stainless steel. It has resistance to corrosion. It has strength at high temperatures. Type 316 grade stainless steel is effective in acidic environments.

Common uses for type 316 stainless steel are heat exchangers, jet motor parts, pharmaceutical and photographic equipment and pumps. It also is used in marine environments (Bell, 2020).

As the insert, Korloy brand DCMT070204-HMP insert has been used. The insert on the tool holder is shown in Figure 3.2. Machining conditions of the insert is shown in Figure 3.3.

Figure 3.2 The lathe insert (Personal archive, 2020)

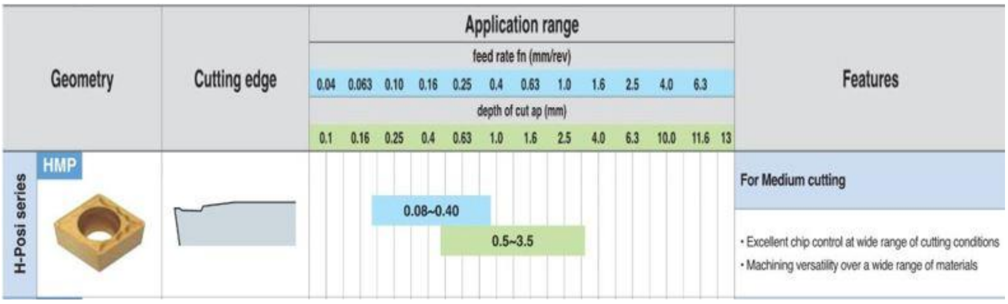

Figure 3.3 Cutting conditions of the insert (Korloy, 2020)

3.2 The turning experiments

In the experiments, 2 pieces 316-L stainless steel shafts with 65 mm length and 30 mm diameter were used. The pieces were divided into 3 machining areas with 15 mm length and 6 experiments were carried out. In the machining processes, 3 passes were made with a 1 mm depth in the diameter. The important thing was that the experiment areas which had the same distance to the chuck must have been compared with each other. So, the flexibility factor for the compared areas were kept same and there were only the effects of different cutting parameter levels. With these experiments, optimum cutting parameter levels of the lathe were determined and the effects of cutting parameters on surface roughness were observed. Effects of the cutting parameters to be monitored in the experiments and their values are given in Table 3.1. Cutting parameter levels in the Table 3.1 have been chosen from the Table 2.1. With these cutting parameters, turning experiments have been made.

Table 3.1 The cutting parameters

Area No	Cutting Speed	Feed
A1.1	200 m/min (2122 rev/min, F:35.3 Hz)	0.1 mm/rev (212 m/min)
A1.2	150 m/min (1591 rev/min, F:27 Hz)	0.1 mm/rev (212 m/min)
A1.3	200 m/min (2122 rev/min, F:35.3 Hz)	0.2 mm/rev (424 m/min)
A2.1	200 m/min (2122 rev/min, F:35.3 Hz)	0.3 mm/rev (636 m/min)
A2.2	250 m/min (2653 rev/min, F:44 Hz)	0.1 mm/rev (212 m/min)
A2.3	200 m/min (2122 rev/min, F:35.3 Hz)	0.05 mm/rev (106 m/min)

After machining processes, surface roughness of the workpieces has been also monitored.

In the experiments, the same parameters were compared with each other separately. For example, A1.1 and A2.1 areas have the same distance to the chuck and the same cutting speed level. So, the effects of different feed levels were compared. A1 workpiece after machining is shown in Figure 3.4.

Figure 3.4 A1 workpiece (Personal archive, 2020)

After machining processes, surface roughness of the areas of A1 workpiece were monitored. The minimum roughness values on this piece were monitored on the area A1.1. Ra value of this area was monitored as 2.033 µm and Rz value of this area was monitored as 12.93 µm. For the area A1.1, the cutting parameter levels are 200 m/min as cutting speed and 0.1 mm/rev as the feed. Surface roughness measurement results of the area A1.1 is shown in Figure 3.5.

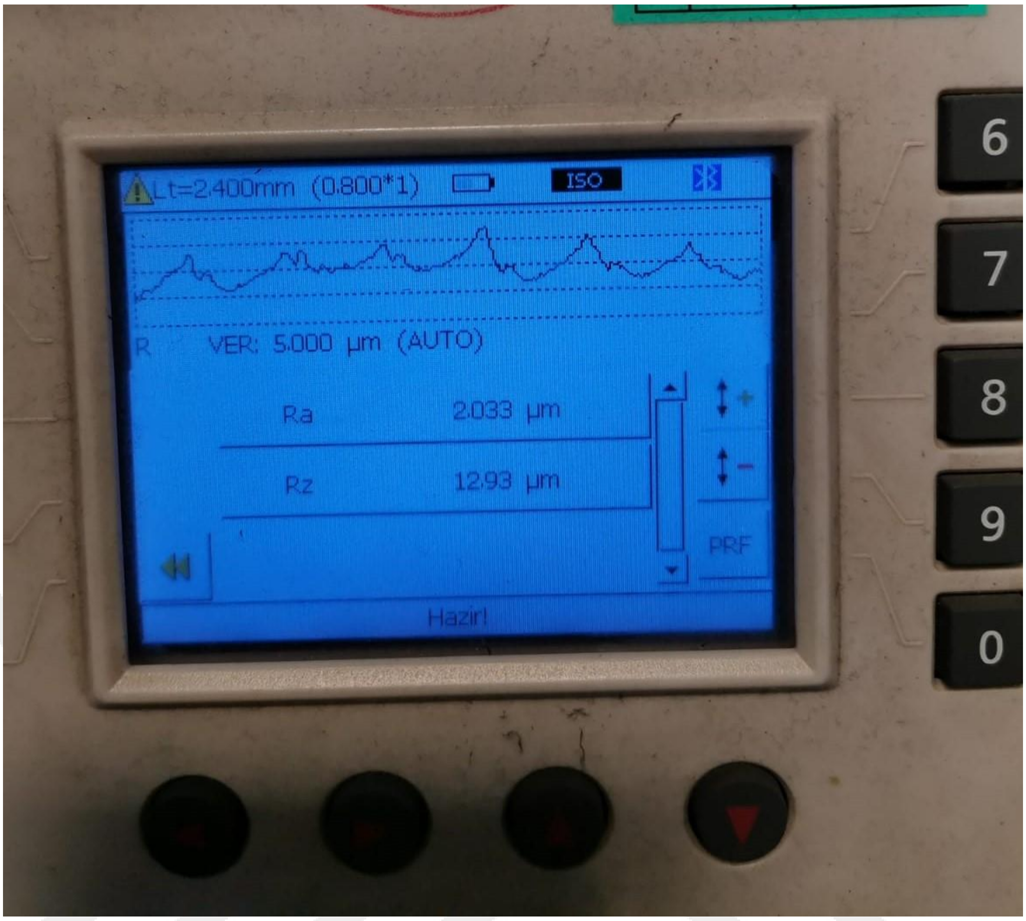

Figure 3.5 Surface roughness values of A1.1 (Personal archive, 2020)

Ra value of area A1.2 was monitored as 2.727 µm and Rz value of this area was monitored as 13.34 µm. For the area A1.2, the cutting parameter levels are 150 m/min as cutting speed and 0.1 mm/rev as the feed. Surface roughness measurement results of the area A1.2 is shown in Figure 3.6.

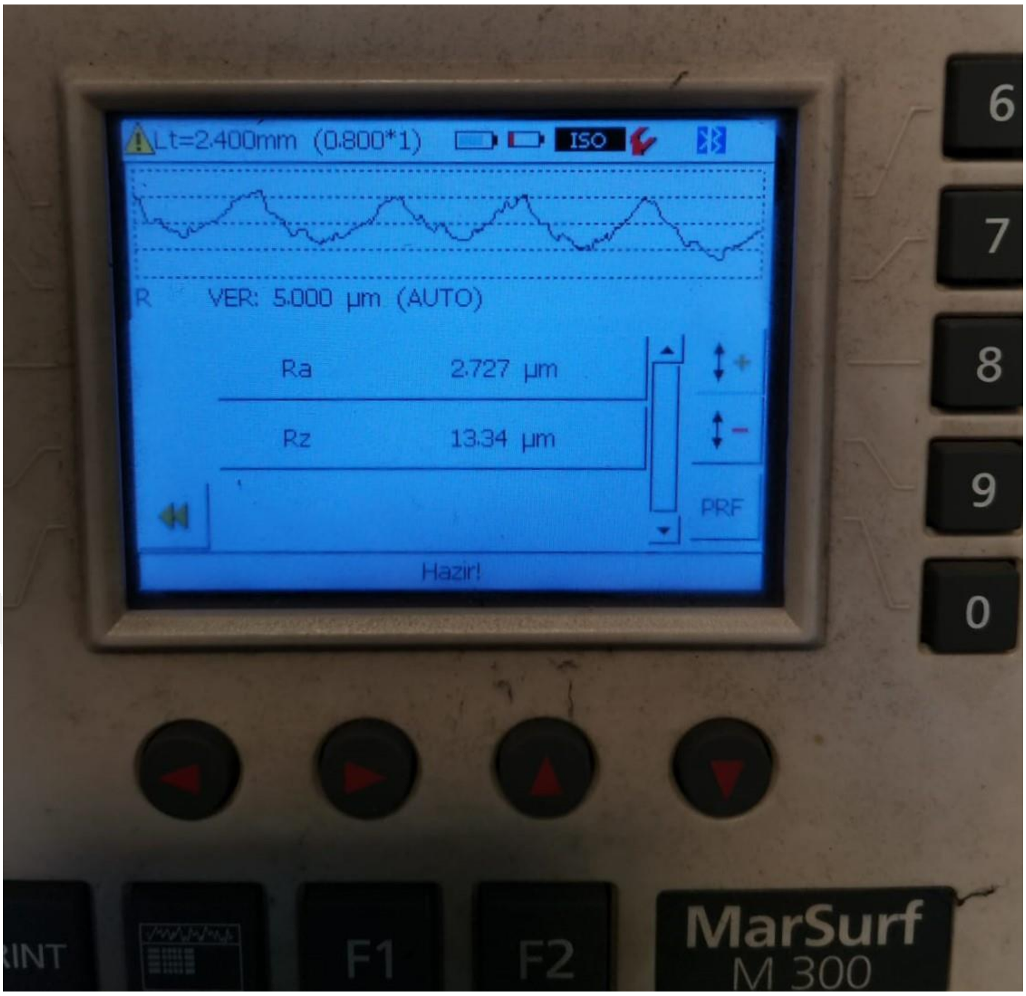

Figure 3.6 Surface roughness values of A1.2 (Personal archive, 2020)

Ra value of area A1.3 was monitored as 4.949 µm and Rz value of this area was monitored as 22.50 µm. For the area A1.3, the cutting parameter levels are 200 m/min as cutting speed and 0.2 mm/rev as the feed. Surface roughness measurement results of the area A1.3 is shown in Figure 3.7.

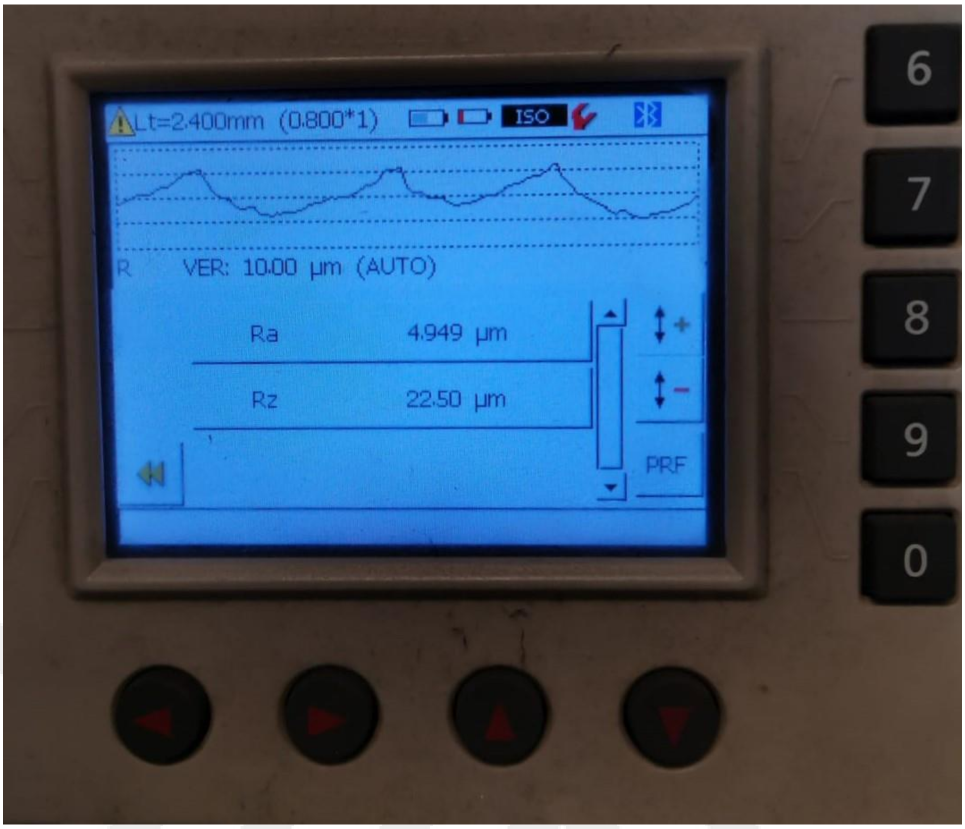

Figure 3.7 Surface roughness values of A1.3 (Personal archive, 2020)

After machining processes, surface roughness of the areas of A2 workpiece were monitored. A2 workpiece after machining is shown in Figure 3.8.

Figure 3.8 A2 workpiece (Personal archive, 2020)

The maximum roughness values on this piece were monitored on the area A2.1. Ra value of this area was monitored as 7.787 µm and Rz value of this area was monitored as 33.17 µm. For the area A2.1, the cutting parameter levels are 200 m/min as cutting speed and 0.3 mm/rev as the feed. Surface roughness measurement results of the area A2.1 is shown in Figure 3.9.

Figure 3.9 Surface roughness values of A2.1 (Personal archive, 2020)

Ra value of area A2.2 was monitored as 2.844 µm and Rz value of this area was monitored as 13.24 µm. For the area A2.2, the cutting parameter levels are 250 m/min as cutting speed and 0.1 mm/rev as the feed. Surface roughness measurement results of the area A2.2 is shown in Figure 3.10.

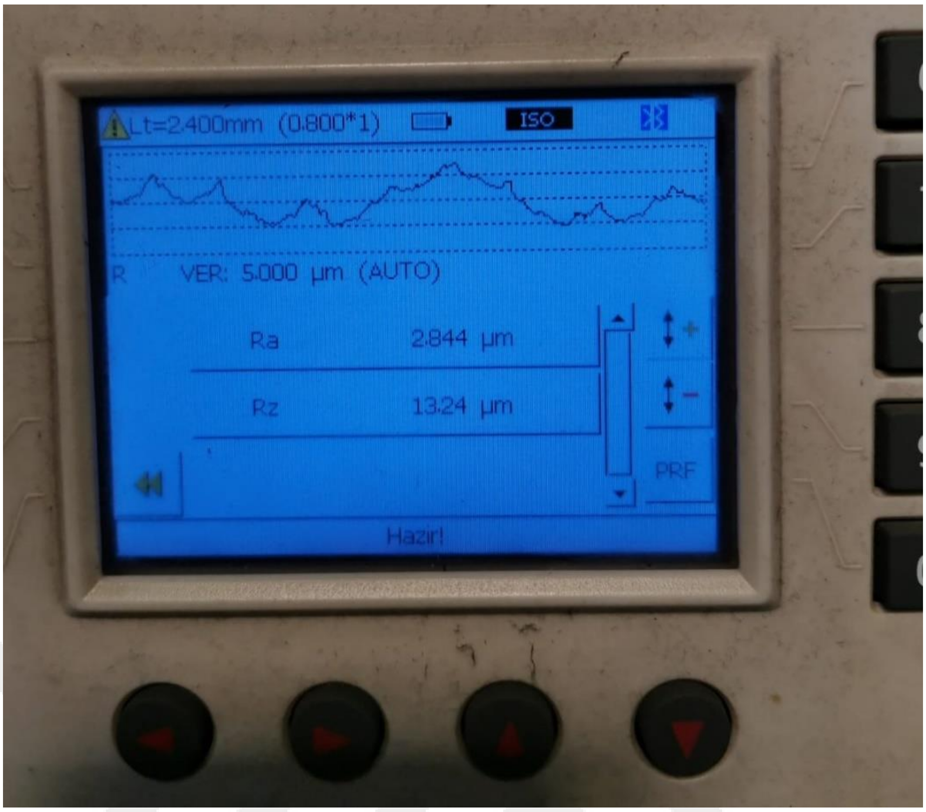

Figure 3.10 Surface roughness values of A2.2 (Personal archive, 2020)

Ra value of area A2.3 was monitored as 2.641 µm and Rz value of this area was monitored as 13.95 µm. For the area A2.3, the cutting parameter levels are 200 m/min as cutting speed and 0.05 mm/rev as the feed. Surface roughness measurement results of the area A2.3 is shown in Figure 3.11.

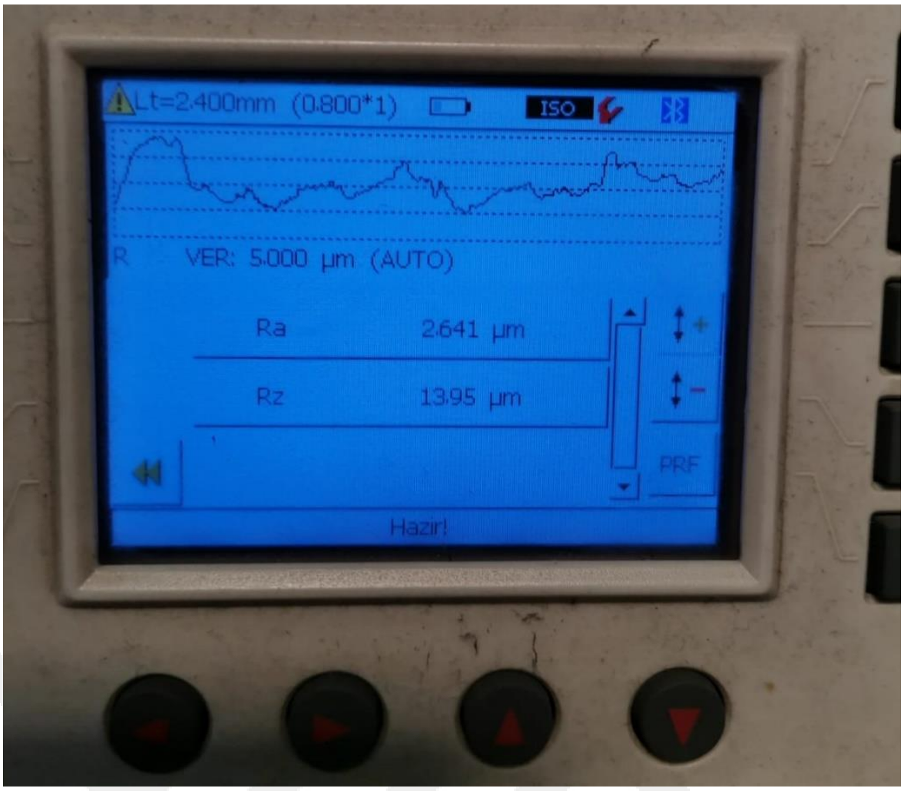

Figure 3.11 Surface roughness values of A2.3

It is seen that cutting speed as 200 m/min and feed as 0.1 mm/rev provide the best surface roughness quality. For the optimum working range of the CNC lathe, these values must be used and chip depth must be 0.5 mm for per passes. Surface roughness measurements shows that the best roughness values occurred on A1.1 area and the worst roughness values occurred on A2.1 area. The best and the worst roughness values is given together in Figure 3.12.

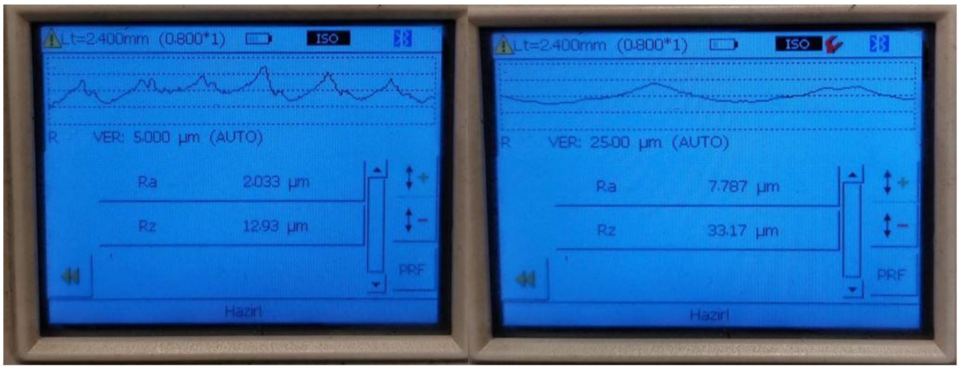

Figure 3.12 The best and the worst roughness values

After the surface measurements of the workpieces the results of the analyzes with respect to cutting force 1 and cutting force 2 have been compared with the surface roughness measurements and CMM results of these related areas. In addition, the comparison of the turned areas with different cutting forces which were not analyzed but used in lathe experiments have been made. The relationships between the turning experiment results are shown in Table 3.2. All of the cutting parameters and cutting force values related to these parameters which were used in the experiments have been chosen from the Table 2.1.

Table 3.2 The study results

Analyzes					**Experiments**				**CMM Measurements**		
Force Name	Fc (N)	Ff (N)	Fr (N)	Total displacement (mm)	Working area	Cutting Speed (m/min)	Feed (mm/rev)	Ra (µm)	Diameter (mm)	Roundness (mm)	Concentricity (mm)
Cutting force 1	1329	804	61	0.1445	A2-1	200	0.3	7.787	26.9171	0.0494	0.0543
Cutting force 2	563	505	19	0.0777	A1-1	200	0.1	2.033	26.7315	0.0185	0.0305
Cutting force 3	562	504	21	0.0744	A2-2	250	0.1	2.844	26.9175	0.0210	0.0430
Cutting force 4	587	537	21	0.0788	A1-2	150	0.1	2.727	26.7406	0.0207	0.0180
Cutting force 5	354	363	7	0.0515	A2-3	200	0.05	2.641	26.8836	0.0120	0.0425
Cutting force 6	933	672	49	0.1073	A1-3	200	0.2	4.949	26.7917	0.0289	0.0176

According to the results in Table 3.2, the cutting regions have been examined. The effect of flexion which changes with respect to the different distances to the chuck is also taken into consideration. According to the results, it is seen that the flexion on the piece decreases as it gets closer to the chuck. This conclusion has been got by considering both roundness and concentricity measurement results. Cutting areas with the same distance from the chuck have been compared to each other too. When the A2.1 and A1.1 cutting areas compared, it is seen that increasing of feed has a negative effect on surface roughness, concentricity and roundness. In other words, as the feed increases, the accuracy of the workpiece decreases. When the A2.2 and A1.2 cutting areas are compared, it is seen that the increasing of the cutting speed does not have a significant effect on the surface roughness and roundness. Besides, he cutting speed has a negative effect on concentricity.

CHAPTER FOUR

AUTOMATION OF THE LATHE

4.1 MACH3 interface settings

The lathe which examined in this study is controlled by the MACH3 program. MACH3 program has been developed to control CNC machines from personal computers with compatible control cards. MACH3 is used to run stepper and servo motors numerically. With MACH3, movements of CNC machines can be adjusted. Default MACH3 interface is shown in Figure 4.1.

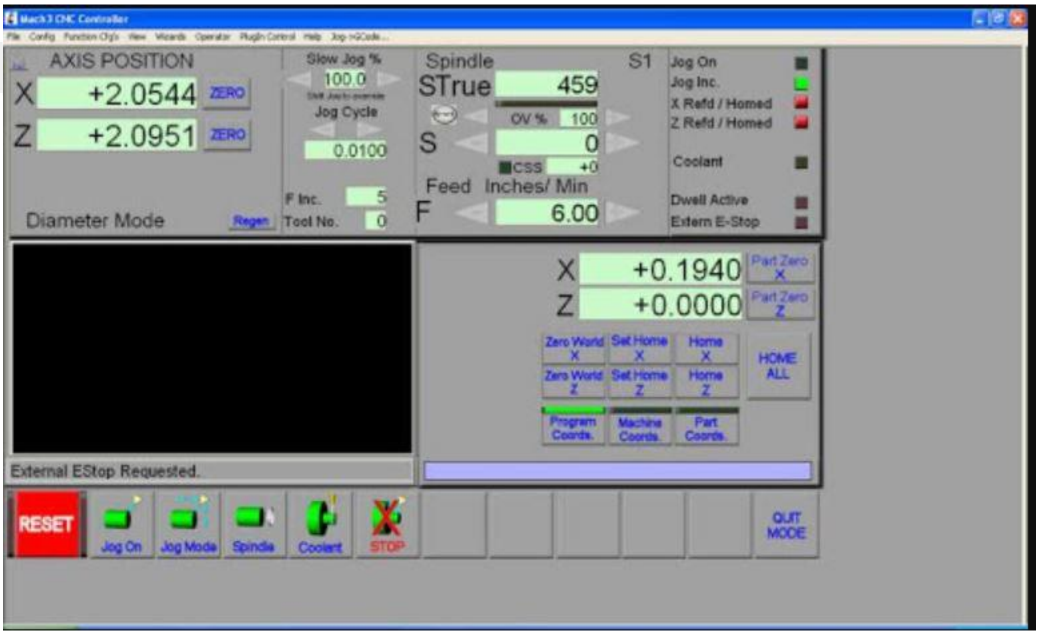

Figure 4.1 Default interface of MACH3

In this study, MACH3 interface has been customized for the existing CNC lathe. In the default interface there were only X and Z axes. The Y-axis that we can control the position of the turret has been added to new MACH3 lathe interface. For this purpose, the lathe set file which has been created as the new interface added to MACH3 directory. Then, load screens button was selected in the view tab of MACH3 CNC controller. Turn files were selected in the list of files of type. #24lathe.Iset file was selected from MACH3 directory. This process loaded the edited screen and changed the default interface. After completing these steps, the Y-axis has been provided to be able to control the turret axis that used for tool changer. For this axis, page up and page down buttons have been attended as control shortcuts on keyboard.

From the configuration page, ports and pins outputs have been edited. View of the MACH3 manual interface is shown in Figure 4.2 and MACH3 auto interface is shown in Figure 4.3.

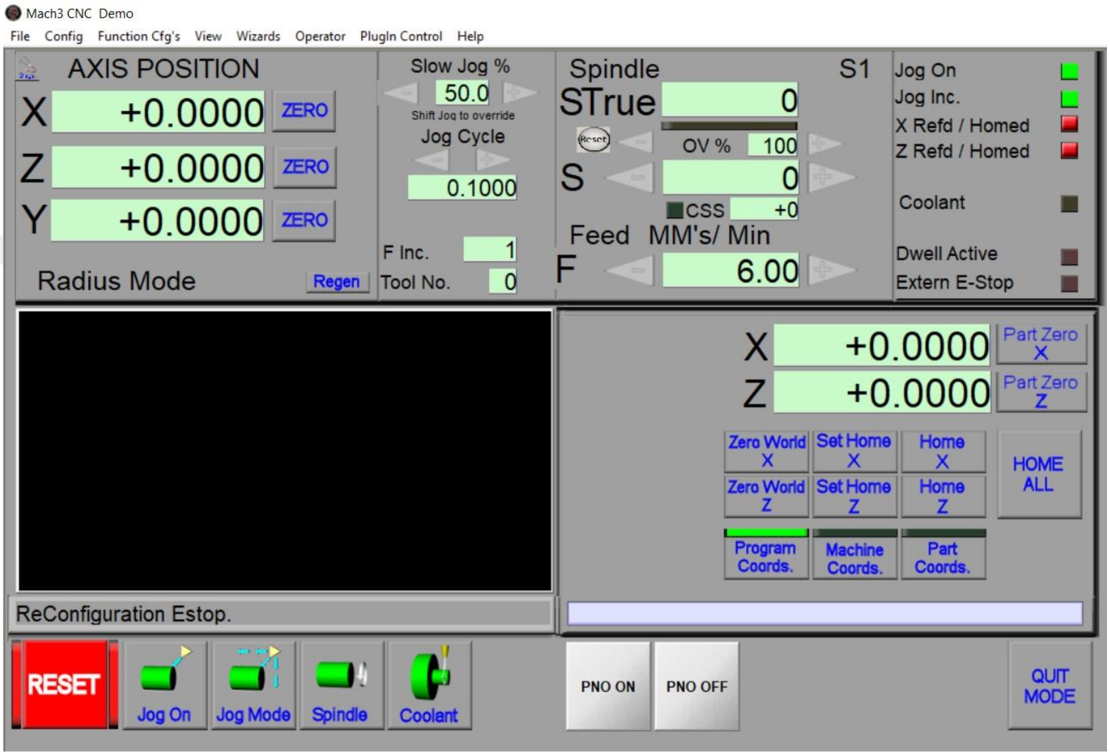

Figure 4.2 Customized MACH3 manual interface

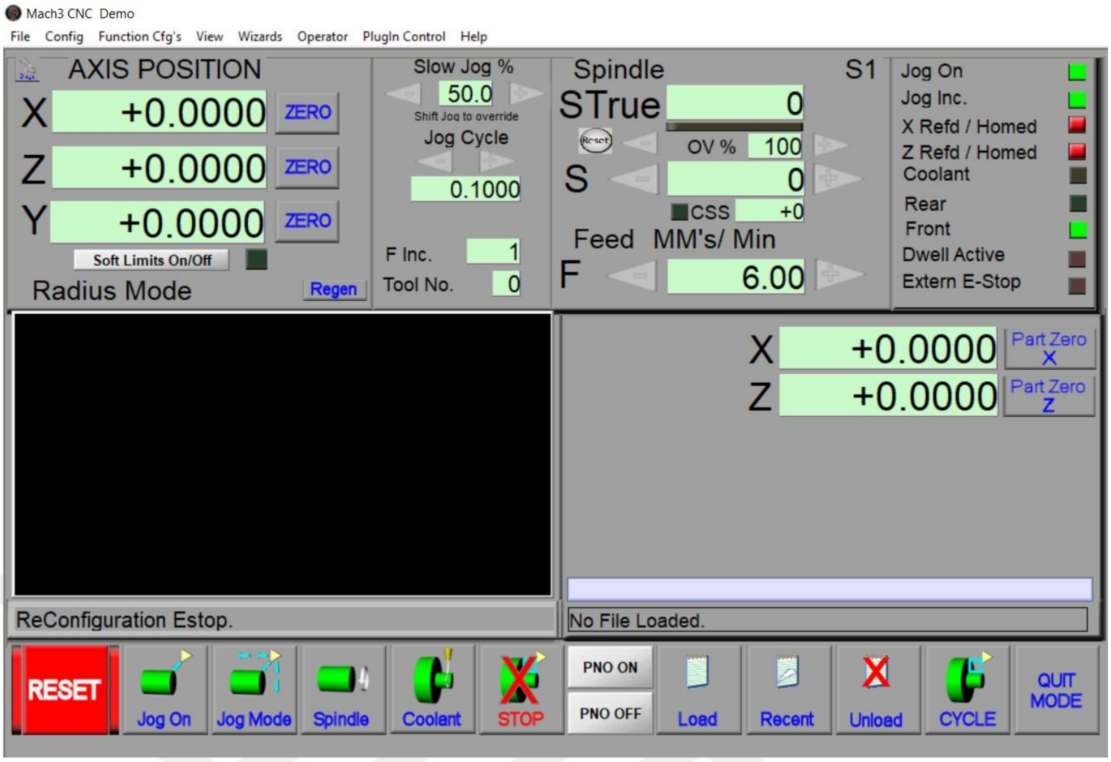

Figure 4.3 Customized MACH3 auto interface

Engine configuration settings of the system are shown in from Figure 4.4 to Figure 4.9.

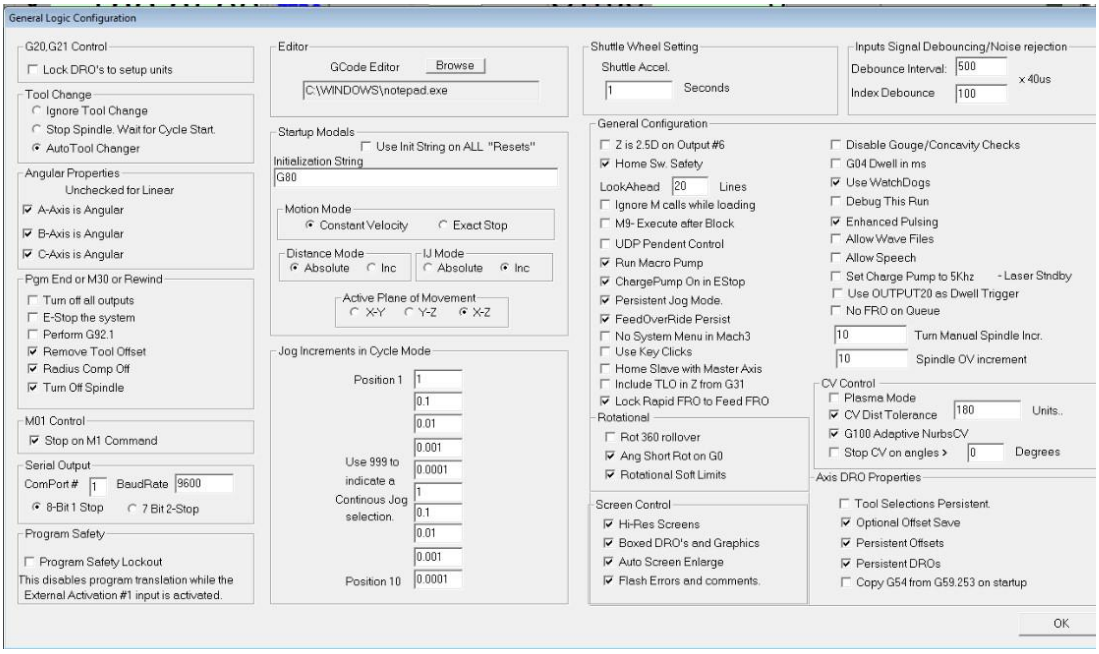

Figure 4.4 General logic configuration

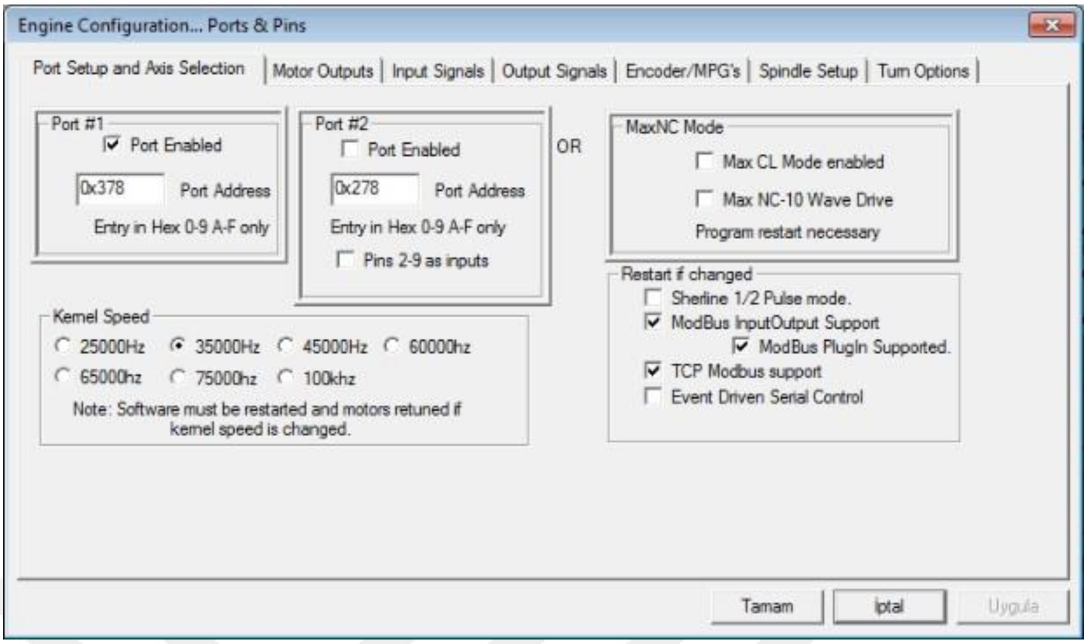

Figure 4.5 Ports and pins configuration

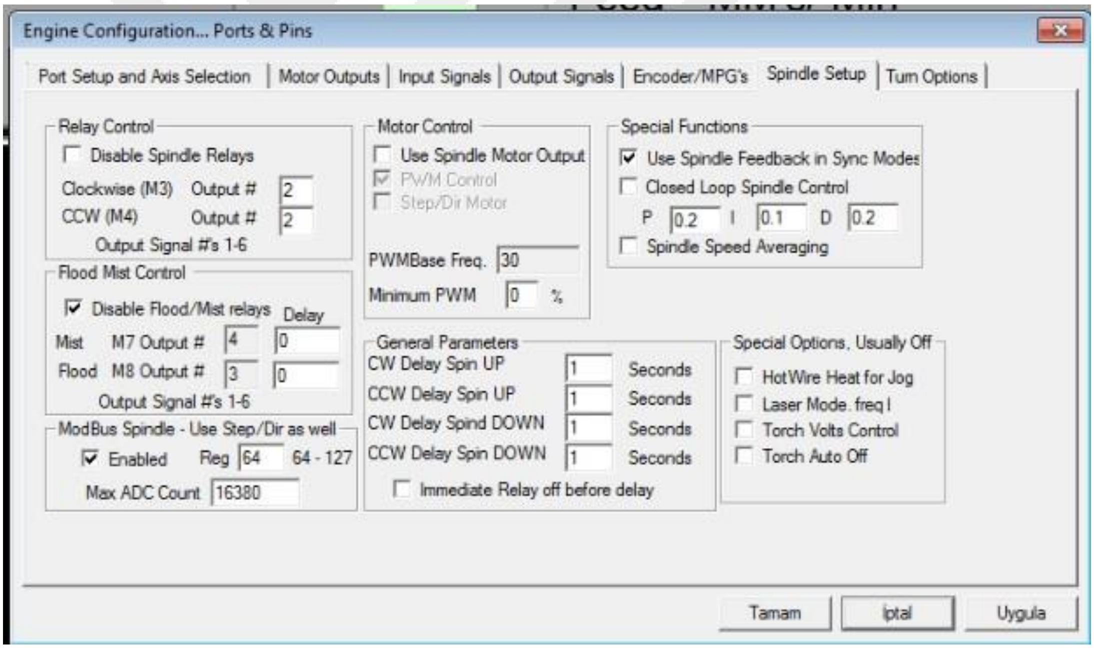

Figure 4.6 Ports and pins configuration

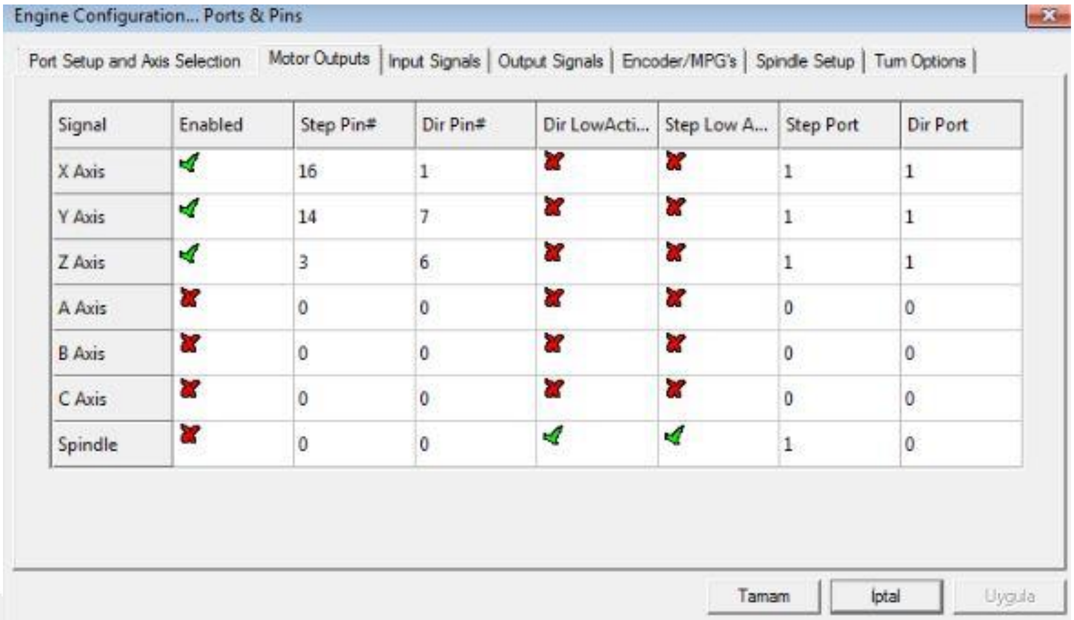

Engine Configuration... Ports & Pins

Port Setup and Axis Selection | Motor Outputs | Input Signals | Output Signals | Encoder/MPG's | Spindle Setup | Turn Options

Signal	Enabled	Step Pin#	Dir Pin#	Dir LowActi...	Step Low A...	Step Port	Dir Port
X Axis	✓	16	1	✗	✗	1	1
Y Axis	✓	14	7	✗	✗	1	1
Z Axis	✓	3	6	✗	✗	1	1
A Axis	✗	0	0	✗	✗	0	0
B Axis	✗	0	0	✗	✗	0	0
C Axis	✗	0	0	✗	✗	0	0
Spindle	✗	0	0	✓	✓	1	0

Tamam | İptal | Uygula

Figure 4.7 Motor outputs

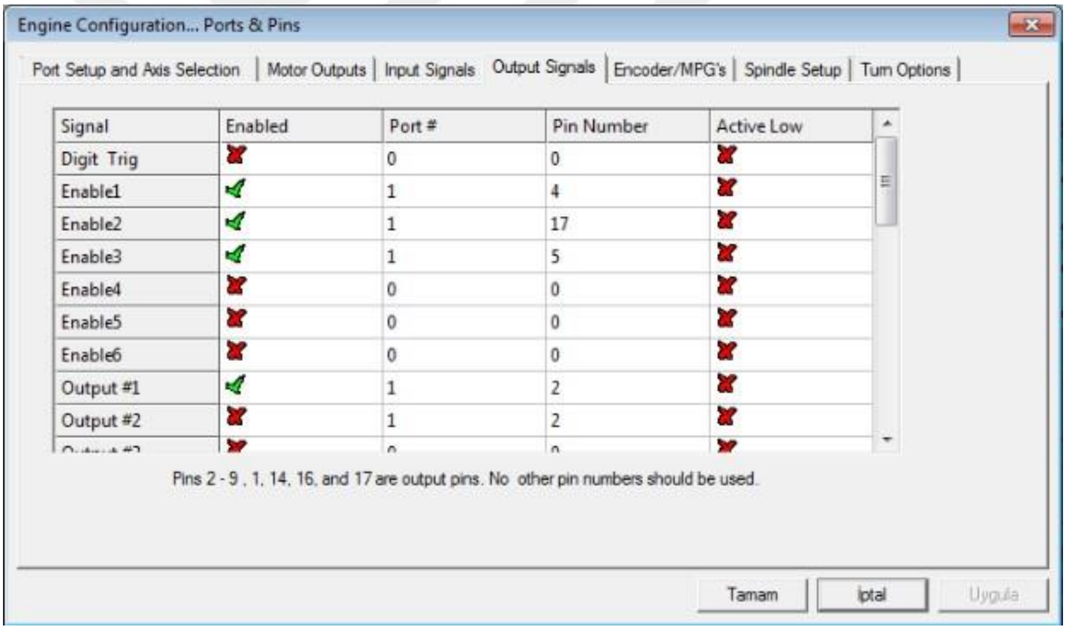

Engine Configuration... Ports & Pins

Port Setup and Axis Selection | Motor Outputs | Input Signals | Output Signals | Encoder/MPG's | Spindle Setup | Turn Options

Signal	Enabled	Port #	Pin Number	Active Low
Digit Trig	✗	0	0	✗
Enable1	✓	1	4	✗
Enable2	✓	1	17	✗
Enable3	✓	1	5	✗
Enable4	✗	0	0	✗
Enable5	✗	0	0	✗
Enable6	✗	0	0	✗
Output #1	✓	1	2	✗
Output #2	✗	1	2	✗

Pins 2 - 9 , 1, 14, 16, and 17 are output pins. No other pin numbers should be used.

Tamam | İptal | Uygula

Figure 4.8 Output signals

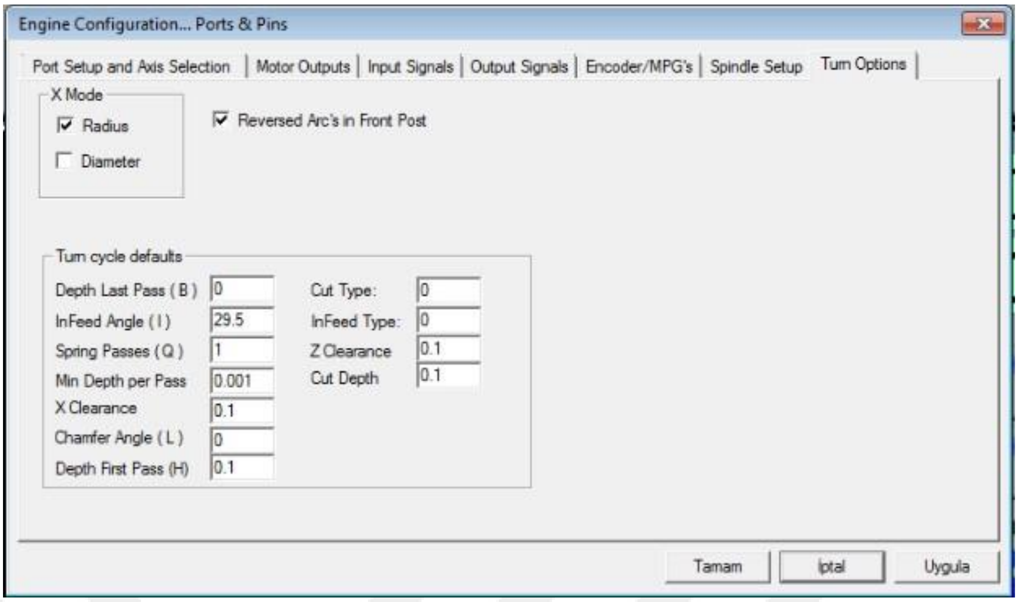

Figure 4.9 Turn options

Toolpath configuration of the system is shown in Figure 4.10.

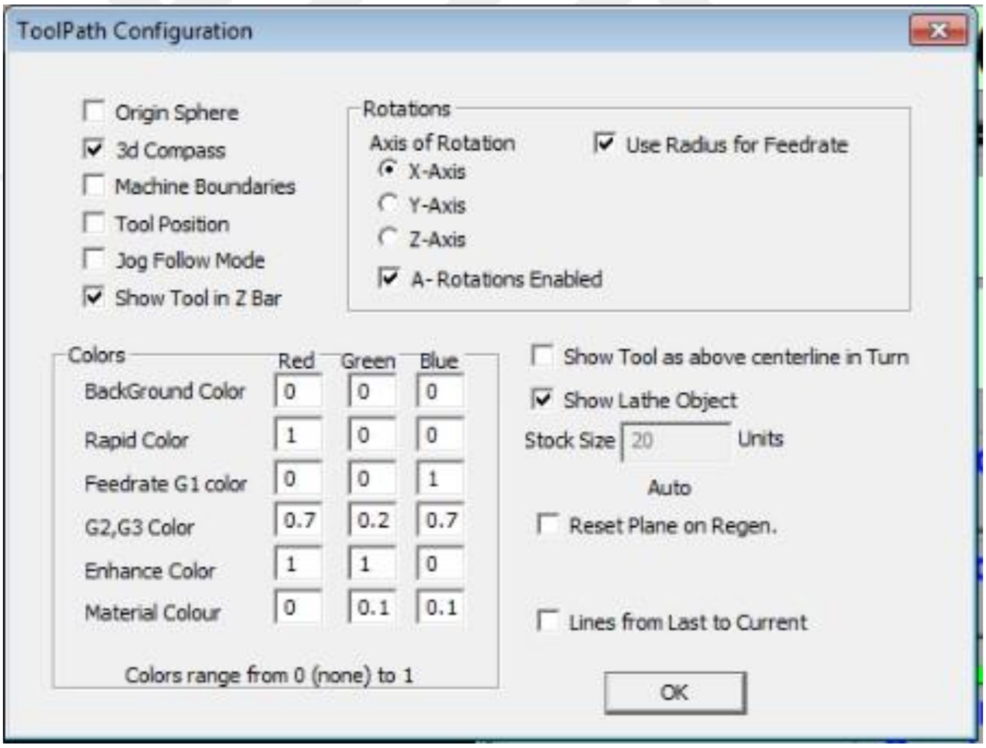

Figure 4.10 Toolpath configuration

Mainly, three upgrades on the system have been made. These are; automation of the pneumatic of the turret, automation of the tool holder and automatic controlling of the spindle motor. Tunings of the step motor movement profiles have also been made.

4.2 Automation of the pneumatic of the turret

Before the automation of the CNC lathe, working of the pneumatic system on the turret had been made manually by the pneumatic power switch on the lathe. Now, the pneumatic system is operated automatically. For this purpose, electronical connections on the lathe have been made and macro codes in the program have been generated.

Pneumatic system is powered by a 24-volt power supply which also powers the mainboard and stepper motors. The solenoid valve of the pneumatic system operates with 24 volts too. When the relay of the mainboard is triggered, the common power supply enables the pneumatic system's solenoid valve to open. Thus, 6 bar pressure air coming from the compressor reaches the turret system. As the solenoid valve closes again, it produces voltage in the opposite direction because of the turning of the coiling of the solenoid valve. This reverse voltage may cause the power supply to short circuit. When this happens, the power supply will turn itself off to protect itself. To prevent this, a 1N4007 diode is positioned between Min and Mout inputs of the relay. 1N4007 diode is shown in Figure 4.11.

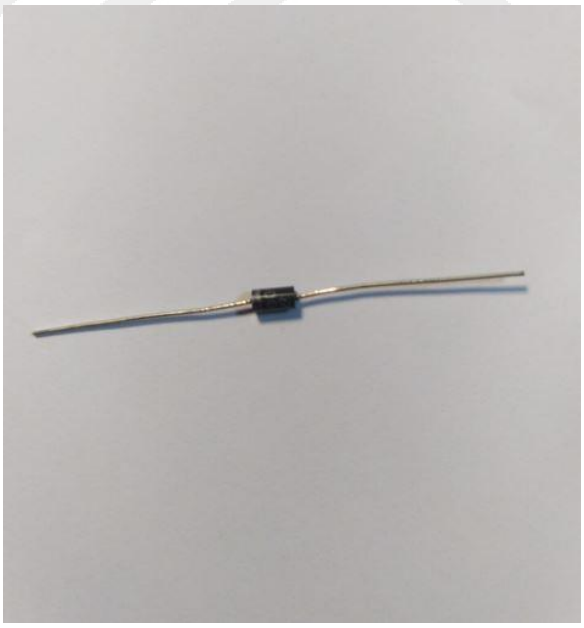

Figure 4.11 1N4007 diode (Personal archive, 2020)

The point we need to pay attention here is that we should connect the anode end of the diode to the same socket (Min) with the cable coming from the cathode pole of the power supply. In the same time, we should connect the cathode end of the diode to the socket (Mout) where we connect the other end of the cable. Pneumatic wiring is shown in Figure 4.12.

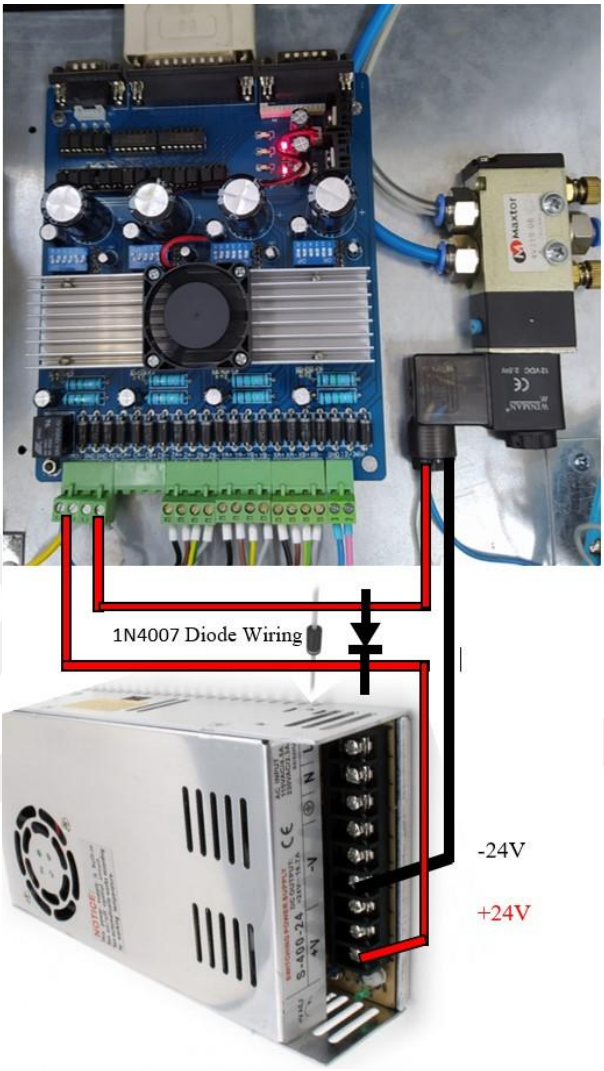

Figure 4.12 Pneumatic wiring (Personal archive, 2020)

In the programming part, macro codes have been written to control the pneumatic automatically in VB script editor. Working of the pneumatic has been made with M6 tool change code. The triggering has been provided by the codes M101 (activation) and M102 (deactivation). The process has been completed by saving the relevant codes from the VB script Editor. M101 code is shown in Figure 4.13 and M102 code is shown in Figure 4.14.

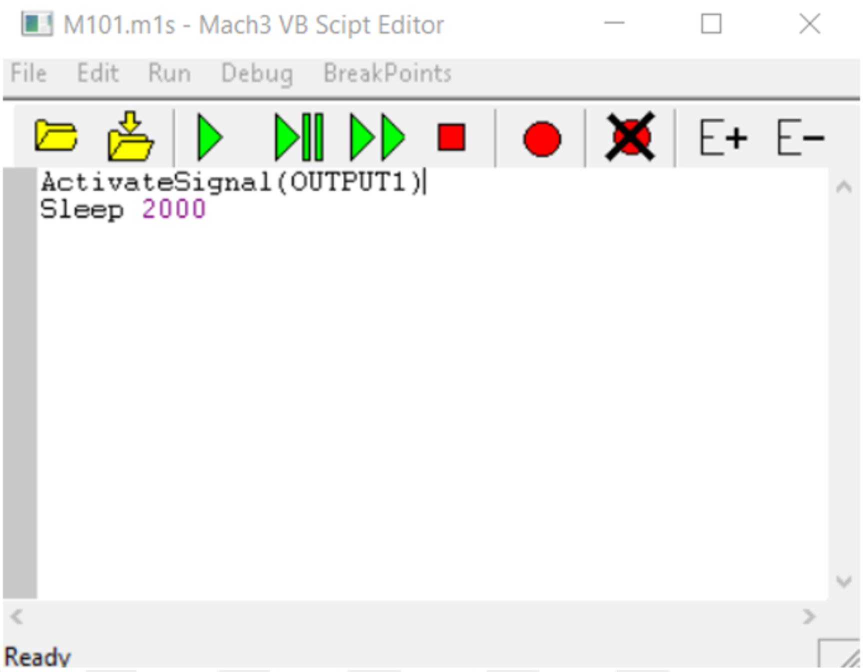

Figure 4.13 M101 code

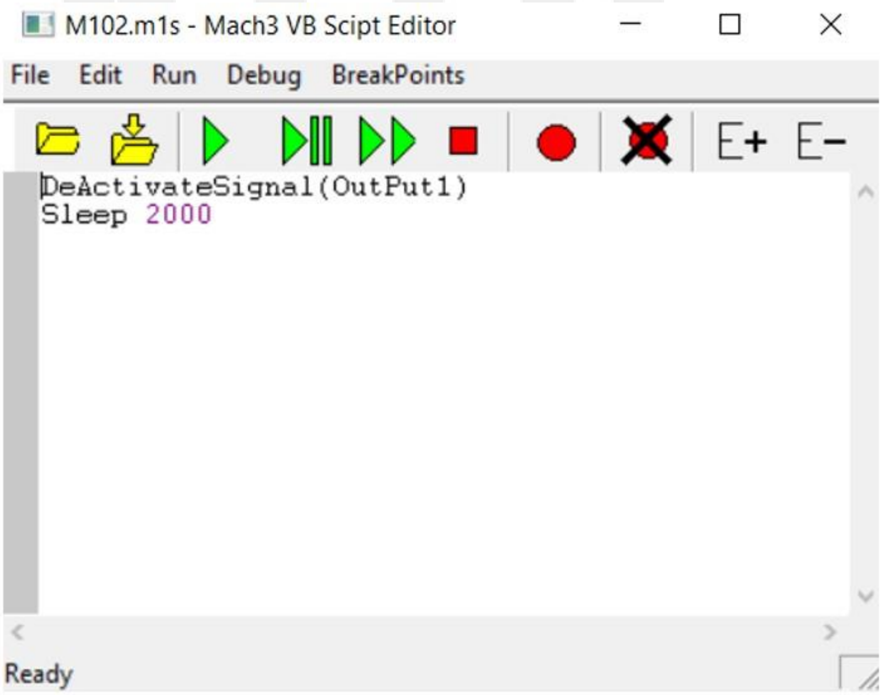

Figure 4.14 M102 code

4.3 Automation of the tool holder

Before this study, the tool holder of the turret had no rotational movement. Now, the automatic rotation movement of the tool holder is possible.

Firstly, the Y-axis has been configured as the turret rotation axis and it has been added to the MACH3 interface. For this purpose, MACH3 interface has been changed and motor tuning parameters of the Y-axis has been arranged.

System settings for the turret control have been activated from the "General Config" tab for the Y-axis. Before this study, Y-axis has not been in use and the lathe had been used X-Z Coordinates. The Y-axis has been added to the program. It is provided to perform the rotational movement on the Y-axis precisely. Motion of the turret is controlled via the shortcut keys "Page Up" and "Page Down" from the "System Hotkeys" tab on the MACH3 interface. Thus, the turret rotation control has been made with the Y-axis on the new MACH3 interface. The toolpath configuration of the Y-axis is shown in Figure 4.15. Figure 4.15 shows that the rotational movement is exist around the x-axis.

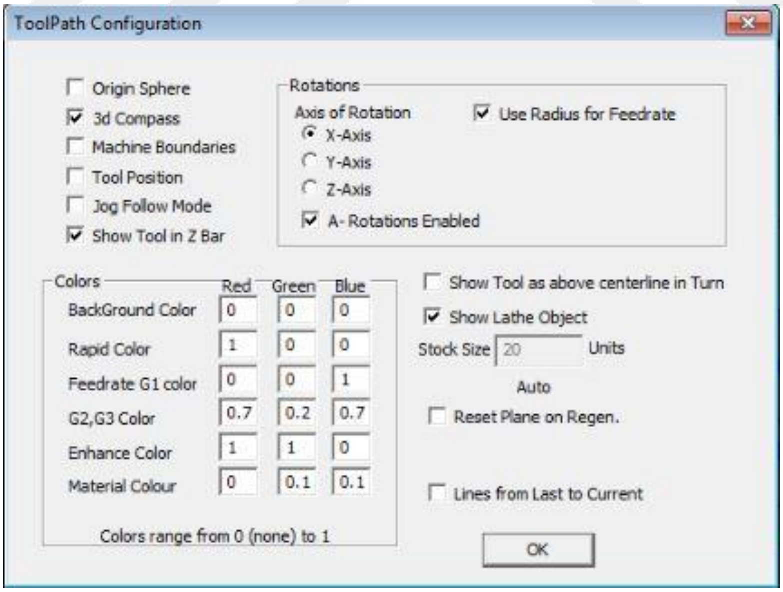

Figure 4.15 Toolpath configuration

Before running the rotation axis, pneumatic of the turret must be turned on. Pneumatic can be run easily from the pneumatic on-off button placed on the computer screen. When the tool change code is given, the pneumatic working process is performed automatically.

For the rotation of the turret, position parameters have been arranged with the macro codes. These codes have been written in VB script editor and each rotation movement have given as 45 degrees. The macro code part of the rotation of the turret is shown in Figure 4.16.

Figure 4.16 Macro codes of the Y axis

4.4 Motor tuning parameters of the axes

Before this study, velocity and acceleration values of the movement axes were not accurate and the axes could not be able to move to their desired positions precisely. With the trials on the motor tuning part of the MACH3 settings, acceleration and velocity values of the X, Y and Z axes have been become more accurate. Motor movement profiles of the axes are shown in Figures 4.17, 4.18 and 4.19.

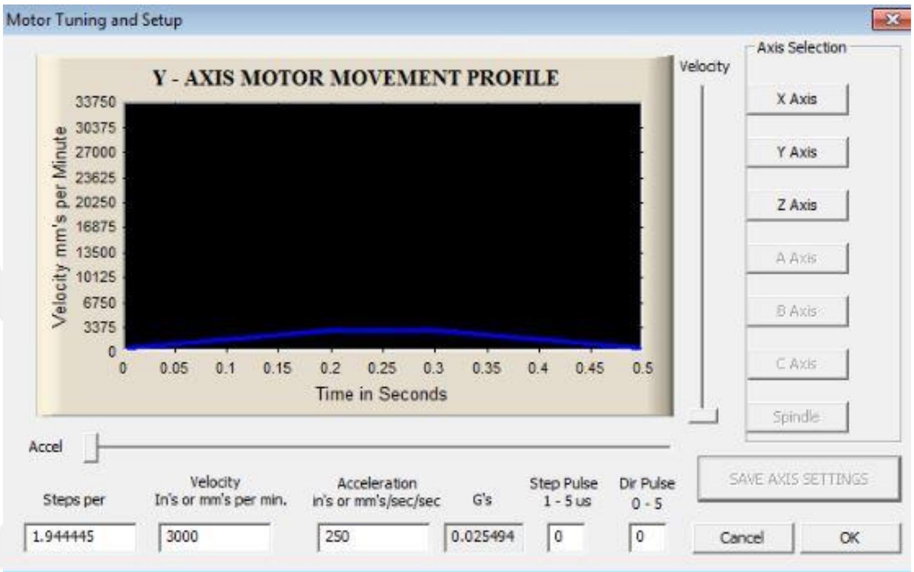

Figure 4.17 y-axis motor movement profile

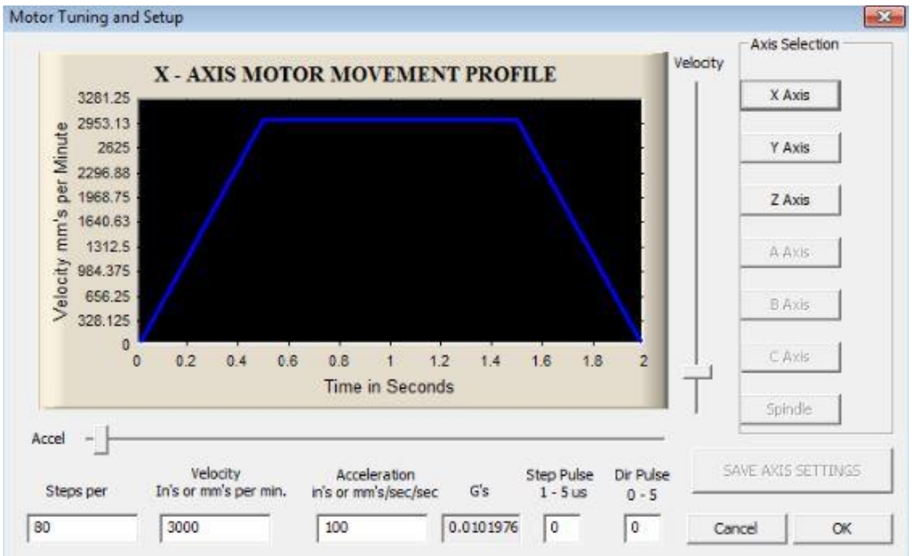

Figure 4.18 x-axis motor movement profile

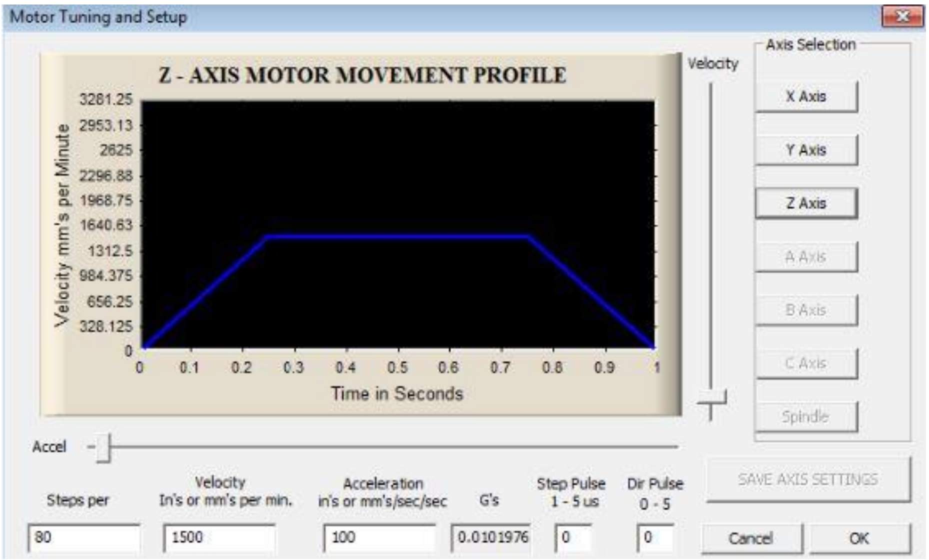

Figure 4.19 z-axis motor movement profile

4.5 Automation of the spindle motor

Before this study, spindle speed control had been made manually only with the potentiometer on the VFD. With the adjustments on the MACH3, the speed control has been made automatically. These adjustments were made by sending 8-bit data over the serial communication port of the computer where MACH3 software has been installed.

By changing the pin/port and input/output settings on MACH3, sending of spindle frequency commands to VFD by using RS485 RJ-45 ethernet port has been activated. Modbus has been used for the transmission of frequency and turning direction information with 8N1 communication protocol over MACH3. 8N1 means basically “8 bytes, no parity, 1 stop bits”. It has been provided to control the spindle speed with the frequency information received from the VFD.

VFD is the motor driver to adjust the rotation speed of the asynchronous motor of the lathe. Various commands for as frequency are run by using the navigation keys and potentiometer on the VFD. View of the VFD on the lathe is shown in Figure 4.20.

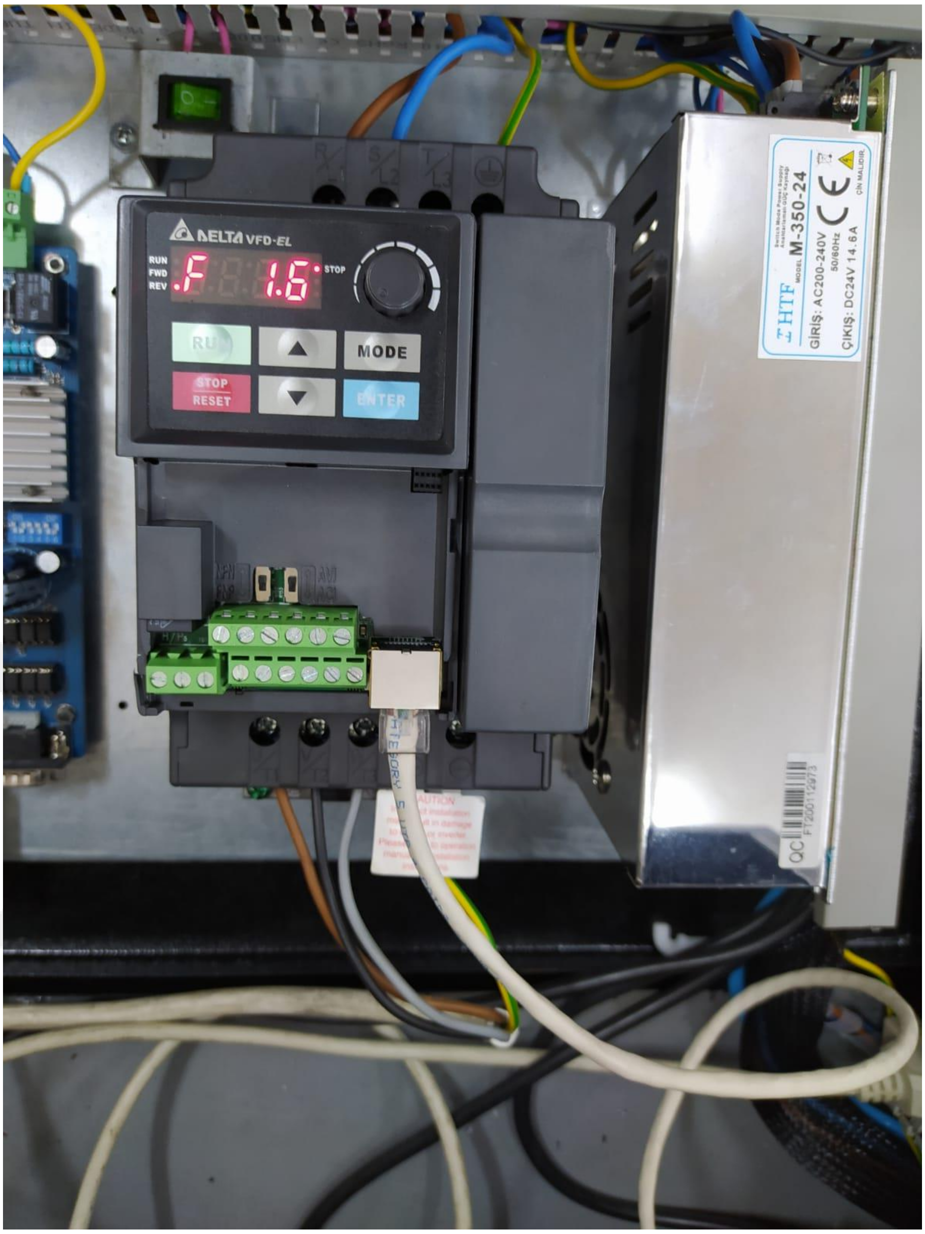

Figure 4.20 The VFD (Personal archive, 2020)

The data transmission has been made over serial communication port (COM1) to the controller board by using RTU device that converts RS282 to RS485 Protocol. This transmission leads us to have less wiring to be able to communicate MACH3 and VFD.

4.5.1 VFD settings

For the automatic rotation of the spindle motor, VFD settings have been made to run with RS485 communication protocol. The reason of choosing RS485 communication protocol is that the control card does not have a PWM output. Since there is no such PWM output on the card, communication has been provided between the computer and the VFD, not between the card and the VFD. If there was a PWM output on the card, the card would communicate with the VFD, and then the card and the computer would communicate. Figures 4.21, 4.22 and 4.23 show the parameters from the VFD manual. The VFD parameters have been set as;

P02.00 = 3 (RS485 RJ-45 communication)

P02.01 = 3 (RS485 RJ-45 communication keypad start/stop enabled)

P09.01 = 1 (9600 baud rate)

P09.04 = 6 (8N1 Modbus RTU)

Group 2 Operation Method Parameters

Parameter	Function	Setting	Factory Setting	Customer
✗02.00	Source of First Master Frequency Command	0: Digital keypad UP/DOWN keys or Multi-function Inputs UP/DOWN. Last used frequency saved. 1: 0 to +10V from AVI 2: 4 to 20mA from ACI 3: RS-485 (RJ-45) communication 4: Digital keypad potentiometer	1	
✗02.01	Source of First Operation Command	0: Digital keypad 1: External terminals. Keypad STOP/RESET enabled. 2: External terminals. Keypad STOP/RESET disabled. 3: RS-485 (RJ-45) communication. Keypad STOP/RESET enabled. 4: RS-485 (RJ-45) communication. Keypad STOP/RESET disabled.	1	

Figure 4.21 Operation method parameters (DELTA VFD-EL User Manual, 2020)

Group 9 Communication Parameters

Parameter	Explanation	Settings	Factory Setting	Customer
09.00	Communication Address	1 to 254	1	
09.01	Transmission Speed	0: Baud rate 4800bps 1: Baud rate 9600bps 2: Baud rate 19200bps 3: Baud rate 38400bps	1	

Figure 4.22 Communication parameters (DELTA VFD-EL User Manual, 2020)

Communication protocol in the DELTA VFD-EL user manual is shown in figure 4.23.

09.04	Communication Protocol	0: 7,N,2 (Modbus, ASCII) 1: 7,E,1 (Modbus, ASCII) 2: 7,O,1 (Modbus, ASCII) 3: 8,N,2 (Modbus, RTU) 4: 8,E,1 (Modbus, RTU) 5: 8,O,1 (Modbus, RTU) 6: 8,N,1 (Modbus, RTU) 7: 8,E,2 (Modbus, RTU) 8: 8,O,2 (Modbus, RTU) 9: 7,N,1 (Modbus, ASCII) 10: 7,E,2 (Modbus, ASCII) 11: 7,O,2 (Modbus, ASCII)	0	

Figure 4.23 Communication protocols (DELTA VFD-EL User Manual, 2020)

Frequency settings were turned off using the keypad on the VFD and the communication feature with RS485 protocol has been activated. In this way, frequency and direction information sending to the inverter automatically with the Modbus protocol has been achieved. Modbus protocols communicate using serial port and internet protocols (RJ45). SG- pin of the ethernet cable has been plugged in to 485- input of the converter and SG+ pin of the ethernet cable has been plugged in to 485+ input of the converter. The converter of the lathe is shown in Figure 4.24 and RJ45 ethernet protocol wireframe is shown in Figure 4.25.

Figure 4.24 The converter

Figure 4.25 RJ45 Ethernet protocol wireframe (DELTA VFD-EL User Manual, 2020)

4.5.2 Modbus

An advantage of using Modbus instead of communicating with the PWM signal is that the small voltage values sent in the PWM signal may vary by small amount because of disturbing inputs from the magnetic field and electronic noise. These changes may lead to sensitivity reduction of the spindle speed. With Modbus communication, 8 bits of data are sent instead of voltage values. With this data, the inverter operates the spindle motor without errors.

For the system working, Modbus communication feature in ports and pins settings and macro pump box in general config must be selected. The setup serial Modbus control window opens to begin the test process. Modbus configuration is shown in Figure 4.26.

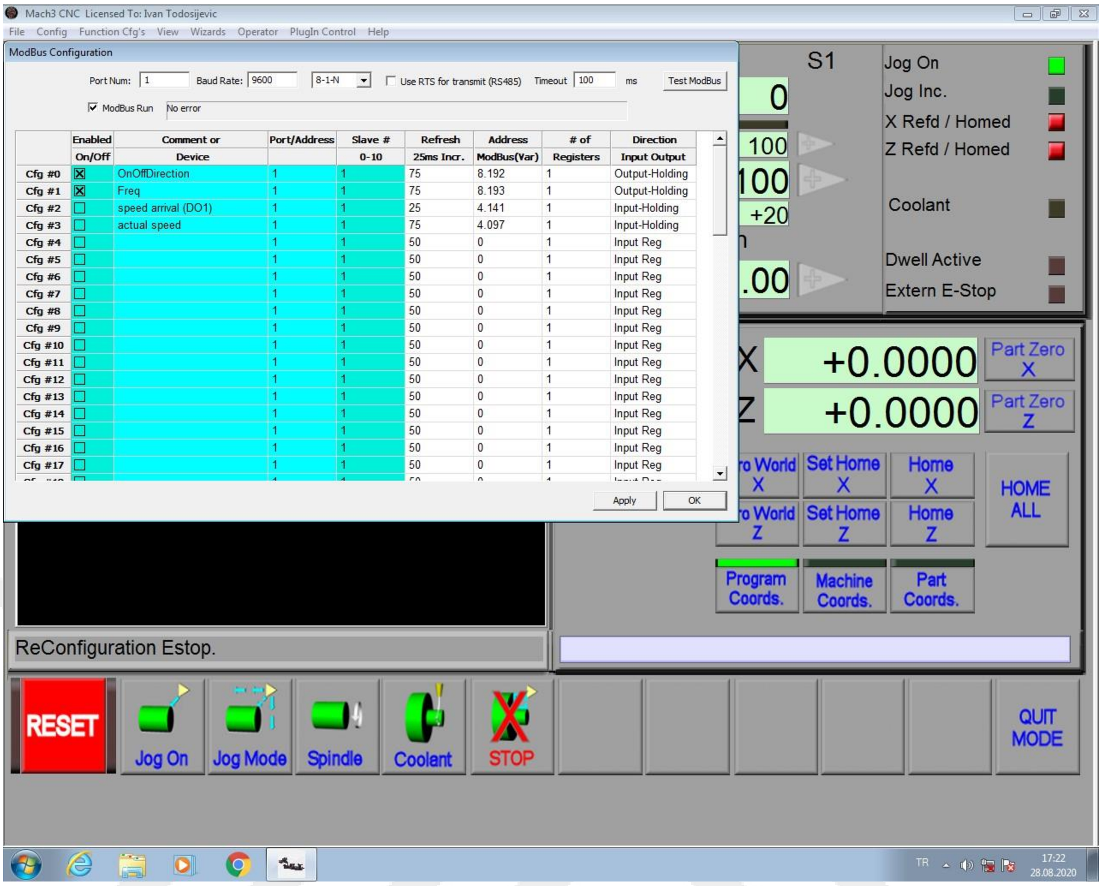

Figure 4.26 Modbus configuration

On the Modbus configuration screen, baud rate, 8N1 and Modbus run options has been selected. Then, the Modbus addresses to which we will send frequency writing, open / close direction information has been written. Then, test Modbus box has been selected and Modbus serial control window has been opened. Modbus serial control window is shown in Figure 4.27.

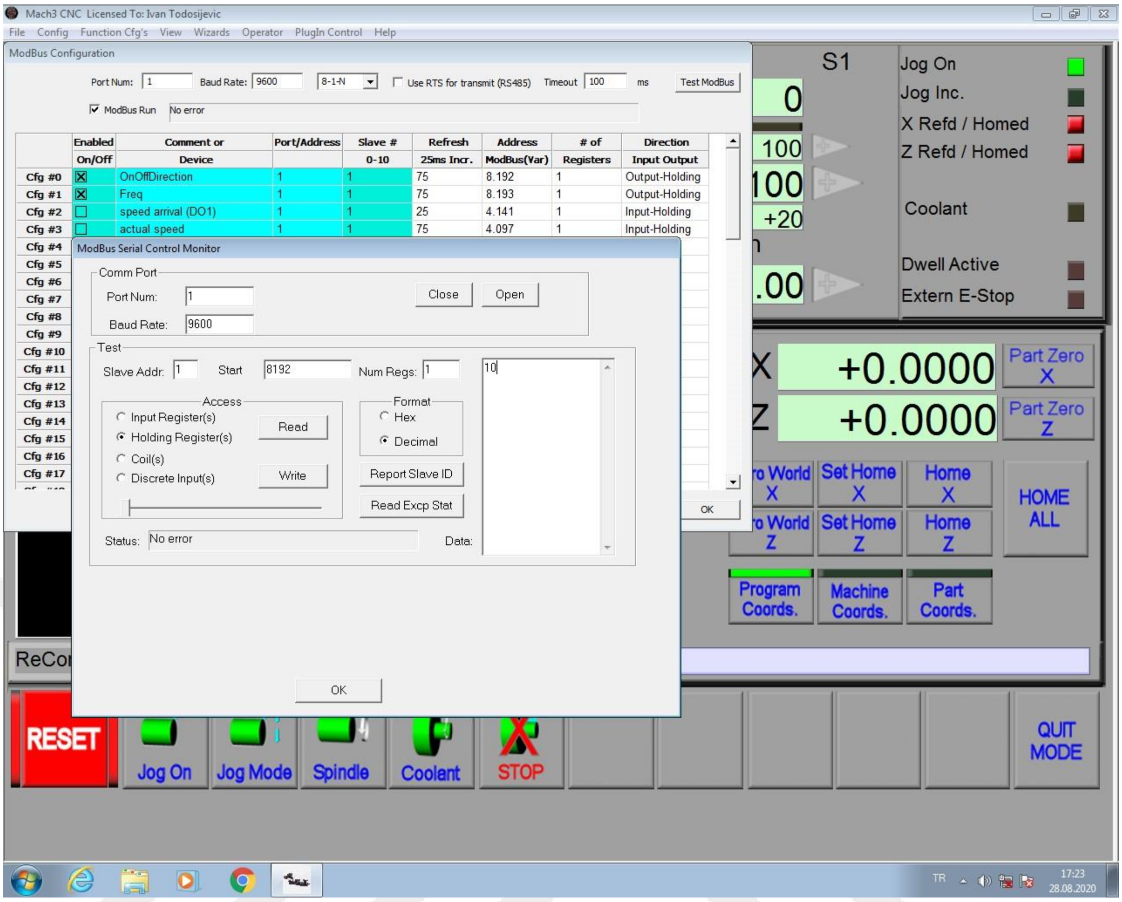

Figure 4.27 Modbus serial control monitor

Port number, baud rate and start address parts which are seen as in Figure 4.27 have been written. Then, open button has been selected. No error text in the status section indicates that the connection is correct. Holding register(s) and decimal boxes must be ticked just as seen in the Figure 4.27. When you type 10 in the information submission screen on the right and click the write box, the spindle works clockwise. When you type 06 and click the write box, it works in the counter clockwise direction. After the test is completed, the spindle motor stops by typing the 01 command.

In the MACH3 user manual, the address where the on / off direction command is sent is given as hexadecimal 2000H. The decimal equivalent of this address is 8192. Similarly, the frequency writing address is given as hexadecimal 2001H. The Modbus equivalent of this address is 8193. Hexadecimal addresses are shown in Figure 4.28.

3.5 Address list

The contents of available addresses are shown as below:

Content	Address	Function	
AC drive Parameters	GGnnH	GG means parameter group, nn means parameter number, for example, the address of Pr 04.01 is 0401H. Refer to chapter 5 for the function of each parameter. When reading parameter by command code 03H, only one parameter can be read at one time.	
Command Write only	2000H	Bit 0-1	00B: No function 01B: Stop 10B: Run 11B: Jog + Run
		Bit 2-3	Reserved
		Bit 4-5	00B: No function 01B: FWD 10B: REV 11B: Change direction
		Bit 6-7	00B: Comm. forced 1st accel/decel 01B: Comm. forced 2nd accel/decel
		Bit 8-15	Reserved
	2001H	Frequency command	
	2002H	Bit 0	1: EF (external fault) on
		Bit 1	1: Reset
		Bit 2-15	Reserved

Figure 4.28 Hexadecimal addresses (DELTA VFD-EL User Manual, 2020)

4.5.3 Macropumps

The macropump is a list of VB commands stored in a file called macropump.m1s in the current profile. Any valid VB script can be used. The Macropump runs about 40 times a second continually. It must be enabled in general config and MACH3 should be restarted to start the process. The reason of using macropump is to instantly detect which command (M3 M4 M5) is run on MACH3.

According to the working purpose of the code which has been written, when the M3 and M4 commands run, the digital LEDs number 164 and number 165 are activated respectively for these commands. If these two LEDs are off, it means M5 command is running. When one of the LED number 164 or LED number 165 is working or none of these are not working, Macropump starts to send 129, 133, 136 bits as decimal information. The counterpart of these bits are information bits that enable the execution of M3, M4, M5 commands sequentially. Macropump codes are shown in Figure 4.29.

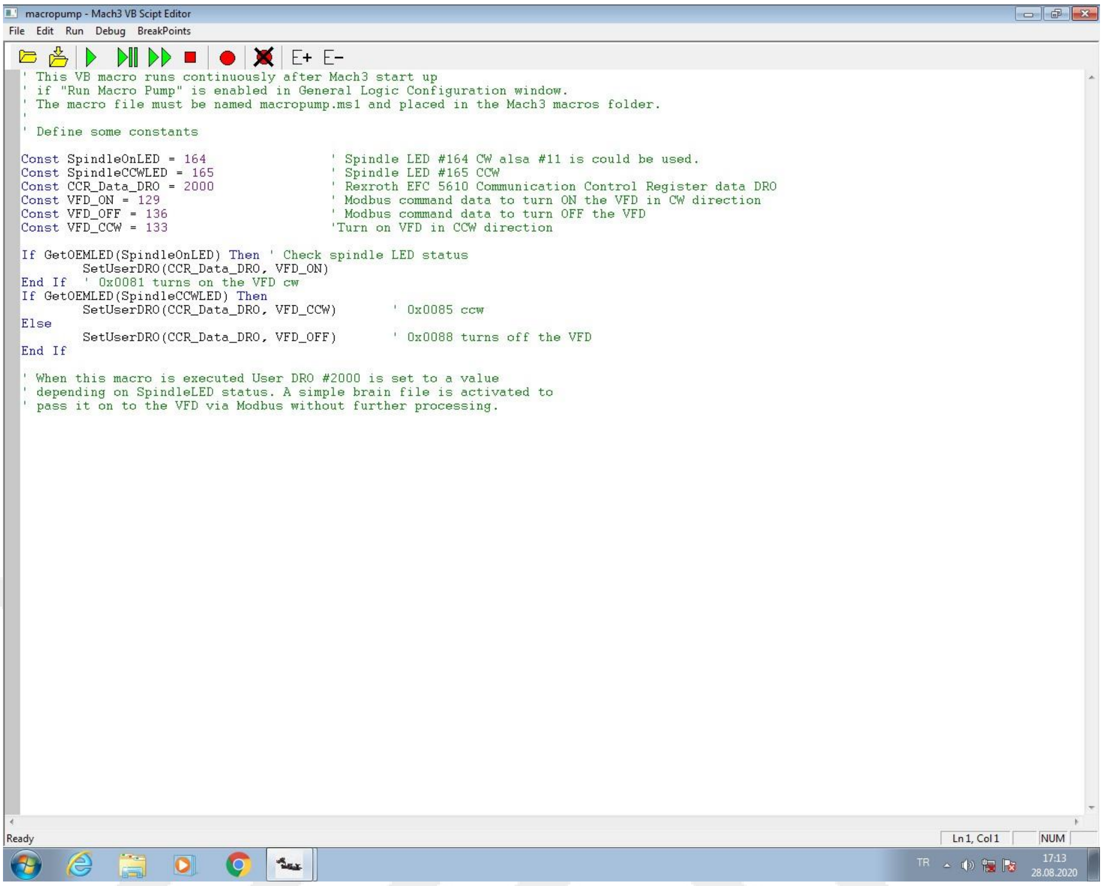

Figure 4.29 Macropump codes

4.5.4 The brain

After the information of executing commands is produced in macropump, it is the task of the MACH3 brain part to convert this information to the use of the inverter. In case M3, M4, M5 commands are executed in the brain section with the information coming from the macropump, 10, 06, 01 bits are sent to the defined Modbus addresses in sequence. This is mentioned in Delta VFD-EL user manual. After configuring the brain part as shown in Figure 4.30 and writing the macropump codes, the stability of the system has been tested on the Modbus test screen.

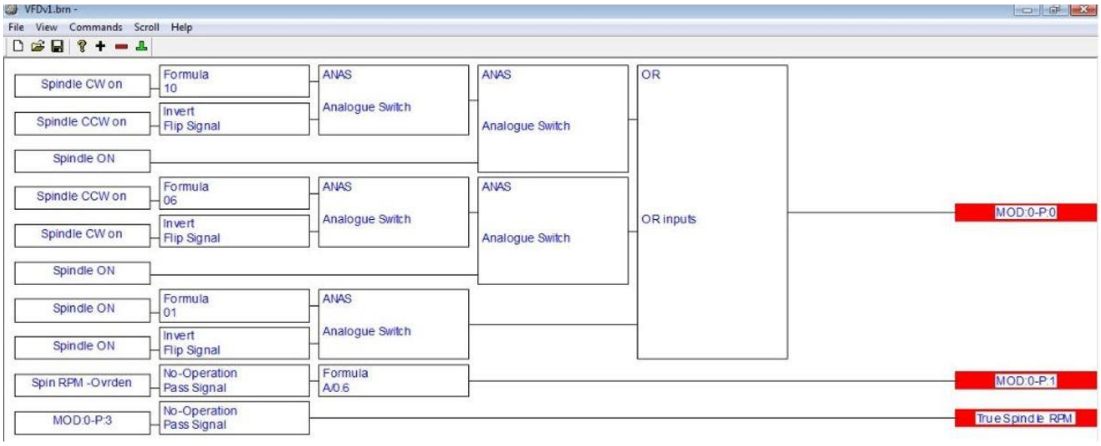

Figure 4.30 Brain structure

When any of the M3, M4 and M5 commands run, the brain only sends the information of the relevant command to the inverter and stops the other two commands. Formula part refers to the information that will be sent when any command is activated. When one of the Spindle CW ON-Spindle CCW ON LEDs which are related to each other is activated, the analogue switch part enables the other deactivated.

Another important part of the brain is the Spindle RPM-Overdriven part. In this section, when commands such as S2000 are received, Modbus allows to send frequency information to the inverter over the frequency write address. Here, the real RPM value is reached by dividing the spindle speed by 0.6 times in the Formula part.

When the M3 command is activated, CW ON and Spindle ON LEDs turn on. Decimal 10 information is sent over the Modbus direction writing address. Inverter runs the spindle motor clockwise direction. The brain activation when the M3 code activated is shown in Figure 4.31.

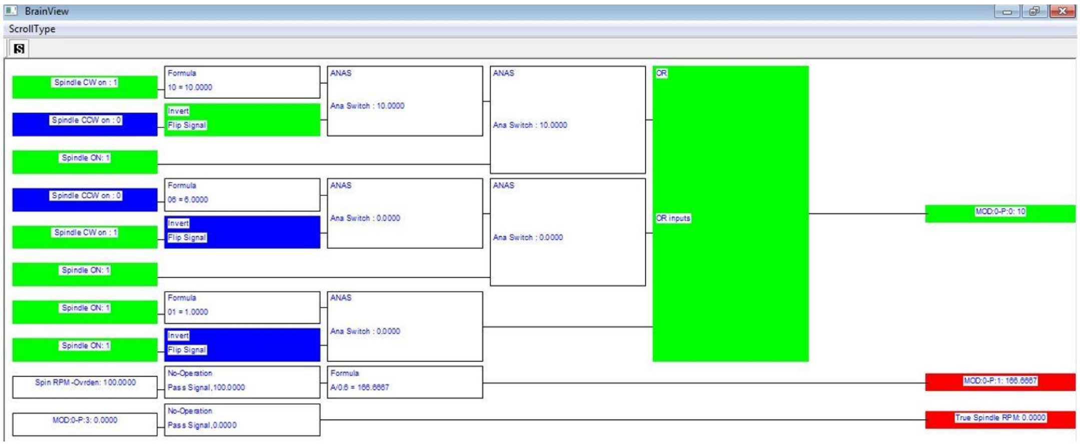

Figure 4.31 Brain with code M3

When the M4 command is activated, CCW ON and Spindle ON LEDs turn on. Decimal 06 information is sent over the Modbus direction writing address. Inverter runs the spindle motor counter clockwise direction. The brain activation when the M4 code activated is shown in Figure 4.32.

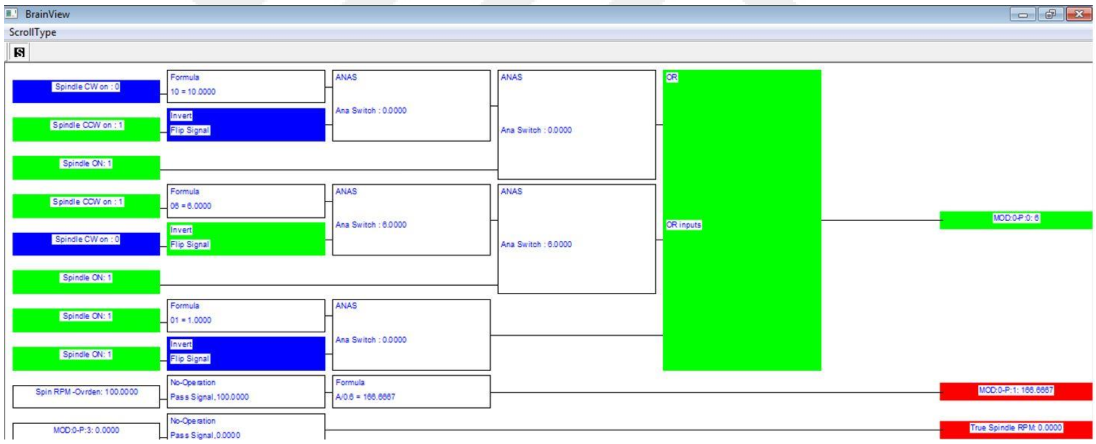

Figure 4.32 Brain with code M4

When the M5 command is activated, M3 and M4 LEDs are turned off. Decimal 01 information is sent over the Modbus direction writing address inverter stops the spindle motor. The brain activation when the M5 code activated is shown in Figure 4.33.

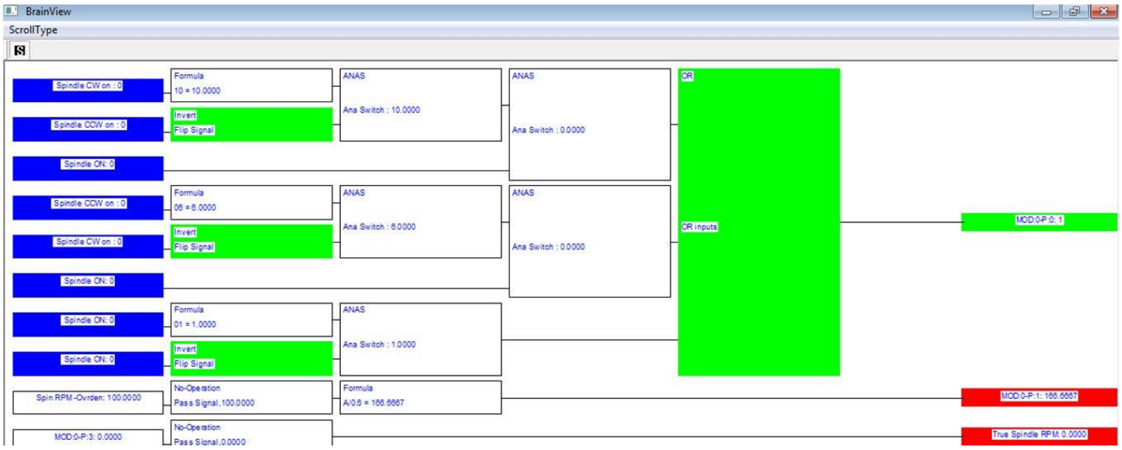

Figure 4.33 Brain with code M5

The system has Toshiba TB6560 card as the motor driver. The connections of the card in the system have been described below the Figure 4.34. The connections of the driver are shown in Figure 4.34.

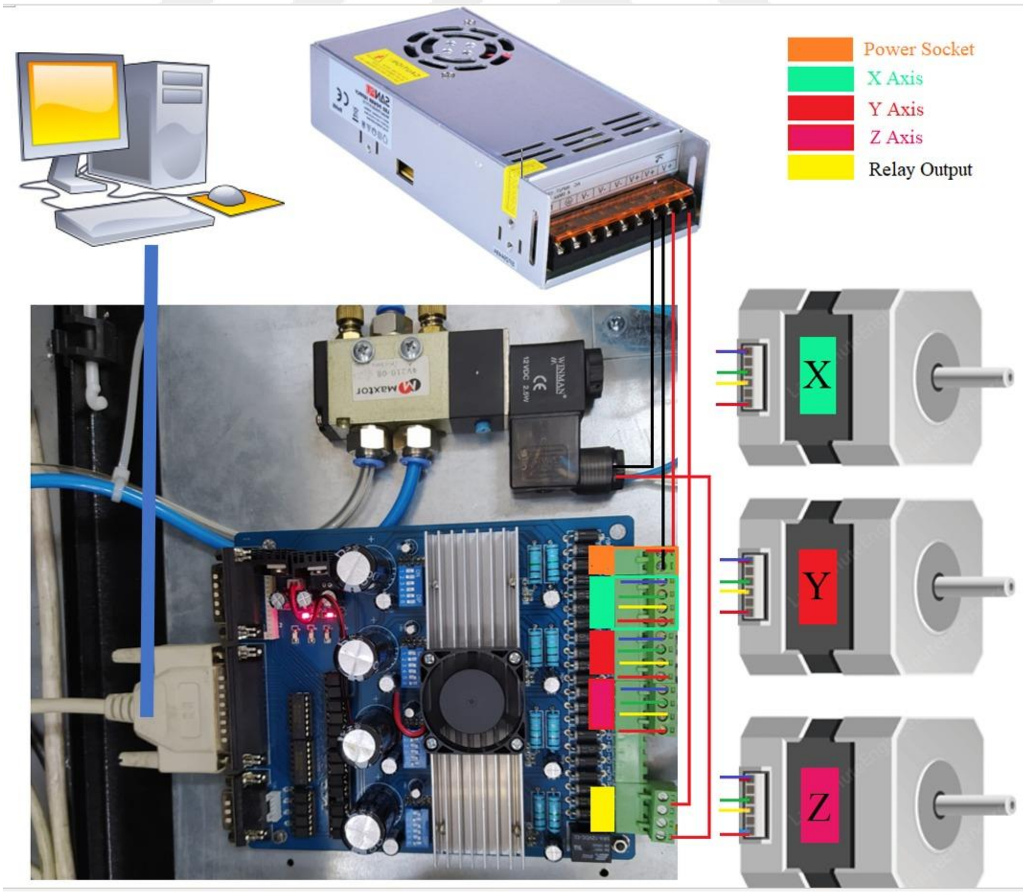

Figure 4.34 Motor driver connection scheme (Personal archive, 2020)

The input shown with a blue colour line is the communication input of the card with the computer. The board communicates with the computer through the computer's parallel port (DB25). The stepper motor connections shown in turquoise, red and purple colours are made in the form of A +, A-, B + and B-. This is called a bipolar connection. In other words, the cables shown in red, yellow, green and blue should be connected to each other. If the motor rotates in the opposite direction to which it is expected to rotate, reverse and reconnect the socket will be enough to correct the direction.

The pneumatic valve is connected to the card's relay. The turret is controlled by the opening and closing of the pneumatic valve by sending a signal to the relay. The power input of the card is powered by a 24-volt power supply. The power requirement of the card and the motors is provided from a single input. Step motor drivers are integrated on the board.

CHAPTER FIVE

CONCLUSIONS

5.1 Conclusions for the analysis part

In this study, the CNC lathe under consideration has been created as a multi-body flexible model in SolidWorks. The assembly model consists of sub-assemblies which are called members. The main assembly consists of three members. These are the main lathe body, the x-axis, and the z-axis. The x-axis member includes the turret. In the sense of deviations at the cutting point, the most important part of the lathe is the turret. The turret was considered as a separate part for a more realistic model. In this way, the deviation on the end point of the cutter has been monitored better. Mesh sizes have been kept high where the effects of the cutting forces insignificant and on the large surface but mesh sizes were kept low where the effects of the forces were significant and on the narrow areas.

After the analysis model had been created correctly, the static analyses have been carried out. Two different static analyses have been performed with cutting force 1 and cutting force 2. The cutting parameters that reveal cutting force 1 were specified as 0.3 mm/rev feed with a cutting speed of 200 m/min and 1 mm chip depth. According to the analysis results the area where the highest stress occured was the cutter tip. Under the determined forces, it was observed that there was a high stress value in the cutter tip region as 900 MPa. The stress increment on the sharp edge is called as stress singularity. In the reality these stress values do not occur. In these sharp edges, the displacement values are more realistic. Stress results should be considered carefully in the corner edges. For this stress value, the displacement of the cutting tool has monitored as 0.115 mm.

After this analysis, cutting parameters were changed and a new analysis has been made with cutting force 2. The cutting parameters that reveal cutting force 2 were specified as 0.1 mm/rev feed with a cutting speed of 200 m/min and 1 mm chip depth. Stress was observed on the cutter tool as 469 MPa maximum. The cutter region in this analysis was safer than the first analysis. For these values, the displacement of the cutting tool has monitored as 0.0639 mm.

5.2 Conclusions for the experimental part

After the analysis steps, experimental processes have been performed. Material of the workpieces to be machined in the turning experiments were chosen as 316 L stainless steel. In the experiments, 2 pieces 316-L stainless steel shafts with 65 mm length and 30 mm diameter were used. The pieces were divided into 3 machining areas with 15 mm length and 6 experiments were carried out. As the insert, Korloy brand DCMT070204-HMP insert has been used.

In the machining processes, 3 passes were made with a 1 mm depth in the diameter. The important thing was here that the experiment areas which had the same distance to the chuck must have been compared with each other. So, the flexibility factor for the compared areas were kept same and there were only the effects of different cutting parameter levels. With these experiments, optimum cutting parameter levels of the lathe were determined and the effects of cutting parameters on surface roughness were observed. In the experiments, the same parameters were compared with each other separately. For example, A1.1 and A2.1 areas have the same distance to the chuck and the same cutting speed level. After machining processes, surface roughness of the areas of the workpieces were monitored.

The minimum roughness values were monitored on the area A1.1. Ra value of this area was monitored as 2.033 µm and Rz value of this area was monitored as 12.93 µm. For the area A1.1, the cutting parameter levels were 200 m/min as cutting speed and 0.1 mm/rev as the feed. The maximum roughness values on this piece were monitored on the area A2.1. Ra value of this area was monitored as 7.787 µm and Rz value of this area was monitored as 33.17 µm. For the area A2.1, the cutting parameter levels were 200 m/min as cutting speed and 0.3 mm/rev as the feed.

According to experimental results, cutting speed as 200 m/min and feed as 0.1 mm/rev provide the best surface roughness quality. For the optimum working range of the CNC lathe, these values must be used and chip depth must be maximum 0.5 mm (1 mm in diameter) for per passes. Surface roughness measurements shows that the best roughness values occurred on the area A1.1 and the worst roughness values occurred on the area A2.1.

5.3 Conclusions for the automation part

For the automation part of the study, the tool holder has been automated with the adjustments on the MACH3 program. In addition, the pneumatic part on the tool holder and the speed control of the spindle motor has been automated with the codes in the program. MACH3 interface has been customized for the existing CNC lathe. In the default interface there were only X and Z axes. The Y axis that we can control the position of the turret has been added to new MACH3 lathe interface. For this axis, page up and page down buttons were attended as control shortcuts on keyboard. With the adjustments on the motor tuning part of the MACH3 settings, acceleration and velocity values of the X, Z and Y axes have been arranged.

By changing the pin/port and input/output settings on MACH3, sending of spindle frequency commands to VFD by using RS485 RJ-45 ethernet port has been activated. Modbus has been used for the transmission of frequency and turning direction information with 8N1 communication protocol over MACH3. Before this study, spindle speed control was made manually only with the potentiometer on the VFD. With the adjustments on the MACH3, the speed control has been made automatically.

The Y axis has been configured as the turret rotation axis and it has been added to the MACH3 interface. Motion of the turret is controlled via the shortcut keys "Page Up" and "Page Down" from the "System Hotkeys" tab on the MACH3 interface. For the rotation of the turret, position parameters have been arranged as the macro codes. These codes were written in MACH3 and each rotation movement have given as 45 degrees. Before running the turret, pneumatics must be turned on. In the previous version of the CNC lathe, running of the pneumatics had been made manually by activating the pneumatic power switch but now the pneumatic system can be operated automatically with M6 tool change code. This process can also be easily made by the pneumatic on-off button placed on the computer screen. The pneumatic is directly connected to the relay of the control board. Output number 1 on MACH3 is the signal output that triggers the relay. The triggering has been provided by the codes M101 (activation) and M102 (deactivation).

5.4 Recommendations for the further improvements

A few recommendations can be given for the further developments of this lathe. Firstly, the chips that appear in the turning process may get stuck in the moving parts like cars. To prevent this, protection bellows may be used. Thus, the system will be more sheltered.

Another issue is the resetting of the coordinate system when the system is restarted. If the resetting process is forgotten and the g codes are loaded, workpieces will be greatly damaged because of the incorrect location. To prevent this, limit switches can be added to the ends of the axes.

Finally, there is no cooling system on the lathe. If large number of parts would be machined in a row, cooling system would be useful.

REFERENCES

Abuthakeer, S. S., Mohanram, P. V., & Kumar, G. M. (2011). Structural redesigning of A CNC lathe bed to improve its static and dynamic characteristics. *Annals of the Faculty of Engineering Hunedoara*, *9*(3), 389.

Arali, S., & Kulkarni, V. V. (2014). Analysis of CNC lathe spindle for maximum cutting force condition and bearing life. *International Journal of Innovative Research in Advanced Engineering (IJIRAE), 1*(6), 346-352.

Aslantaş, K., Çiçek, A., & Kara, F. (2015). ANN and multiple regression method-based modelling of cutting forces in orthogonal machining of AISI 316L stainless steel. *Neural Computing & Applications*(26), 237-250.

Bell, T. (2020). *Machinery*. Retrieved August 2020, from Thoughtco.com: https://www.thoughtco.com/type-316-and-316l-stainless-steel-2340262

Cakir, M. C., & Yahya, I. S. (2005). Finite element analysis of cutting tools prior to fracture in hard turning operations. *Materials & Design, 26*(2), 105-112.

Das, B., Rai, R. N., & Saha, S. C. (2013). Analysis of surface roughness on machining of Al-5Cu alloy in CNC lathe machine. *International Journal of Research in Engineering and Technology, 2*(9), 296-299..

DELTA VFD-EL User Manual (2020). *Turkey*. Retrieved July 2020, from http://destek.delta-turkey.com/viewtopic.php?t=29

Eker, B., Ekici, B., Kurt, M., & Bakır, B. (2014). Sustainable machining of the magnesium alloy materials in the CNC lathe machine and optimization of the cutting conditions. *Mechanics, 20*(3), 310-316.

Elmunafi, M. H. S., Mohd Yusof, N., & Kurniawan, D. (2015). Effect of cutting speed and feed in turning hardened stainless steel using coated carbide cutting tool under minimum quantity lubrication using castor oil. *Advances in Mechanical Engineering, 7*(8), 1-7.

Erkekli, K. (2017). *Mechanical design for a hydraulically actuated quadruped robot.* Doctoral dissertation, Sabanci University, Istanbul.

First CNC Machine. (n.d.). Retrieved 10 June 2020, from https://ykoren.engin.umich.edu/research/cnc/

Hackaday (1962). *A magnetic tape controlled vertical profiler.* UK. Retrieved May 2020, from https://hackaday.com/2016/11/11/an-introduction-to-cnc-machine-control/

Kara, F., Aslantas, K., & Çiçek, A. (2015). ANN and multiple regression method-based modelling of cutting forces in orthogonal machining of AISI 316L stainless steel. *Neural Computing and Applications*, *26*(1), 237-250.

Korloy tools. (n.d.). Retrieved August 10, 2020, from http://www.korloy.com/tr/download/cata.do?searchType=CP&findtype=M

Kumar, N. S., Shetty, A., Shetty, A., Ananth, K., & Shetty, H. (2012). Effect of spindle speed and feed rate on surface roughness of carbon steels in CNC turning. *Procedia Engineering*, *38*, 691-697.

Le Hieu Giang, M. D. D., & Duc, P. M. (2016). Investigation of effects of tool geometry parameters on cutting forces, temperature and tool wear in turning using finite element method and Taguchi's technique. *International Journal of Mechanical Engineering and Applications*, *4*(3), 109-114.

Maniar, N. P., Vakharia, D. P., & Patel, C. M. (2009). Design & manufacturing with modeling, dynamic balancing & finite element analysis of rotary fixture for cnc turning centre to function as HMC. *ASME Early Career Technical Journal*, *8*, 86-93.

Parts of the CNC lathe. (n.d.). Retrieved, June 10, 2020, from http://www.helmancnc.com/cnc-lathe-main-parts/

Senapati, A. K., Bhatta, A., Senapati, A., Mishra, O., & Mohanty, S. (2014). Effect of machining parameters on cutting forces during turning of mild steel on high speed lathe by using Taguchi Orthogonal Array. *Global Journal of Advanced Research, 1*(1), 28-35.

The first nc machine tool in Europe. (n.d.). Retrieved June 10, 2020, from https://www.mybrightonandhove.org.uk/topics/technology/inventions/technology

Tutkun & Akdağ, (2020). Modelling and finite element analysis of a desktop cnc lathe as an example of a flexible multi-body system. *International Conference on Materials Science, Mechanical and Automotive Engineerings and Technology,* 43-48.

Umbert, S. M., & de Grau, T. T. D. F. (2017). *Cutting forces in turning operations.* NTNU: Norwegian University of Science and Technology.

Vrtanoski, G., & Dukovski, V. (2005). Design of polymer concrete main spindle housing for cnc lathe. In *13th International Scientific Conference on Achievements in Mechanical and Materials Engineering,* 695-698.

Xing, Y., & Moan, T. (2013). Multi-body modelling and analysis of a planet carrier in a wind turbine gearbox. *Wind Energy, 16*(7), 1067-1089.

Yadav, U. K., Narang, D., & Attri, P. S. (2012). Experimental investigation and optimization of machining parameters for surface roughness in CNC turning by Taguchi method. *International Journal of Engineering Research and Applications, 2*(4), 2060-2065.

Yao, C., Zhou, Z., Zhang, J., Wu, D., & Tan, L. (2017). Experimental study on cutting force of face-turning Inconel718 with ceramic tools and carbide tools. *Advances in Mechanical Engineering, 9*(7), 1-9.